

© 2009

Judith D. Sorge

ALL RIGHTS RESERVED

HYDROTHERMAL GROWTH AND CHARACTERIZATION OF TITANIUM DIOXIDE
NANOSTRUCTURES FOR USE IN DYE SENSITIZED SOLAR CELLS

By

JUDITH D. SORGE

A Dissertation Submitted to the
Graduate School – New Brunswick
Rutgers, The State University of New Jersey
in partial fulfillment of the requirements

for the degree of

Doctor of Philosophy

Graduate Program in Materials Science and Engineering

written under the direction of

Dr. Dunbar P. Birnie, III

and approved by

New Brunswick, NJ

May 2009

ABSTRACT OF THE DISSERTATION

Hydrothermal Growth and Characterization of Titanium Dioxide Nanostructures for Use in Dye Sensitized Solar Cells

by JUDITH D. SORGE

Dissertation Director:

Dr. Dunbar P. Birnie, III

As the world's energy needs continue to grow, next generation photovoltaic cells are in high demand because they offer the possibility of an inexpensive alternative to current energy production techniques. Dye sensitized solar cells (DSSC's), utilize common materials and low cost commercialization techniques, which make them a compelling choice for research in this area. This research focuses on the titanium dioxide coating, which transfers electrons from the photoactive dye to the electrode. 3-4% efficient DSSC's using doctor bladed titanium dioxide coatings with a specific surface area of 55-60m²/g have been demonstrated in our laboratory. To enhance the efficiency of these cells, both the surface area and the electron conduction of the titania layer must be optimized. This has been done by utilizing high aspect ratio nanoparticles of titania instead of mesoporous layers formed with spherical particles. Anodization of titanium metal or anodic alumina membrane templating are common ways to produce nanorods, but involve complex processes leading toward expensive commercialization. This research instead focuses on the hydrothermal growth of nanofibrous titania on a titanium

metal substrate, removing the need for dispersion and deposition procedures as well as using a low temperature processing method. Depending upon the formulation utilized, a variety of structures can be produced, from thick carpets of nanofiber strands to large platelets. The composition and morphology of the products have been characterized with respect to the growth conditions using electron microscopy, energy dispersive spectroscopy and x-ray diffraction. The compositional analysis is used to investigate the complicated reaction mechanisms in the system. Coatings of titania nanotubes were then tested in the DSSC's, as were those with the titanium metal substrate acting as the photo anode. Modeling the geometric parameters of the different pore structures of the coatings helps us to understand the advantages afforded by these new cells.

DEDICATION AND ACKNOWLEDGEMENTS

While there were many people that have helped me along the way, this thesis is dedicated to my family. They have been my greatest source of support, encouragement and laughter throughout my time at graduate school, and especially during the writing of this thesis.

I would also like to thank my advisor, Dr. Dunbar P. Birnie, III for always being there with a smile and reminding me that everything matters, even when it was the last thing I wanted to hear. Thanks also go to my groupmates and undergraduates who helped me brainstorm creative ideas and also put up with boring labwork. I also want to thank everyone in the Rutgers Materials Science and Engineering Dept. because getting a PhD is a team effort. The support of the Malcolm G. McLaren / HED / John Dennis fellowship has also been greatly appreciated.

TABLE OF CONTENTS

ABSTRACT.....	ii
DEDICATION AND ACKNOWLEDGMENTS.....	iv
TABLE OF CONTENTS.....	v
LIST OF TABLES.....	viii
LIST OF FIGURES.....	ix
CHAPTER 1: INTRODUCTION.....	1
CHAPTER 2: LITERATURE REVIEW.....	4
2.1: Dye Sensitized Solar Cells.....	4
2.1.1: Design of DSSC's.....	6
2.1.2: Electrical Characteristics.....	19
2.2: Hydrothermal Growth of Nanostructures in Solution.....	23
2.2.1: Morphology.....	24
2.2.2: Composition.....	30
2.2.3: Mechanism and Structure.....	35
2.3: Hydrothermal Growth on Substrates.....	43
2.4: Use of High Aspect Ratio Titania in Dye Sensitized Solar Cells.....	46
CHAPTER 3: METHOD OF ATTACK.....	52
CHAPTER 4: EXPERIMENTAL PROCEDURES.....	53
4.1: Dye Sensitized Solar Cells.....	53
4.1.1: Materials.....	53
4.1.2: Building DSSC's.....	60
4.1.3: Solar Cell Characterization Methods.....	62

4.2: Hydrothermal Growth of Nanostructures.....	64
4.3: Characterization of Hydrothermal Products.....	67
4.3.1: X-Ray Diffraction.....	67
4.3.2: Scanning Electron Microscopy.....	68
4.3.3: Transmission Electron Microscopy.....	68
CHAPTER 5: DYE SENSITIZED SOLAR CELLS.....	70
5.1: Results.....	70
5.1.1: Cell Design Tests.....	70
5.1.2: Electrolytes.....	82
5.1.3: Titania.....	82
5.2: Discussion.....	88
5.2.1: Comparison of Efficiency.....	88
5.2.2: Titania.....	94
5.2.3: Electrolytes and Titania Interaction.....	95
CHAPTER 6: HYDROTHERMAL REACTIONS.....	104
6.1: Results.....	104
6.1.1: Solution Growth of High Aspect Ratio Nanostructures.....	104
6.1.2: Nanostructures Growth on Substrates.....	120
6.1.3: Results of High Aspect Ratio Nanostructures in DSSC's.....	135
6.2: Discussion of Hydrothermal Growth Method.....	140
6.2.1: Morphology.....	140
6.2.2: Phase and Composition of Hydrothermal Growth Products.....	147
6.2.3: High Aspect Ratio and Titanium Substrate Solar Cells.....	154

CHAPTER 7: CONCLUSIONS	156
7.1: Dye Sensitized Solar Cells.....	156
7.2: Hydrothermal Growth of High Aspect Ratio Nanostructures.....	158
7.3: The Use of High Aspect Ratio Nanostructures in DSSC's.....	160
CHAPTER 8: FUTURE WORK.....	162
REFERENCES.....	164
CURRICULUM VITAE.....	173

LIST OF TABLES

Table 2.2.1: Review of Hydrothermal Reaction in the Literature.....	26
Table 2.4.1: Characteristics of High Aspect Ratio DSSC's.....	47
Table 4.1.1: Electrolyte Recipes.....	55
Table 5.1.1: Characteristics of Initial DSSC's.....	71
Table 5.1.2: Binder Clip Cells with Sputtered Pt Electrodes.....	72
Table 5.1.3: Sealing Method and Pt Electrode Comparison.....	73
Table 5.1.4: Comparison of Additional Layers of TiO ₂	75
Table 5.1.5: Barrier Layer and Platinum Electrode Comparison.....	76
Table 5.2.1: Optimal Spherical Nanoparticle TiO ₂ Coating.....	98
Table 5.2.2: Modeled Nanorod Coating with SA = Spherical Coating.....	99
Table 5.2.3: Properties of Template Coatings.....	100
Table 6.1.1: List of Hydrothermal Solution Samples.....	105
Table 6.1.2: Products Formed by Hydrothermal Growth on Titanium Metal.....	123
Table 6.2.1: Intensity and Position of Closest Peak to 15.9° in Various Sodium Titanate Compounds.....	148

LIST OF FIGURES

Figure 1.1: Comparison of Solar Cell Types and Their Efficiencies.....	2
Figure 2.1.1: Schematics of a Dye Sensitized Solar Cell.....	5
Figure 2.1.2: Electron Configuration in a DSSC.....	7
Figure 2.1.3: Absorption and Emission Spectra.....	12
Figure 2.1.4: Molecular Structure of N3.....	13
Figure 2.1.5: IPCE Comparison.....	14
Figure 2.1.6: Redox Couple Comparison.....	18
Figure 2.1.7: Grätzel IV Curve.....	20
Figure 2.1.8: Bonding Surfaces.....	22
Figure 2.2.1: TEM Images of Nanotube Formation.....	29
Figure 2.2.2: Comparison of XRD Patterns of Hydrothermal Growth Products....	33
Figure 2.2.3: Solubility of Ti with pH and Temperature.....	37
Figure 2.2.4: TEM of Intermediate Hydrothermal Product.....	39
Figure 2.2.5: Schematic of Growth Mechanisms.....	40
Figure 2.2.6: TEM Images of Nanotube Products.....	41
Figure 2.4.1: Composite Nanorod / Nanoparticle Coatings.....	50
Figure 4.1.1: Binder Clip Method.....	57
Figure 4.1.2: Hot Melt Sealant Method.....	58
Figure 4.1.3: Solar Simulator and Characterization Equipment.....	63
Figure 4.2.1: Schematic of Hydrothermal Reaction System.....	66
Figure 5.1.1: Reproducibility of Early DSSC's.....	77

Figure 5.1.2: Testing Non-Platinum Back Electrodes.....	78
Figure 5.1.3: Effect of Thickness on Efficiency.....	79
Figure 5.1.4: Geometry of Titania Coatings.....	80
Figure 5.1.5: IV Curves of Cells with Different Geometries.....	81
Figure 5.1.6: Direct Comparison of Ionic Liquid and Volatile Electrolytes.....	83
Figure 5.1.7: Effect of the Evaporation of Volatile Electrolyte.....	84
Figure 5.1.8: Comparison of Ionic and Volatile Electrolytes Over Time.....	85
Figure 5.1.9: Cells Made Using Battery Separator.....	86
Figure 5.1.10: FESEM Images of Titania Mesoporous Coatings.....	87
Figure 5.1.11: Templated Cells Tested with Different Electrolytes.....	89
Figure 5.1.12: FESEM Images of Templated Films.....	90
Figure 5.2.1: Changes in Efficiency Over Time wrt Sealing Method.....	91
Figure 5.2.2: Barrier Layer and Platinum Electrode Interaction.....	93
Figure 5.2.3: Comparison of Testing Methods with Corning, Inc.....	96
Figure 5.2.4: Schematic of Titania Coatings.....	101
Figure 5.2.5: Pore Structure in Templated Coatings.....	103
Figure 6.1.1: Sequence of Hydrothermal Product Formation.....	106
Figure 6.1.2: Comparison of End Products.....	108
Figure 6.1.3: Changes in Morphology with Reaction Sequence.....	109
Figure 6.1.4: Changes in Composition with Reaction Temperature.....	110
Figure 6.1.5: Changes in Morphology with Reaction Temperature.....	111
Figure 6.1.6: Hydrothermal Reaction Time Comparison.....	112
Figure 6.1.7: Effect of P25 Amount on the Product Composition.....	114

Figure 6.1.8: Composition of Final Products.....	115
Figure 6.1.9: Changes in Surface Area due to NaOH Concentration.....	116
Figure 6.1.10: Morphology of Reactant Particles.....	117
Figure 6.1.11: Amorphous Structures in Initial Product.....	118
Figure 6.1.12: Initial Product Morphology.....	119
Figure 6.1.13: Nanotube Morphology Maintained After Acid Wash.....	121
Figure 6.1.14: Deposited High Aspect Ratio Nanostructures.....	122
Figure 6.1.15: FESEM Image of Untreated Titanium Metal.....	125
Figure 6.1.16: Range of Microstructures Grown on Titanium Metal.....	126
Figure 6.1.17: Images of Coatings Formed on Ti - No P25 Added.....	127
Figure 6.1.18: Images of Coatings Formed on Ti with P25 Added.....	128
Figure 6.1.19: Composition of Preliminary “Ruffle” Structures.....	130
Figure 6.1.20: XRD Patterns of Platelet Coatings.....	131
Figure 6.1.21: Composition of Nanofibers on Titanium Metal.....	132
Figure 6.1.22: Product of Hydrothermal Reaction with Sol-Gel Layer.....	133
Figure 6.1.23: Changes in Morphology due to Acid Treatment.....	134
Figure 6.1.24: EDS Analysis After DIW Aging Treatment.....	136
Figure 6.1.25: Effect of Post Treatment on XRD Patterns.....	137
Figure 6.1.26: Composition of Coatings Through Reaction Sequence.....	138
Figure 6.1.27: Photovoltaics Produced with Nanotubes.....	139
Figure 6.1.28: Characteristics of Cells Made with a Titanium Electrode.....	141
Figure 6.1.29: IV Curve of Titanium Cell Made with Ionic Liquid Electrolyte....	142
Figure 6.2.1: Images of Platelet Coatings on Both Sides of Ti Substrate.....	145

Figure 6.2.2: PDF Cards for Sodium Titanate Phases.....	149
Figure 6.2.3: PDF Cards for Anatase and Rutile Titania.....	150
Figure 6.2.4: XRD Pattern of Untreated Ti Metal.....	152
Figure 6.2.5: EDS Mapping of Platelet Structures.....	153

CHAPTER 1: INTRODUCTION

Renewable and environmentally sound energy production technology is necessary for the replacement of fossil fuels. Currently, most of the world's energy derives from fossil fuels, and the supply can no longer keep up with the demand. This scarcity and the environmental hazards caused by fossil fuels have led towards a revitalization of research in renewable and sustainable energy production. Technology in the conversion of solar, wind and geothermal energy to usable electrical energy has gained much popularity and further research is necessary for these techniques to become efficient and competitive with fossil fuels.

Solar cells are an alternative energy source that have been utilized in various forms for many years, which convert radiation from the sun into usable electricity. Common solar cells are based on doped silicon semiconductors with a p-n junction where a depletion region produces an electric field that separates charges. This separation of charges produces electrical flow. While they are commercially available, these cells are not economically competitive with fossil fuels currently and have a current module cost of approximately \$2/watt¹. The inset in figure 1.1 illustrates the goals for cost and efficiency of solar cells. A variety of types solar cells are being investigated, with different materials that hope to fit into the third generation type of cell. The methods these materials use to convert the energy and how they are affected by sunlight, heat and time must be investigated in great depth to determine if they are suitable for long-term energy production. Figure 1.1 demonstrates the increased efficiencies in all areas of solar cells over the past thirty years.

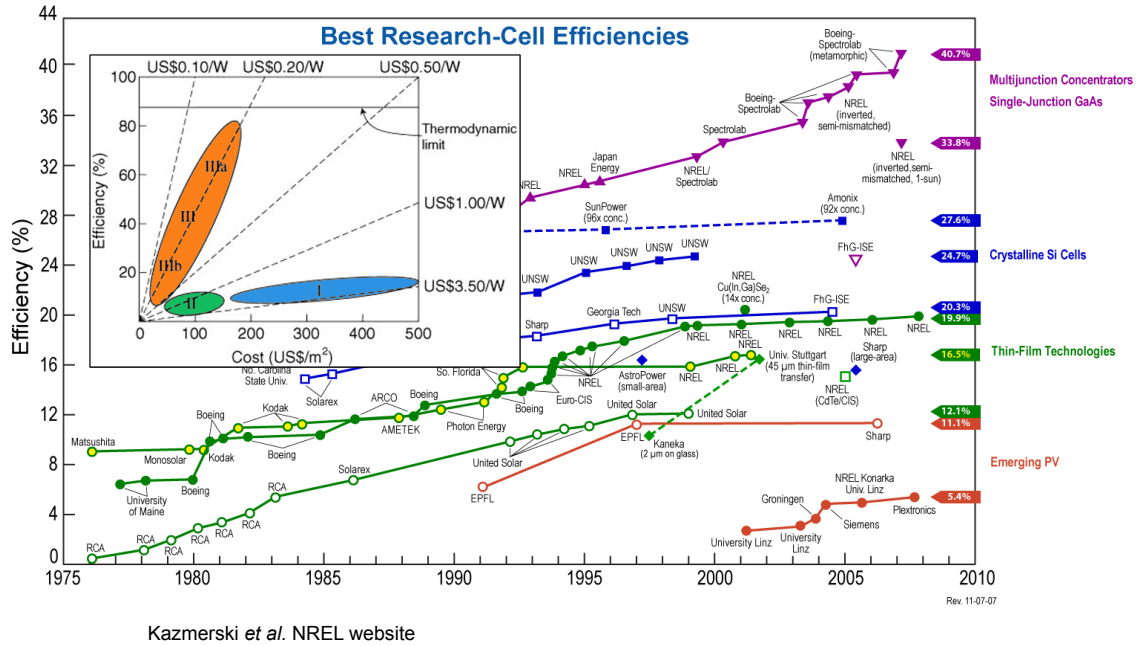


Figure 1.1. Large graph demonstrates the state of photovoltaics at the end of 2007. Inset illustrates the aim towards third generation solar cells: I) low efficiency, high cost; II) low efficiency, low cost and III) high efficiency, low cost².

Dye sensitized solar cells (DSSC's) are one type of emerging photovoltaic cell with an efficiency reaching 11%^{3,4} that consist of low cost materials. Research in these cells surged in 1991 when efficiencies of 7.1-7.9% were reported by a group in Switzerland under the direction of Michael Gratzel⁵. DSSC's involve a layered system with two electrodes, one an active layer of dye chemisorbed to titanium dioxide and the other a platinum layer, both coated on a transparent conductive oxide layer on glass. An electrolyte between the electrodes is used to replenish the electrons in the active dye layer. The focus of this research is the structure of the titanium dioxide layer and how different particle and film geometries affect the charge transport in the solar cell.

Titanium dioxide is a ubiquitous material used for pigments, photocatalysis, and sensors among many other applications, so that while this research focuses on a photocatalytic application, much of the structure and growth characterization work is applicable to other product areas. A hydrothermal growth method was utilized to produce different nanostructures of titanium dioxide. High aspect ratio nanostructures, such as nanotubes and nanofibers, produce high surface area coatings that maintain the necessary design parameters for DSSC's. It has been found that nanotubes have different properties than those of their bulk materials, and that their structure may be able to enhance certain properties. This would affect the efficiency of the DSSC's as recombination losses at the grain boundaries of titania nanoparticles cause current losses. Growing, characterizing and utilizing high aspect ratio nanostructures offers great promise for increased efficiency in DSSC's as well as furthering understanding of the hydrothermal growth process.

CHAPTER 2: LITERATURE REVIEW

2.1: Dye Sensitized Solar Cells

Using dye molecules instead of chlorophyll, DSSC's mimic the process that occurs in green, leafy plants where the molecule is excited by the sun and high energy conversion occurs⁶⁻⁸. DSSC's have a simple structure, shown in figure 2.1.1, with five layers working together to produce and transfer current. The top electrode consists of a glass substrate coated with a transparent conductive oxide (TCO) and dense barrier layer that hinders recombination. Dye molecules are chemisorbed onto a wide bandgap semiconducting film deposited or grown over the barrier layer. The semiconductor is simply used for electron transfer while the dye is the photoactive layer. The interlayer spacing between this film and the bottom electrode is filled with an electrolyte, which reduces the dye, allowing for a renewable process. The second electrode consists of a sputtered layer of platinum on a TCO coated glass substrate.

Unlike a silicon p-n junction cell, the light absorption and charge separation in a DSSC are separated in space and time. The activation of this cell occurs when light strikes a dye molecule and the electron is excited into a higher energy state. From this higher energy state, it passes to the semiconductor electrode. Because the electron injection to the semiconductor is much faster than electron relaxation in the sensitizer, charge separation occurs with a high efficiency. The dye molecule is reduced by the electrolyte, which is in turn reduced at the counter electrode. The difference between the Fermi level and the potential of the counter electrode equals the maximum voltage output of the cell⁹. In figure 2.1.1b, the arrows illustrate the direction and series of electron

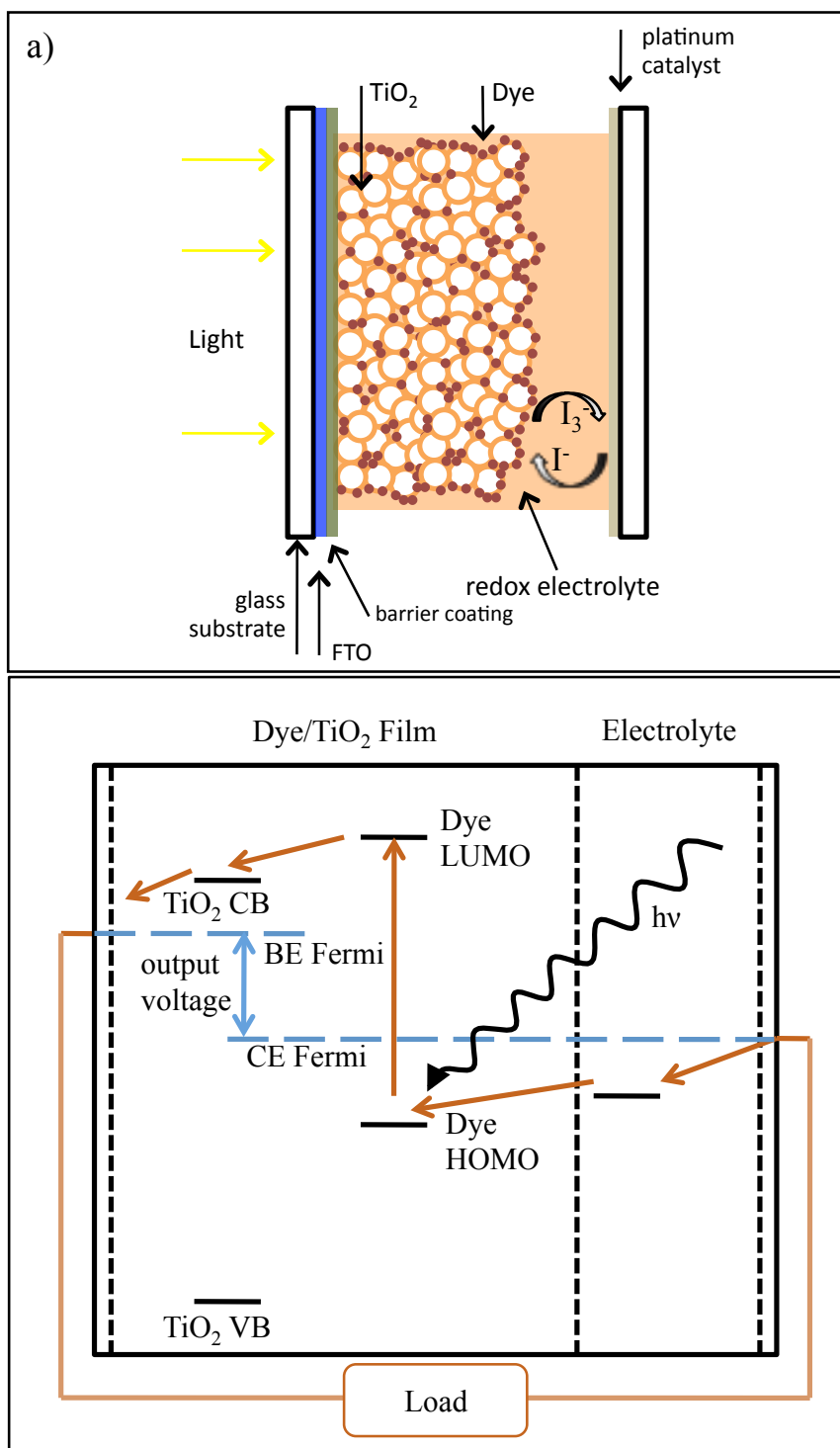


Figure 2.1.1. DSSC schematics depicting a) the design of the cell and b) the electron transfer that occurs after light impinges on the dye molecule. CE and BE Fermi portray the relative levels of the Fermi level for the counter electrode and back electrode, respectively.

movement when the cell is light activated. Path 1 is excitation of the dye electron by light absorption, then electron injection into the semiconductor occurs, and after the electrons pass through the load, the electrolyte reduces the dye.

2.1.1: Design of DSSC's

The different layers of the solar cell each have specific design parameters for the cell to function well. The electrode substrates are designed for mechanical strength, as they must withstand contact and eventually weather the elements, and maximum light transmission, necessary for the light to activate the dye. The anode, with the titanium dioxide film attached, is the contact through which the cell is illuminated because it has been shown that this increases the efficiency. If light shines through the platinum cathode instead, when only catalytic platinum is used, recombination losses increase because more electrons must pass through a greater distance, making it more likely for trapping to occur¹⁰ and current decreases as a metal backing increases electron collection due to reflection. TCO coated glass maintains both transparency and mechanical strength. The TCO that is most commonly used is fluorine doped tin oxide and its thickness is in the range of $0.5\mu\text{m}$ ¹⁰ with a resistance of 8-10 Ω /sq. Other doped tin oxides are often utilized, such as indium doped tin oxide, but empirical studies show that the fluorine doped tin oxide markedly increases the efficiency. The work function of the metal on the back electrode determines how large the output voltage can be, as shown in figure 2.1.2. Platinum is used because with its high work function of 5.6eV, it gives a large possible output voltage. If, for example, gold were used, which has a work function of 5.1eV, the 0.5V difference becomes a loss in the cell.

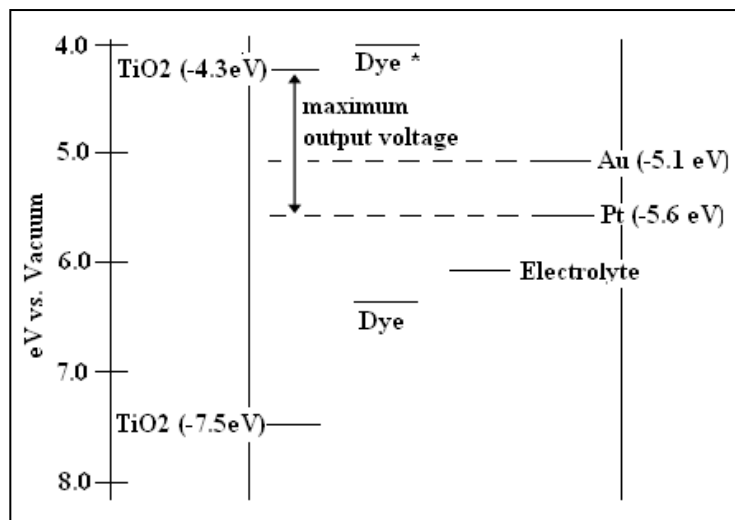


Figure 2.1.2: This diagram illustrates the electron configuration in the DSSC. The changes in output voltage due to the work function of platinum versus that of gold are illustrated¹¹.

The mesoporous, wide bandgap semiconductor adheres to the TCO/glass surface and transfers electrons from the dye molecules to the TCO electrode. Currently titanium dioxide has been found to give the highest efficiencies. Zinc oxide¹²⁻¹⁴ has been utilized often, but has a lower current conversion efficiency and takes much longer to adsorb dye on the surface than the titanium oxide¹⁵. The lower efficiency of zinc oxide cells appears to be due to lower dye to semiconductor electron injection or an increase in recombination losses¹⁵. SnO_2 ^{6,16}, Fe_2O_3 ¹⁷, Nb_2O_5 ¹⁸ and CdS ^{12,19} and CdSe ¹⁹ have also been researched as possible electrode materials, and results illustrate that although photocurrents are produced, the efficiencies are less than that of titanium dioxide.

Other properties of the semiconductor electrode include mechanical strength, such that the coating does not flake off, uniform thickness, high surface area and rapid dye adsorption throughout the film. High surface area is a necessity because the current output is directly related to the amount of dye molecules adsorbed on the titanium dioxide. Tsubomura, et al proved this by illustrating that a monomolecular layer of dye on the flat surface of zinc oxide gave very low efficiencies, while the use of a more porous system produced greater photocurrents²⁰. A thicker layer of dye on a flat surface does not produce high photocurrents because, although light excitation occurs, the electron injection into the semiconductor only occurs through the dye molecule / titania bond. Mesoporous titanium dioxide is often used, defined by IUPAC as a film with pores in the range of 2-50nm, as the dye molecules fit closely into pores on the smaller side of this. High surface area coatings are simply produced by using nanoparticles which increase the roughness factor of the optimized electrodes by over 1000 and the surface area increases to at least $100\text{m}^2/\text{g}$ ²¹. Nanoparticles also speed electron transfer without

the need for doping as the addition of one photoinjected electron allows it to become n-type²¹, unlike bulk titania. Recombination losses may rise due to the increase in trapped states, such as grain boundaries and surface states, when nanoparticles are used, but as the charge separation and reduction of the dye are rapid, these losses are not assumed to be detrimental to the efficiency of the cell²¹⁻²⁴. The electrolyte causes a screening effect on the surface of the particles because of its overall negative charge which allows electrons to transfer through the semiconductor with low recombination losses^{24,25}. As it conducts holes away from the dye molecule, it also minimizes recombination by protecting the titania from the holes.

The production of the titanium dioxide layer has been completed by a variety of methods to determine which produces the cell with the greatest efficiency. Sol-gel methods^{26,27}, dispersion methods²⁸, and hydrothermal growth methods²⁹, among others, have all been researched. The properties of the particle and the film that affect the efficiency of the cell that are a part of this layer are many and varied. Thickness, particle size, surface area, porosity, pore size, pore size distribution, and even surface chemistry all have a profound effect on the cell's overall efficiency. Grätzel utilized mesoporous thin films of spherical titanium dioxide for his 10.6% efficiency cell. These particles are well formed, with a narrow size distribution, and are made from a hydrothermal sol-gel synthesis with titanium isopropoxide as the precursor³⁰. The titanium dioxide layer may also be made by a dispersion of a commercially available product, P25, which consists of approximately 70% anatase and 30% rutile titanium dioxide²⁶ while a sol-gel produced titanium dioxide usually consists of wholly anatase, due to a heat treatment at 450°C.

Anatase has a larger bandgap than rutile, 3.2eV and 3.0eV respectively, and is reported to be more photocatalytically active.

The sensitizer, or dye monolayer, is the active layer in which an electron gets bumped from the ground state to an excited state when solar energy impinges upon the cell. The layer itself must be thin because only the layer of dye molecules in direct contact with the semiconductor and the electrolyte can transfer charge and any further layers of dye may impede electron transfer from the electrolyte to the dye molecules^{20,31}. A monolayer of coverage on a high surface area semiconductor is ideal²⁴ as it allows for absorption of the greatest amount of photons and gives up the least losses due to relaxation of the excited state electron because there is always a semiconductor surface nearby to accept the electron into the conduction band.

A photon is absorbed by the dye and the electron moves from the ground state to the carboxylate ligand by metal to ligand charge transfer (MLCT). Then electron injection occurs from the carboxylate ligand to the conduction band. This transfer is on the order of picoseconds because the π^* orbital of the carboxylate overlaps with the 3d manifold or conduction band of the titanium dioxide^{24,25}. Electron injection from the ligand to the conduction band is favored energetically, as the conduction band energy levels is below that of the lowest unoccupied molecular orbital (LUMO) of the dye where the electron is excited to, and entropically, since once in the conduction band, the electron will be averaged over many states. For these reasons, the back reaction is unfavored. Electron injection from the dye to the titanium dioxide is reported to be hindered by impurities in the titania, such as iron. It has been shown empirically that this can be lessened by depositing a layer of high purity titania nanoparticles on the surface of

the titania electrode by hydrolyzing titanium tetrachloride. The surface area increases because of the small particle size and the speed of the electron injection increases with the high level of purity²⁸. Currently, this topic is in debate because there is a lack of evidence that these are the only reasons that the surface layer of pure titania increases the efficiency of the cell.

The sensitizer must be designed for maximum absorption across the solar spectrum, contain ligands that readily attach to the titania surface, a high efficiency transfer of the excited electrons to the conduction band²¹, and a high reduction potential so that reduction is rapid compared to relaxation. Figure 2.1.3 portrays the absorption and emission spectra of an early dye³². As will be expanded upon below, the energy levels of the sensitizer and the semiconductor should be well matched, such that the excited state of the sensitizer lies just above the conduction band of the semiconductor in order for electron injection to be a low energy, rapid process. The ground state energy level should be just below that of the electrolyte and be of sufficient reduction potential to be easily reduced by the redox electrolyte. The sensitizer most commonly used is labeled N3 and is $\text{cis-Ru(2,2'-bipyridyl-4,4'-dicarboxylate)}_2(\text{NCS})_2$ which is shown in figure 2.1.4^{21,28}. The absorption maxima lie at 518 and 380nm with extinction coefficients of 1.3 and $1.33\text{M}^{-1}/\text{cm}$, and the dye emits at 750nm with a 60s lifetime. The dye degrades in water, and bonds via a bridging ligand to the titanium atoms in the titania electrode. The 10.4% efficiency cell actually used a second dye, $\text{tri(cyanato)-2,2'2''-terpyridyl-4,4'4''-tricarboxylateRu(II)}$, known as black dye, but the N3 dye with a self-assembly additive has produced the 10.6% cell^{21,33}. Figure 2.1.5

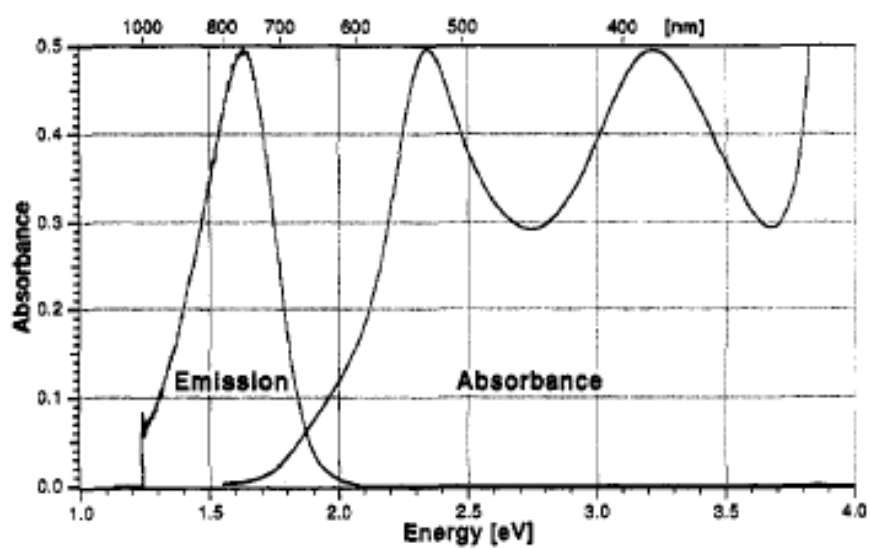


Figure 2.1.3. The absorption and emission spectra of an early type of dye: cis-di(thiocyanato)bis(2,2'-bipyridal-4,4'-dicarboxylate)ruthenium(II)³².

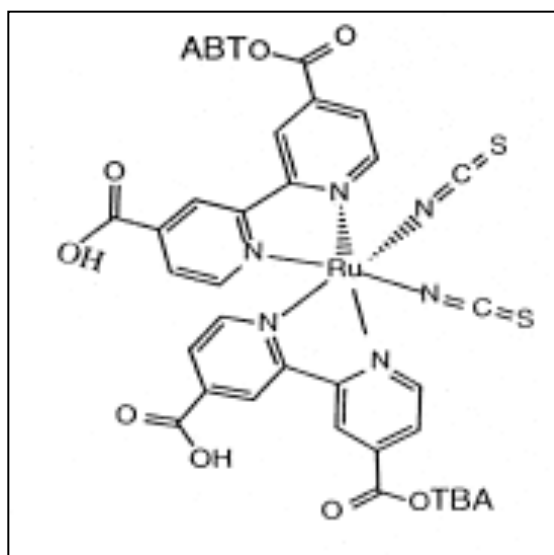


Figure 2.1.4. Molecular structure of the N3 dye³⁴.

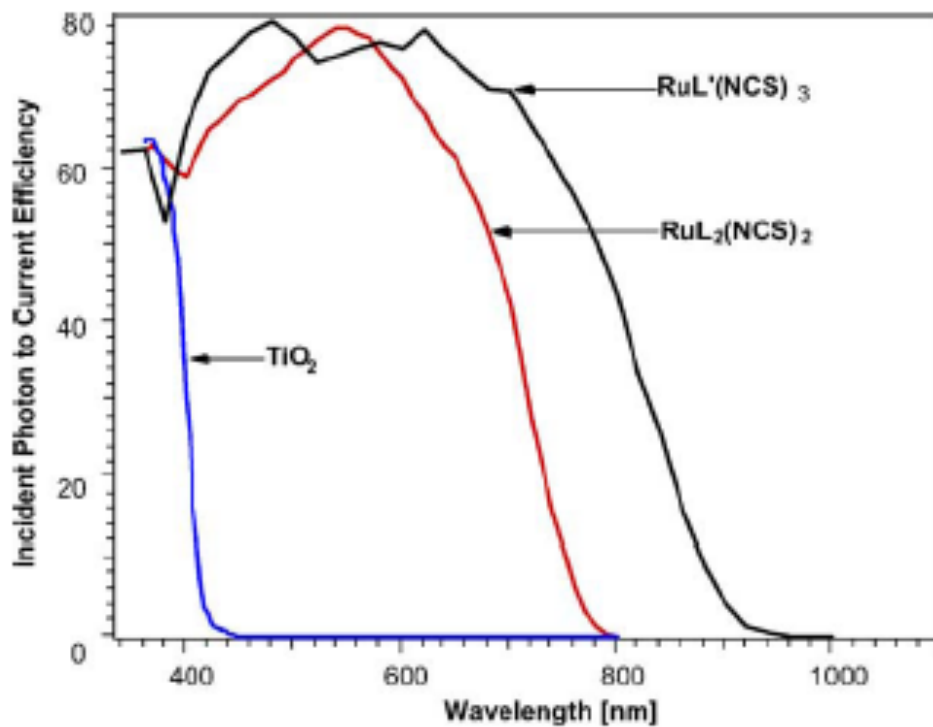


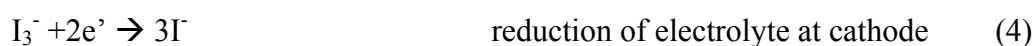
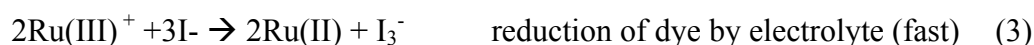
Figure 2.1.5. Comparison of the IPCE of different dyes²¹. Black dye has a higher IPCE and offers the promise of high efficiency cells, but the highest efficiency cell yet made was prepared with N3 due to an electrolyte additive.

illustrates the incident photon to current efficiency (IPCE) for each dye, the N3 and the black, which demonstrates how much current is generated for each photon. The black dye is labeled $\text{RuL}'(\text{NCS})_3$ and the N3, $\text{RuL}_2(\text{NCS})_2$. These dyes both show IPCE of almost 80%, which is equivalent to a 100% efficiency because of the losses through the TCO coated glass²¹. Dyes have improved greatly over the past twenty years, as a new dye in 1985 had an unprecedented IPCE of 44%, with three bipyridal groups and two chlorine ligands³⁵. Most of this increase has come from the movement towards two bipyridal groups and three thiocyanate ligands. Novel sensitizers utilizing quaterpyridyl derivatives may demonstrate increased IPCE values for a larger region of wavelengths rather than the peak behavior of current dyes³⁶.

The electrolyte is a system of reduction-oxidation (redox) molecules that reduce the sensitizer after photoexcitation and are reduced at the counter electrode. The redox couple must have a reduction potential between the platinum work function and the sensitizer reduction potential which creates a driving force for electron transfer. An iodide/iodine complex has been used because of its appropriate reduction potential and rapid kinetics since early photoelectrochemical cells²⁰. It is produced simply by mixing iodine with an iodide salt in an appropriate solvent, such as acetonitrile³⁷. Adding guanidinium thiocyanate to the electrolyte screens the coulombic interactions between the dye molecules, producing a more dense dye layer that decreases recombination losses²¹.

At the platinum electrode, the electrons that have passed through the circuit are donated to the redox molecule, which has an excess hole after it has reduced the dye. This molecule then donates an electron to the sensitizer molecule, which is positive because it has donated its excited electron to the conduction band of the semiconductor.

The sensitizer must be reduced rapidly because as soon as it has an electron back in the ground state, the electron in the excited state cannot relax down and cause losses. The following reactions illustrate these processes:



Recombination losses:



Relaxation of the excited electron does not occur because the electron injection happens more rapidly, on the order of picoseconds ($\tau < 7\text{ps}$)²⁸ and the metal to ligand charge transfer process that occurs in electron injection is much more rapid in the forward direction, as discussed in more detail below. As one can see from the equations above, the iodide/tri-iodide complex uses two electrons in each oxidation/reduction process. Hypotheses by Nusbaumer, et al have questioned whether electrolytes that use only one electron would have a lower activation barrier at oxidation, and therefore would increase the speed of dye reduction³⁹. Another possible way to increase the output voltage would be to decrease the difference in potential between the redox couple and the sensitizer. The N3 dye has a reduction potential of 0.85eV³², while the iodide/tri-iodide complex holds at 0.15eV, versus a standard calomel electrode. If an electrolyte with a higher

reduction potential, perhaps 0.6eV, instead of the 0.15eV, were chosen, the open circuit voltage of the cell could increase by that difference, 0.45eV, which may increase the efficiency of the cell. $(\text{SCN})_2/\text{SCN}^-$ and $(\text{SeCN})_2/\text{SeCN}^-$ complexes have been tested due to their higher reduction potential, but the efficiency of the cell did not increase, most likely due to a slower dye regeneration rate^{39,40}. Figure 2.1.6 compares the IV curves for cells produced with different electrolytes, demonstrating that the I^-/I_3^- redox couple is much more efficient than others tested.

In all of the electrolytes discussed above, there is a degradation problem due to the use of a liquid phase. Although the liquid phase allows for the electrolyte to fill all of the pores and small crevices in the mesoporous electrode with ease, it often degrades in air and/or under thermal stresses so that sealing must be done perfectly to make a cell with a long lifetime. Specifically, degradation occurs after a short duration at 80-85°C, causing a problem for DSSC's used in outdoor conditions²¹. The degradation is caused by crystallization of the iodide salt. Currently, research is being done on solid state electrolytes to prevent degradation and leakage complications. Polymer matrix electrolytes offer fewer leakage problems, but still have degradation issues as well as low efficiency because of their slow ionic conductivity⁴¹⁻⁴³. Nanocomposite gel electrolytes illustrate an effective manner of mixing the solid state with the liquid electrolyte. A matrix composed of an inorganic material, such as silica, is produced and then the inner pores contain the organic that is the active ionic conductor⁴⁴. This organic can be optimized for speed of ionic conductivity, but percolation conditions are necessary to allow for greatest conductivity. In this way, the liquid is more stable because there is less

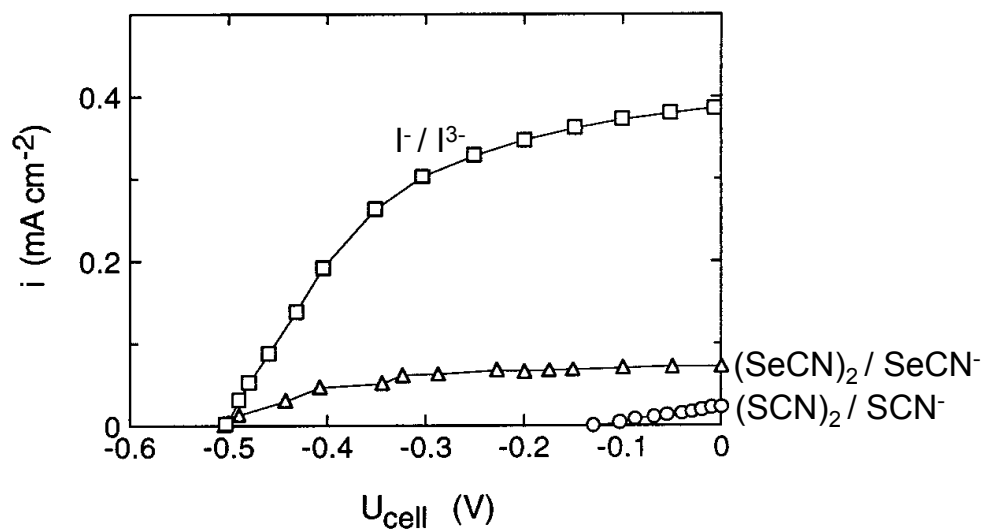


Figure 2.1.6. Changing the redox couple in the electrolyte is shown to have a drastic effect on the photocurrent generated⁴⁰.

chance of environmental degradation and the inorganic actually acts as a sealant as well. Electrolytes will continue to change as the DSSC's evolve, and it appears that the polymer composite matrices will be utilized in the commercial products.

2.1.2: Electrical Characteristics

Solar cells are characterized by a number of factors, most generated from the current versus voltage (IV) curve generated by measuring the current in the cell across a range of voltages. Figure 2.1.7 illustrates an IV curve for a high efficiency cell made by the Grätzel group. The efficiency number (η) is generated from equation (1) and is used to characterize what percentage of photons is converted into electrical energy.

$$\eta = PP / (I_s * A) \quad (1)$$

PP is the peak power generated in the cell, labeled " P_{\max} " in Figure 2.1.7, I_s is the intensity of illumination, usually corresponding to 1000W/m^2 for the AM1.5 solar spectrum, and A is the active area of the cell. The peak power is simply the peak voltage multiplied by the peak current, which are usually near 0.6V and 12mA per 1cm^2 for high efficiency cells. The fill factor (FF) demonstrates how much of the possible power is being generated, and is used often to quantify solar cells. Equation (2) illustrates how this is calculated based upon the peak power and the open circuit voltage times the short circuit current which is the theoretical maximum power that could be generated by the cell if fewer losses occurred.

$$FF = PP / (V_{oc} * I_{sc}) \quad (2)$$

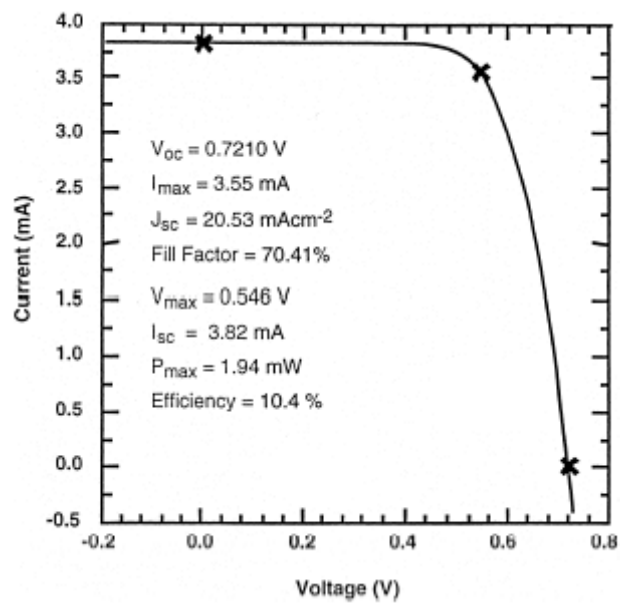


Figure 2.1.7. IV curve for a 10.4% cell by the Gratzel group illustrating characteristics of a solar cell, including open circuit voltage and short circuit current³⁴.

Finally, the incident photon to current efficiency (IPCE) is another comparison factor used, usually to quantify dye absorption and charge transfer. The IPCE is an experimental measurement that provides the current generated at various wavelengths. With the amount of photons incident on the solar cell at each wavelength known, the efficiency of current generation at each wavelength is calculated, as in equation 3¹⁸. Figure 2.1.5 illustrates an IPCE curve comparison for two dyes, N3 and black dye.

$$\text{IPCE} = (1250 * i_{\text{ph}}) / (\lambda * I_s) \quad (3)$$

The overall efficiency of the cell is increased by optimizing the titanium dioxide electrode and rapid electron transfer, and also simple design parameters of the cell such as thickness of the semiconductor layer, electrolyte properties, sheet resistance of the TCO, and other characteristics that may cause increased resistance⁴⁵. In this research, nanotubes or nanorods will be used to increase electron transfer through the titania and maximize surface area based on geometrical constraints to increase the efficiency of the cell.

The interface between the sensitizer and the semiconductor is important because it affects the electron injection into the semiconductor and should be optimized to lower recombination losses. The surface density of the dye monolayer, the bonding configuration between the two layers, and the coherence of the semiconductor with the dye monolayer are all very important aspects of this interface.

The dye is attached to the titania via chemical bonding between the titanium atoms and the carboxylate ligands on the sensitizer. Other groups that can be used as the bonding ligands include phosphonates or hydroxamates. Two of the carboxylate groups are attached to the titanium atoms via a bidentate configuration on the surface faces of the

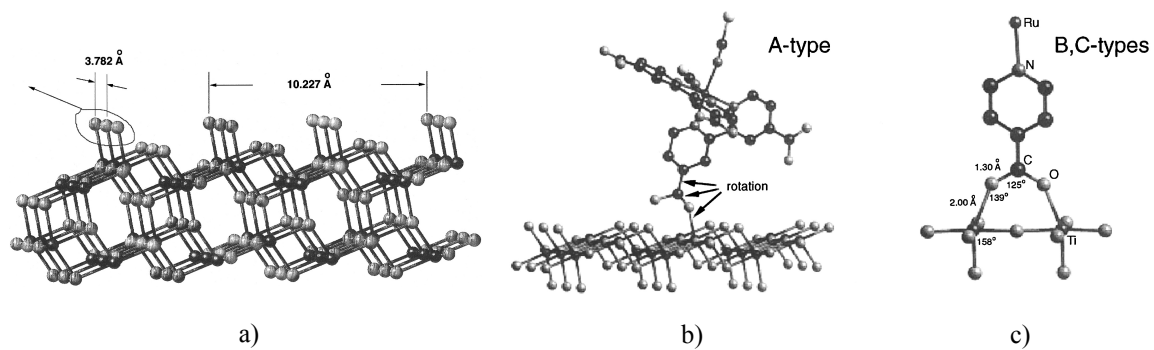


Figure 2.1.8. a) Anatase (101) surface. Cleaves to leave mostly Ti atoms that are open for bonding with carboxylate ligands of the sensitizer. b) Initial bond by only one Ti – O – C group c) bidentate bridging with 2 Ti – O – C bonds.⁴⁶

titanium dioxide, which are predominantly (101). Figure 2.1.8 portrays both the most likely bonds between the dye and the titania as well as the (101) face. Other configurations have been studied and modeled, but the bidentate configuration is the most likely because of its low energy and the molecule is already sterically in place for this configuration⁴⁶.

The dye molecules can act as a steric or electrostatic hindrance to a dense monolayer, which will decrease light absorption. Depending on the face of the titanium dioxide, the dye molecules may be more or less likely to attach in an organized manner. The optimization of the dense monolayer of dye molecules that allow for rapid electron injection into the semiconductor is more difficult than originally thought. Spherical titania particles have an average of different faces across them, so the dye bonding is not optimized. However, knowledge of the dye bonding on individual planes of the titania will allow for a more uniform dye-titania interface.

2.2: Hydrothermal Growth of Nanostructures in Solution

The first stage of the hydrothermal research project aimed to produce high aspect ratio titanium dioxide nanoparticles, such as nanotubes or nanofibers, for direct application in a dye sensitized solar cell (DSSC). The desired properties of the titania nanostructures include high conductivity, which translates to few defects, and high surface area for increased dye adsorption. The nanostructure with the highest surface area is a nanotube with a diameter just large enough for dye molecules, with about 2nm diameter, and electrolyte to pass through. These types of structures have been produced by a variety of different routes including anodization,⁴⁷⁻⁵² templating⁵³⁻⁵⁷, and

solvothermal^{58,59} or hydrothermal growth⁶⁰⁻⁶⁴ processes. Anodization and templating are both processes that produce nanotubes or nanorods on a substrate with compositional regularity; however, these are batch processes that can be expensive to commercialize. The advantages of the hydrothermal growth method include low temperature processing and ease of commercialization. The reaction system can also be easily modified for nanostructure design variability and for production in solution or on a substrate. Unlike the anodization and templating procedures, the product of the hydrothermal reactions is not anatase titania, but a sodium titanate that needs post processing. Hydrothermal methods were chosen over the other options despite their compositional variations for the ability to choose the nanotube morphology based on the reaction design, for possible production on flexible substrates, and because it is a low cost, low temperature reaction system.

2.2.1: Morphology

The first hydrothermal reaction producing sodium titanate was completed in 1961 by Andersson, et al who demonstrated that the combination of sodium carbonate and titania can form sodium titanate of the phase, $\text{Na}_2\text{Ti}_3\text{O}_7$ ⁶⁵. In their case, the morphology was not taken into account in the study. Kasuga, et al worked with a similar reaction system in 1998, and found that hydrothermal treatment of sodium hydroxide and anatase titania nanoparticles form titania nanotubes, after a hydrochloric acid post treatment step is applied^{61,66,67}. Debate in the literature has contested many of Kasuga's conclusions, including whether the final product is anatase and when during the reaction the nanotubes form. This appears to be due to the large variation in possible reaction conditions. There

are many variables in this reaction system, including not only the concentration of sodium hydroxide (NaOH) and the ratio of NaOH to titania in the hydrothermal step, but also the type of acid used, its concentration and the pH of the final solution in the post treatment process. Each research group in the literature has a slight variation on the reaction system. It has been proposed that even slight differences in the duration and temperature of the hydrothermal system causes the product to be fully formed nanotubes or layered intermediate structures⁶⁸. By comparing the reactions done by different research groups, some patterns are found in this system; however, determining conclusively what makes nanotubes form over nanosheets and which phase of sodium titanate is formed is still elusive. It is recognized by most researchers that the initial product, after the hydrothermal reaction, consists of sodium titanate. Then, the acid washing converts the sodium titanate to a hydrogen titanate, and upon heating, the hydrogen is removed and titania is formed. However, whether nanotubes form during the hydrothermal reaction or in the acid wash appears dependent upon the reaction conditions.

Although the products are very dependent on the experimental conditions, it has been found that open ended, multiwalled nanotubes with diameters in the range of 5-9nm can generally form after the hydrothermal reaction of 10M sodium hydroxide with titanium dioxide at temperatures between 130 - 170°C unless reaction time or concentration of TiO_2 to NaOH differs greatly^{60,69-74}. Besides the nanotubes, intermediate species of nanosheets, nanowires and nanoplates, which are mostly amorphous, can also be found^{74,75}. The interlayer spacing between the walls of the

Table 2.2.1: Review of Hydrothermal Reactions in the Literature

	Thorne	Tsai and Teng 2006	Tsai and Teng 2006	Bavykin	Chen Adv Mat 2002	Ferreira	Weng, 2006, J Eur Cer Soc	Yao, APL, 2003	Yuan, Coll and Surf, 2004	Kasuga, Adv Mat, 1999
Amt (g)	8g	2	2	0.75	unk	2	1		0.1-0.3g	12.5
Type/Size particles	rutile/200nm	P25	P25	anatase	anatase/80-200nm	anatase	anatase-rutile mix/20nm	pretreated anatase	P25	rutile/20nm
Conc NaOH (M)	10M	10	10	10	10	10	10	10	10	10
Amt NaOH (mL)	20	70	70	300	130	60	10	150	20	100
Temp (°C)	150	130	130	120	130	170	110	150	150	110
Time (hrs)	72.00	24	24	22	72	170	24	12	24	20
Acid type	HCl	HCl	HCl	H2SO4		HCl; til pH=3-4	HCl	HNO3	HCl	HCl
Amt	1L	1L	1L						until pH<7	150mL
Conc (M)	0.1M	pH = 0.38	pH = 1.6	0.05		0.1	pH = 3	0.1	0.1	0.1
Water rinse	water wash first at 50C, then acid wash			before acid rinse vacuum 50C	no acid wash	DIW til pH=11; then acid wash 50C, 24hrs		rinsed after acid		before and after acid wash
Drying	none	100C, 3hrs	100C, 3hrs		monoclinic H2Ti3O7 - no Na	Na2Ti3O7; Na/Ti = 0.67	80C		60C	
Prod before acid wash	Na2Ti3O7 - some crystallinity			unk				anatase w/ new peaks in Raman due to structural chgs		amorphous
Prod after acid	H2Ti3O7 - no peaks in xrd	anatase	H2Ti2O5*H2O + anatase	H2Ti3O7 or Na2Ti2O4(OH)2		Na2-xHxTi3O7*H2O; Na/Ti = 0.20	H2Ti3O7	anatase w/ new peaks in Raman due to structural chgs SAED- (101) and (200) seen	H2Ti3O7	anatase, some rutile
Composition Charact.				XRD	EDX, EELS	EDS	XRD - few peaks		XRD, Raman	
Morphology, before acid		NOT nanotubes	NOT nanotubes	unk	nanotubes 9nm in diamter, 100nm long	multiwalled, open ended nanotubes, 5nm inner diam, 9nm outer diam	8nm nanotubes			large, thin plates with holes 200-300nm diam; poor crystallinity
Morphology after acid	open ended nanotubes; 7 walls one side, 8 on the other	small coagulated particles	nanotubes w/ defects	2-20nm inner diamter, nanotubes, open ended; few nanosheets in samples		multiwalled, open ended nanotubes, 5nm inner diam, 9nm outer diam	8nm nanotubes	10nm wide, 100/5nm long, open ended nanotubes	8-10nm diameter, 1-ended, 5-6nm inner diameter, crystalline nanotubes	crystalline nanotubes, 5-8nm in diameter

nanotubes ranges from 0.72nm to 0.78nm^{60,69-71,73}. The wall spacing increases with dehydration and extends to 0.9nm with drying⁷⁶. The formation of multiwalled nanotubes is independent of amount of anatase powder used as reactant^{73,75,76} and the size of the reactant particles⁷⁵, although there are some conflicting reports that the size of the reactant particle does affect the size of the nanotube^{77,78}. The reactant titania must be crystalline as amorphous titania forms only nanofibers⁷⁹. The reaction temperature is a very important variable as it ranges from 100-200°C, the size, shape, and surface area of the nanotubes is affected. From 120°C to 150°C, the average diameter of the nanotubes increases slightly as shown by the pore volume distribution⁶⁰. At temperatures above 170°C, non-nanotube but high aspect ratio structures tend to form, such as wide belts or thin nanofibers at 190°C^{60,78,80,81}. At lower temperatures, around 110°C, reactant nanoparticles can still be seen among the nanotubes showing lack of complete reaction^{78,81}, the product is less crystalline than that reacted at 150°C⁸² and the nanotubes are of a wider range of thicknesses from 10-30nm⁷⁸. It has also been shown that the thickness of the walls increases with reaction temperature⁸³. The surface area of the product is also dependent on temperature as it increases from 180m²/g at a reaction temperature of 100°C to 270m²/g at 150°C and then decreases to 205m²/g at 200°C⁷⁸. Other researchers have found similar patterns with a maximum surface area of 400m²/g at 130°C⁸⁴. The crystallinity of the nanotubes is not only dependent upon the temperature, but also on the reaction time and the filling fraction of the autoclave as the crystallinity of the nanotubes increases after ten days⁸⁵ and with high filling fractions, greater than 84%⁷³. The efficiency of the reaction grows with reaction time from 24-48 hours and with increased temperatures, up to 150°C such that a larger yield of nanotubes is

produced, but a change in their average size is not shown^{70,75}. At longer reaction times, nearer to 168 hrs, the dimensions of the nanotube structures do increase slightly^{82,86}. After ten days at 160-180°C, the titanates formed have a nanobelt structure⁸⁵. There is no change seen in the morphology of the structures when the sodium hydroxide concentration varies from 5-10M⁸¹. Although the size of the reactant particles does not scale the product size⁷⁰, smaller particles do cause the reaction to occur more rapidly⁸². The morphology of the product is not changed with a washing step, as it has been shown that washing with acetone, water or ethanol maintains the nanotube structure⁷⁰. Thermal treatments do affect the morphology as heating above 650°C causes nanorods to form, and above 800°C, only aggregated spherical particles remain^{69,73,79,84,86}.

The morphology characterization is generally done by transmission electron microscopy (TEM) and figure 2.2.1 portrays an image illustrating the morphology of structures immediately after the hydrothermal reaction as compared to those after acid washing. It is obvious that the nanotube morphology is enhanced by the acid wash stage; however, it is open to interpretation whether the non-acid washed structures are nanotubes or nanosheets⁸⁴. There are a fair number of researchers that agree with Kasuga, et al that the nanotubes only form after the acid washing process^{67,84,87}, and others that still conclude that they are produced in the hydrothermal bath^{82,86}. As most reactions that lead to non-nanotube structures before the acid wash occur at low temperatures, it is possible that the yield is simply so low in these cases that the small sample size seen in the TEM does not include any of the nanotubes. Then the washing with hydrochloric or nitric acid completes the reaction and a large yield of nanotubes is

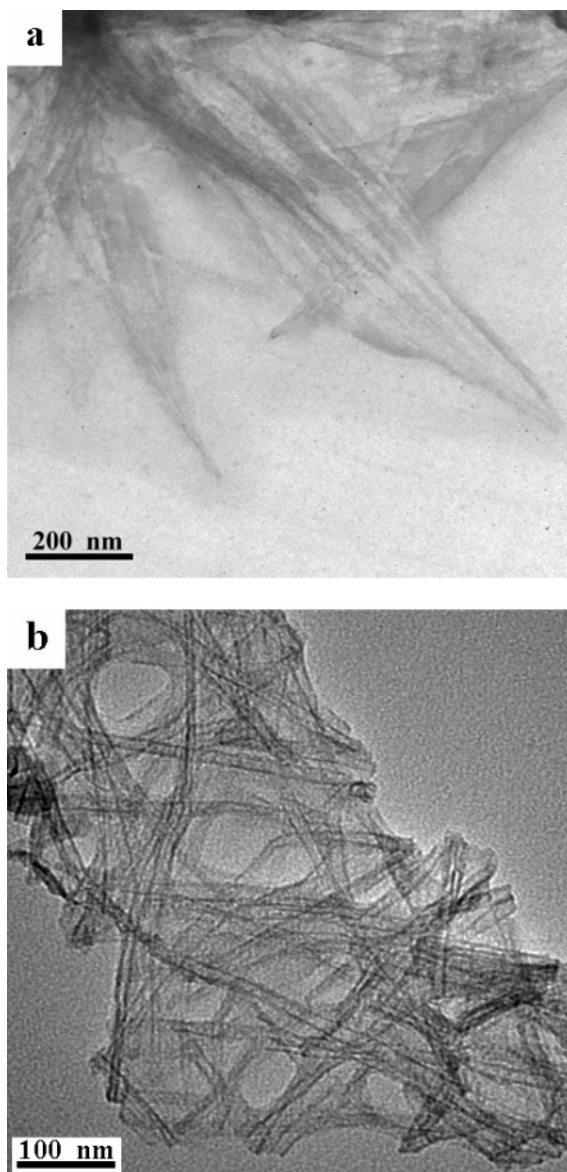


Figure 2.2.1. Whether nanotubes are formed in the sodium hydroxide hydrothermal reaction or only after the acid wash step is complete is an ongoing debate. Above, a) the nanostructures before acid washing and b) after acid washing are illustrated. It appears here that the acid wash merely enhances the nanotube formation and completes the scrolling of reactant sheets⁸⁴.

seen. Whether the nanotubes are completely formed or not, the acid treatment is still necessary to produce compositional changes, as will be discussed below, although it does cause some morphological changes. Studies have shown that the acid wash can increase the number of defects on the nanotubes⁷¹ or completely transform the product nanotubes to small particles when they are washed in HCl at a pH less than 1 or a concentration greater than 2M^{68,73}. The surface area of the nanotubes increases after the HCl wash from 160m²/g when rinsed in DIW to 185m²/g and 200m²/g when 0.1M and 0.5M HCl were used, respectively⁸². Nitric acid (HNO₃) has also been used in this process and may maintain the nanotube structure better than HCl as well-formed 8-12nm nanotubes have been seen after rinsing⁸¹.

2.2.2: Composition

It is reasonable that since different nanostructures can be formed depending upon the reaction conditions, a variety of phases can be produced during hydrothermal synthesis as well. Small changes in the conditions, i.e. reaction time, amount of TiO₂, or temperature, can cause a different major phase to be formed. Table 1 demonstrates the variety of phases found due to the numerous differences in the methods used throughout the literature. Characterization of the phase is most often by x-ray diffraction (XRD), energy dispersive spectroscopy (EDS) in the scanning electron microscope (SEM) and small angle electron diffraction (SAED) and electron energy loss spectroscopy (EELS) in the (TEM). Both XRD and SAED use small particles, x-rays and electrons, respectively, that hit the sample and deflect based on the unit cell structure, which creates a signal that can be interpreted to determine the composition. Both are only viable for crystalline

materials. EDS and EELS have a slightly different system where the results portray only the types of elements in the sample, and then the intensities can demonstrate composition. Some variations in the results occur as the nanotubes have such small diameters (5-9nm) that most characterization techniques used are at their limits of resolution so that it is difficult to distinguish between remaining reactant particles, intermediate sheets and nanotubes. The composition of the products that different research groups find is largely variable from seeing no sodium in the immediate product^{70,71} to seeing an Na/Ti ratio of 0.67 via EELS⁷². Those researchers that have found the hydrothermal product to be TiO_2 with minimal post treatment process tend to use incomplete characterization data^{78,84}. EELS and EDS were used, by separate groups, to demonstrate that the ratio of O:Ti is ~ 2 , although these characterization techniques do not demonstrate accurate composition analysis on their own^{73,88}. Raman data with peaks that are not identified was used to show that the nanotubes are titania that has a different structure from the anatase form⁸³. Thorne, et al found, by EDS analysis, that a single nanotube has a complete lack of sodium while the bulk sample contains large amounts. This is most likely due to lower ratios of sodium in the nanotube which do not appear as a readable peak⁸⁹, again demonstrating that more than one technique should be used for characterization of the nanotube composition. Different phases of sodium titanate appear to form concurrently in the same reaction, as when four nanotubes were characterized, again with EELS, and the Ti:O ratio across them varied by 20%⁶⁹. Interpreting the results from the characterization techniques can also cause confusion as there are especially narrow differences in peak position between $\text{Na}_2\text{Ti}_3\text{O}_7$, $\text{H}_2\text{Ti}_3\text{O}_7$ and $\text{Na}_2\text{Ti}_2\text{O}_4(\text{OH})_2$ in the XRD results⁶⁰, which comprise the compositions that are most often reported as products. The

complexity of reading the characterization results is also shown in figure 2.2.2, where image a) portrays clear XRD data from the hydrothermal product after drying to 120°C while image b) demonstrates a more commonly found spectrum taken directly after hydrothermal growth. Increased drying temperature may also lead to XRD patterns that show different compositions as the sodium titanate crystallizes⁷³. These images illustrate the difficulty in determining the original hydrothermal product, as the clear data has water removed and so hydration levels are unknown.

Some phases that have been suggested for the hydrothermal reaction product include specific compositions of $\text{Na}_2\text{Ti}_n\text{O}_{2n+1}$ ($n = 3$ or 4)⁶⁹ or $\text{Na}_{2-x}\text{H}_x\text{Ti}_2\text{O}_4(\text{OH})_2$ ($0 < x < 2$)⁹⁰. $\text{Na}_2\text{Ti}_4\text{O}_9$ was reported after a reaction time of 10 days and rinsing with distilled deionized water and was then seen to transform to $\text{Na}_2\text{Ti}_3\text{O}_7$ and $\text{Na}_2\text{Ti}_6\text{O}_{13}$ after heating above 900°C⁸⁵. $\text{Na}_2\text{Ti}_6\text{O}_{13}$ tends to be found upon heating to temperatures in the range of 500-600°C. The most commonly proposed composition is $\text{Na}_2\text{Ti}_3\text{O}_7$ that then transforms to $\text{H}_2\text{Ti}_3\text{O}_7$ after proton exchange in the acid wash^{71,72,91}. Hydrated phases of $\text{H}_2\text{Ti}_3\text{O}_7$ ⁹² and $\text{H}_2\text{Ti}_4\text{O}_9$ ⁸² have also been suggested as the level of hydration is dependent on the drying temperature used⁹². The effect of the acid wash on composition is simply to exchange protons for sodium cations. This proton exchange reaction is reversible as shown by the conversion from $\text{Na}_2\text{Ti}_2\text{O}_5$ to $\text{H}_2\text{Ti}_2\text{O}_5$ ⁶⁸ and back. Nitric acid (HNO_3) produces the same exchange reaction as HCl after a 10hr rinse at room temperature⁹². Most researchers tend to use dilute HCl, commonly 0.1M, as this was used by Kasuga et al, even though the reaction does not always go to completion as EDS has shown a 0.20 ratio of Na:Ti after the acid wash^{72,73}. The need for the dilute concentration is supported by the findings of Tsai and Teng who showed that washing with a solution with $\text{pH} < 1$

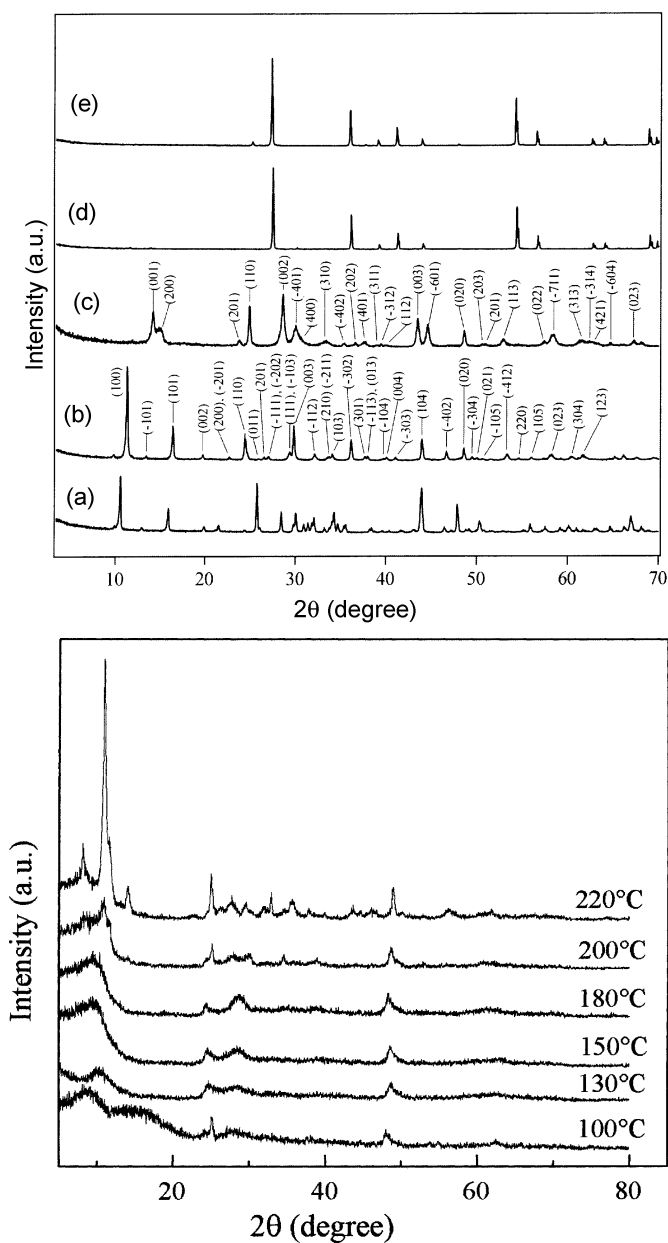


Figure 2.2.2. i) Clear XRD patterns are demonstrated after products are dried to 120°C for one hour. XRD patterns portray a) $\text{Na}_2\text{Ti}_3\text{O}_7$, b) $\text{H}_2\text{Ti}_3\text{O}_7$, c) $\text{TiO}_2(\text{B})$, d) product heated to 900°C becomes TiO_2 , and e) commercial rutile TiO_2 ⁹². ii) XRD patterns resulting from different hydrothermal reaction temperature conditions from 100°C to 220°C in 10M NaOH for 24hrs⁷⁹. The low intensity and broad peaks are most likely due to water in the products.

leads to titania formation but nanotube breakdown. In most cases no sodium is found in either EELS or EDS demonstrating a completely washed product⁸⁷. Although rarely mentioned outright in the literature, the completeness of the washing step is most likely due to the number of washes that were done and would be dependent on the final pH of the product solution^{76,89}. Some compositions are suggested that include both sodium and hydrogen ions, demonstrating the equilibrium concentration may not be a completed wash.

One suggested composition that has been seen in the XRD characterization is lepidocite, $H_xTi_{2-x/4}\square_{x/4}O_4$ ($x \sim 0.7$, \square =vacancy)⁸⁷. This group, Ma et al, compares this structure to that of hydrogen trititanate, the more common compositional product by looking closely at the XRD. As evidence of lepidocite, they contend that the 001 peak that is often claimed as proof of $H_2Ti_3O_7$ should not be taken as such without a strong 200 peak, which is not found. The common interwall spacing of 0.78nm can be ascribed to 0.8nm if dehydration is taken into account, and this matches well with the d_{020} spacing of lepidocite⁸⁷. Using thermal gravimetric analysis (TGA), Ma's group was able to demonstrate that the product dehydrates rapidly, as lepidocite would do since it is more difficult to remove protons from $H_2Ti_3O_7$. In the bulk, $H_2Ti_3O_7$ transforms to $TiO_2(B)$ at 350°C,⁹² but the hydrothermal product formed by Ma et al produces anatase when heated, as lepidocite should⁸⁷.

$H_2Ti_3O_7$ is the most commonly found composition and appears to be found at a variety of temperatures in the 130-150°C range. Many XRD patterns demonstrate that this composition clearly exists after acid washing^{69,79,89}, and some have shown that it can be formed by simple washing with distilled deionized water⁷⁶. The nanotubes, when

heated to 800°C, do form $\text{TiO}_2(\text{B})$ rather than anatase which confirms the $\text{H}_2\text{Ti}_3\text{O}_7$ composition⁷⁴. Infrared spectroscopy illustrates large amounts of OH bonds which suggest the hydrogen trititanate rather than titania⁷⁹. Further discussion into the reaction will assume the product of the hydrothermal growth and acid wash is $\text{H}_2\text{Ti}_3\text{O}_7$, unless otherwise stated.

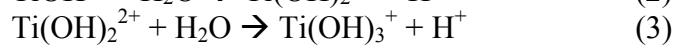
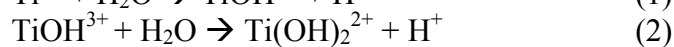
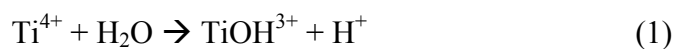
Further transformations in composition can occur by heating or by changing the acid washing method. These are less researched, but demonstrate some interesting possibilities. Stirring bulk $\text{Na}_2\text{Ti}_3\text{O}_7$ in 3M HNO_3 for six days can form small rutile nanorods⁹². Two accounts demonstrate that if the original hydrothermally grown nanotubes are washed in dilute nitric acid, and then hydrothermally reacted a second time in nitric acid, anatase nanorods are formed^{62,76}.

2.2.3: Mechanism and Structure

It is important to understand how the final product is formed in order to be able to better design the experiment for specific product properties. Similar to the morphology and composition, the mechanism of the reaction between titanium dioxide and sodium hydroxide in a hydrothermal solution is difficult to understand and has caused much debate in the literature. Determining the mechanism of growth is complicated, as one must compare the composition and morphology of the original reactants, the intermediates and the products, which will imply how the reaction occurs. The first step in determining this particular mechanism is to establish how the titanium dioxide reacts with the sodium hydroxide, whether the outer edge of the spherical nanoparticles grows

in a specific direction or if these nanoparticles dissolve in solution and then re-precipitate as the product.

The dissolution of titanium dioxide in an aqueous medium and the effects of pH and temperature have been studied to demonstrate that this mechanism is feasible. The solubility of rutile titania is shown to increase dramatically with pH when experimentally tested and through theoretical calculations^{93,94}. Figure 2.2.3a illustrates a plot of the changes in titanium concentration with pH. However, it is apparent that even at high pH, titanium has a very low solubility in aqueous media, on the order of 0.00001m at 150°C⁹³. The reactions that lead to the solubility of titania in solution are the following:



As the pH of the solution increases, the species convert from Ti(OH)_2^{2+} to Ti(OH)_3^+ , and finally to Ti(OH)_4 in alkaline solutions⁹⁴⁻⁹⁶. The solubility of titanium also increases with increasing temperature, as shown in figure 2.2.3b. It is important to note that the solubility of TiO_2 at high pH and increased temperatures remains low, but that the species that is found in solution in the hydrothermal reaction system is Ti(OH)_4 .

Although some report that the reactant particle size affects the nanotube morphology^{77,78}, which would present evidence for a seed crystal growth mechanism, the solution/re-precipitation method has a stronger basis as it has been shown more reliably that different sizes of titania particles used as the reactant do not lead to variations in the size of nanotubes⁷⁰. Next, it is important to recognize the intermediate structures that form in this process. A variety of authors have illustrated that layered titanates form originally in the hydrothermal reaction conditions, and then these sheets react in some

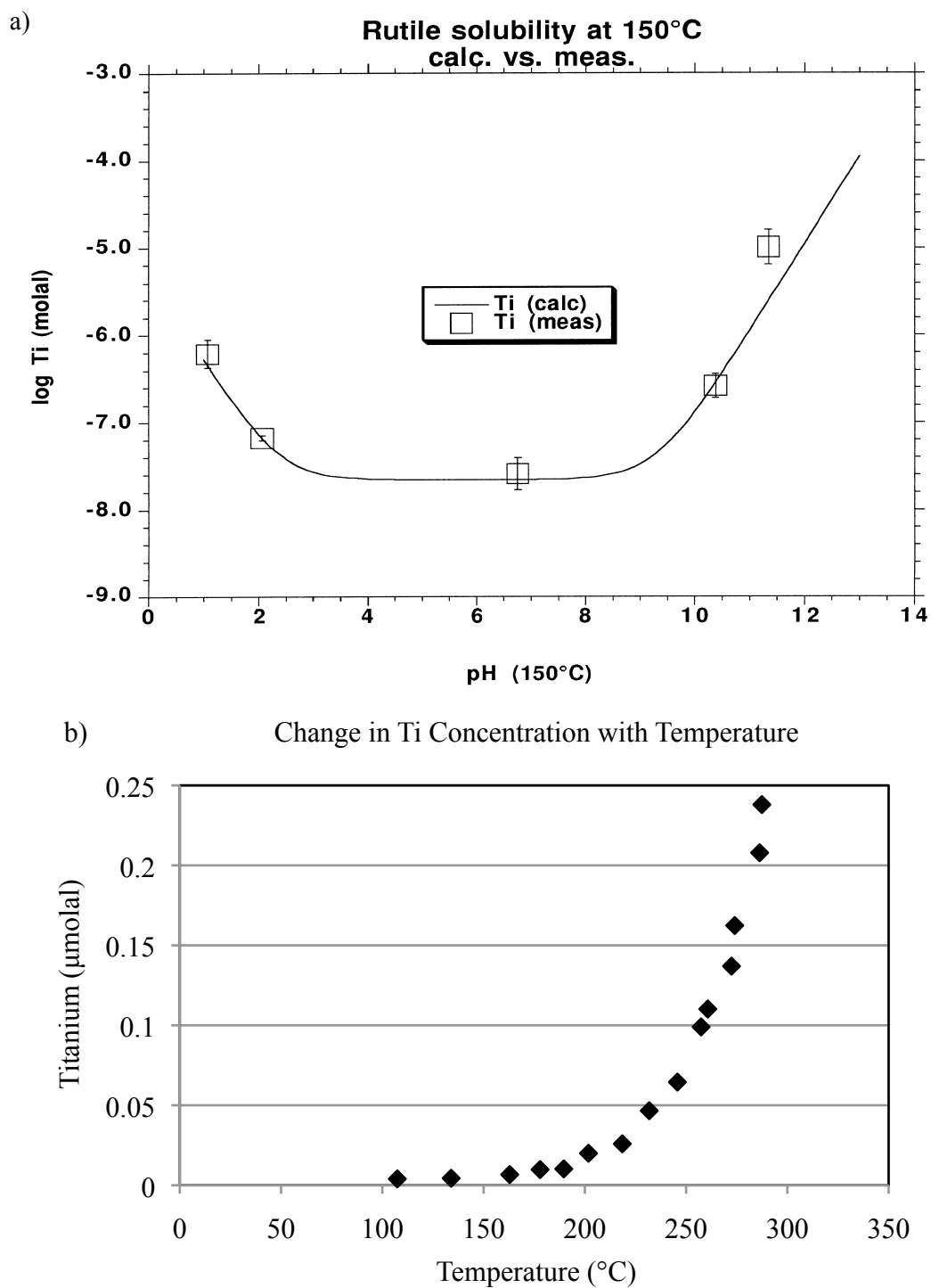


Figure 2.2.3. The above plots illustrate the effect of a) pH⁹³ and b) temperature⁹⁵ (at pH =11) on the concentration of Ti⁴⁺ in aqueous solution.

way to form nanotubes^{66,70,82,97}. Chen, et al formed nanotubes from the reaction of titanium dioxide in 10M sodium hydroxide at 130°C for 72 hours and figure 2.2.4 illustrates the layered sheets that formed as a byproduct of the nanotubes. Zhang, et al stopped the reaction every two hours to determine the intermediate structures which were first highly disorganized sheets that then crystallized into $\text{H}_2\text{Ti}_3\text{O}_7$ ⁶⁴. These sheets are formed by edge-sharing TiO_6 octahedra⁸⁶. It is a feasible mechanism that the layered sheets form first, and then form nanotubes since alkali metal reactions in general often produce layered lepidocite sheets that can be phase transformed to titania after acid washing⁹⁸. It is suggested that the Ti- O-Ti bonds of titania break above 120°C causing the sheets to form due to electrostatic repulsion among the sodium cations^{83,84}. It is under debate whether the sheets are $\text{Na}_2\text{Ti}_3\text{O}_7$ or $\text{H}_2\text{Ti}_3\text{O}_7$, but the second appears more likely as computer simulations were done demonstrating that hydrogen deficiencies on the surface are a driving force for the curving of the layers⁶⁴. Zhang, et al also found that the sodium ions are weakly bound to the surface, so it is feasible that nanotubes do not have sodium cations in their unit cell structure. The formation of the nanotubes from sheets can occur by either scrolling, when one single layer sheet wraps from one end to the other, or by creating a seam at one point on the nanotube as both sides of the sheet curve up towards each other and meet⁶⁰. The transformation from layered sheets to nanotubes and back again is reversible by acid or alkali addition⁶⁸. Evidence used for the scrolling mechanism has included a variation in the number of walls on opposite sides of the same tube⁸³, *ab initio* calculations that demonstrate an asymmetrical chemical environment⁶⁴ and TEM studies^{69,70,87,99}. Figure 2.2.5 from Bavykin, et al demonstrates a schematic of the different nanotube formation possibilities. Figure 2.2.6b is a TEM image of the end

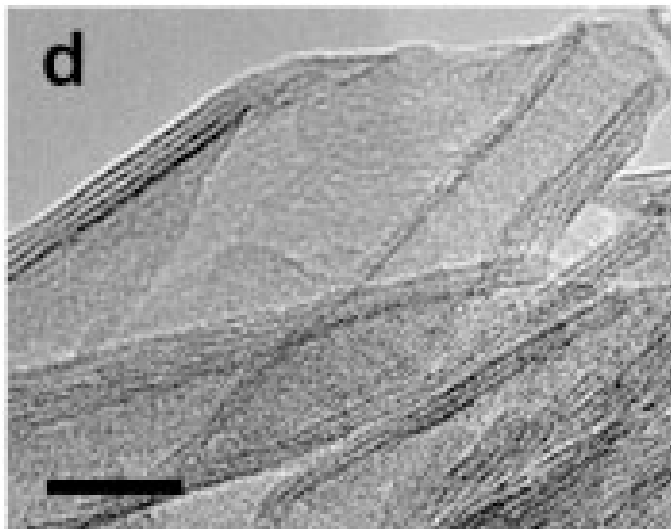


Figure 2.2.4. TEM image demonstrating layered sheets found either as a byproduct of the hydrothermal reaction⁷⁰.

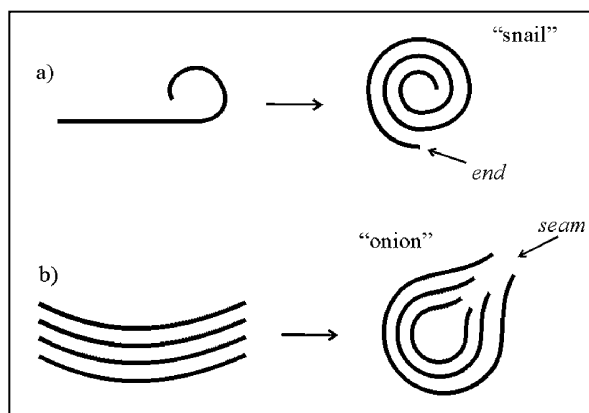


Figure 2.2.5. Bavykin, et al discusses a variety of ways that nanotubes might form from layered sheets of titanate. This schematic shows two such methods, a) scrolling of 1 sheet into a multi-walled nanotube and b) rolling up of numerous sheets so that a seam forms.

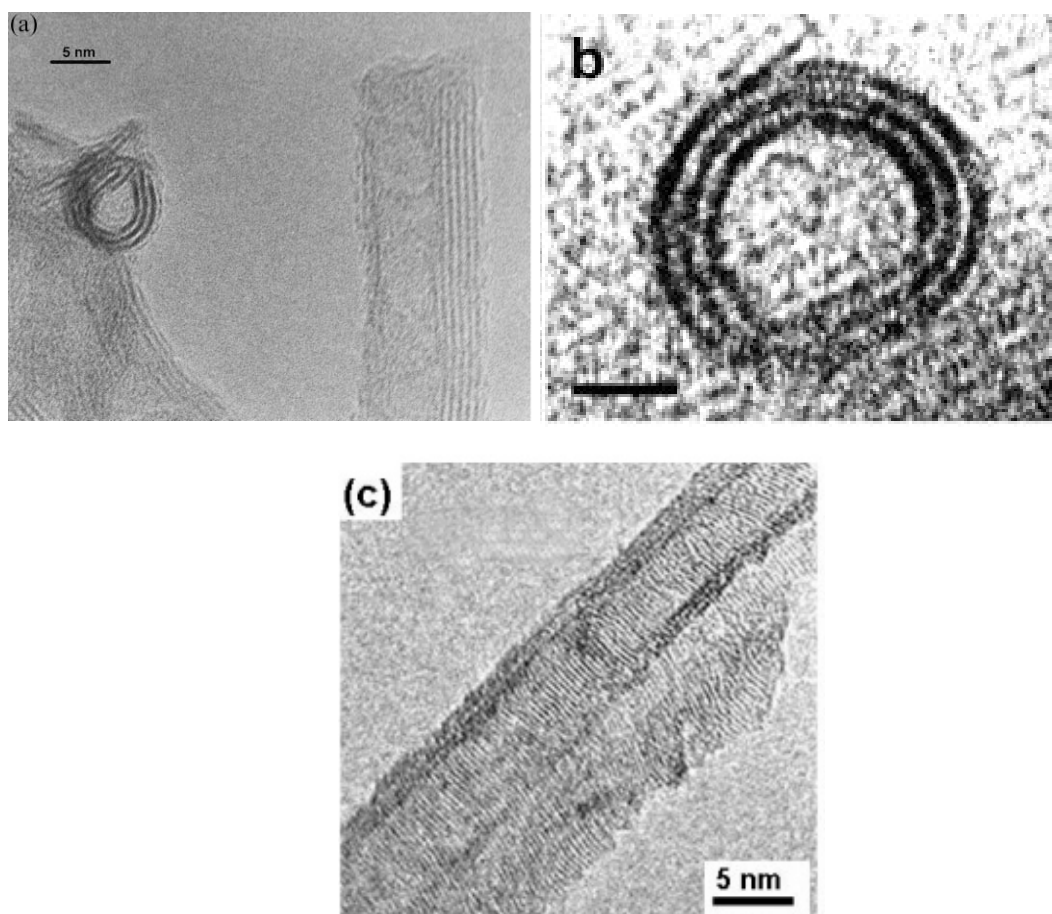


Figure 2.2.6. TEM analysis of nanotubes demonstrates the difficulty of determining the growth mechanism. Image a) illustrates a conjoined nanotube or “onion” formation⁶⁰ while b) and c) show the scrolling of nanotubes perpendicular to its length⁶⁹ and on axis⁸⁹, respectively.

of a nanotube that appears to be scrolled from one single titanate sheet⁷⁰ and figure 2.2.6c portrays a nanotube that is in process of rolling up⁸⁹. An image of an unfinished seam apparently formed from the conjoining of edges of multilayered sheets is seen in figure 2.2.6a, also from Bavykin et al who discuss the driving force for this type of growth as asymmetry due to preferential doping of the layered sheets and differences in surface energy⁶⁰. Similarly, scrolling is governed by surface tension and must occur very rapidly according to computer simulations that have been done⁶⁴. That both of these methods can be illustrated in a transmission electron micrograph evidences the difficulty of determining which method is correct. The suggested composition of the nanosheets is Na_2TiO_3 ⁶⁰.

In an effort to determine the reaction process, some groups have attempted to use different hydroxide solutions, including potassium hydroxide and lithium hydroxide, but neither produced a similar morphology. The KOH led to nanorods and nanoplates and the LiOH simply produced nanoparticles; however, both products showed greater crystallinity than that seen in the reactions with NaOH⁷⁰. Unlike Chen et al, Nakahira et al found that KOH can produce nanofibers in the same manner as NaOH⁸². The reaction time for the second group was lower, 110°C in comparison to 130°C, which could have caused some effect, but this does illustrate it is possible to grow high aspect ratio nanostructures in KOH although they are of a slightly different phase than that grown in NaOH. Therefore, it questions whether the Na^+ cation is necessary to the reaction. If a similar reaction is run in distilled deionized water, with no base or acid additives, with 5nm anatase particles, the particles coarsen and produce faceted structures due to differences in growth rates in the [001] and [101] directions¹⁰⁰. If 1.5g TiO_2 is

hydrothermally reacted with 4-10M KOH at 160-180C for 48hrs, well formed nanobelts of pure, monoclinic $K_2Ti_8O_{17}$ form reproducibly⁸⁵.

Once both the composition and mechanism have been proposed with some certainty, the structure of the nanotube and its unit cell can be determined. As previously discussed, the nanotubes are reported to form from the wrapping of multilayered nanosheets. These sheets have been proposed to be layers of titanate, $Ti_3O_7^{2-}$ with the sodium cation in an interlamellar position^{69,89}. Then, the acid washing simply exchanges the sodium cation with the proton. Further evidence for this type of structure, rather than having the cations situated inside each layer, is found in fourier transform infrared spectroscopy (FTIR) where the greatest effect of proton exchange is found in the cation bonds⁷². The structure of $H_2Ti_3O_7$ includes corrugated ribbons of edge sharing TiO_6 octahedra where each ribbon is three octahedral wide which join at the corners to produce sheets⁸⁷. Not only $H_2Ti_3O_7$, but the whole family of $A_2Ti_nO_{2n+1}$ is known for having layered and/or tunnel shaped structures⁹². The nanotubes are highly symmetric and achiral, as most have a [010] directed axis, characterized by high resolution TEM (HRTEM)⁶⁴.

2.3: Hydrothermal Growth on Substrates

When titanium metal is a reactant in the sodium hydroxide hydrothermal treatment instead of titanium dioxide nanoparticles, coatings of nanowires and nanotubes are produced, depending on the reaction conditions. Titanium metal enters the reaction with a passivation layer of TiO_2 because of its rapid oxidation in air¹⁰¹. Although not a highly reactive metal, titanium has been shown to react with hydrogen peroxide, forming

an amorphous titania gel^{102,103} layer or producing a meshlike morphology¹⁰⁴. In the presence of sodium hydroxide, an alkali titanate layer is formed on the titanium¹⁰².

Biomedical research has looked at growing sodium titanate through this hydrothermal process as a method to improve the attachment of simulated body fluid to titanium^{105,106}. In these cases, the morphology of the film is often ignored because it is the effect of the coating that is important; however, it has been reported that an amorphous, hydrated titania layer forms on titanium in alkali solution during heating although annealing temperatures of up to 600°C are necessary for the film to crystallize¹⁰⁷.

The morphology of the hydrothermally grown films depends on certain reaction conditions, and the effects are often similar to those of the hydrothermal solution growth process. After 20 hours at 160°C, 20µm coatings of titanate nanotubes were produced via the reaction of titanium metal in 10M NaOH on plates, wires and other geometries of titanium¹⁰⁸. Lower temperatures, such as 140°C, produce a net-like morphology¹⁰⁹ or an array of nanobelts¹¹⁰. At higher temperatures, the thickness of the nanotube layer increases from ~400nm up to 5µm at 200°C¹⁰⁹ and nanowires form at 180°C for 4 hours with 70-80nm widths instead of nanotube formation. Incomplete formation of the nanotubes also occurs at low concentrations of NaOH, such as 5M, leading to production of belts or sheets⁹¹. The size of the nanostructures increases directly with the NaOH concentration, and at longer times, oriented growth begins to occur⁹¹. Wang et al suggest a mechanism for how the nanobelts/sheets convert to nanowires when the hydrothermal reaction system is run at higher temperatures. Their research utilized HRTEM and found that the nanobelts had a large number of defects, which caused large strains as they grew longer. Finally, the strain is high enough that the nanobelts are suppressed and multilayer

nanowires form¹¹⁰. When KOH is used in place of NaOH, at 150°C for 24 hours, high aspect ratio nanostructures are formed on the titanium similar to those produced by NaOH¹¹¹.

Reported phases of sodium titanate formed are similar to those reported for the solution hydrothermal growth system, including $\text{Na}_2\text{Ti}_6\text{O}_{13}$ and $\text{Na}_2\text{Ti}_3\text{O}_7$, among others⁸. It has also been suggested that there may be more than one sodium titanate phase present in the final coatings⁶. Characterization with XRD and SAED illustrates that the final coatings are actually $\text{H}_2\text{Ti}_5\text{O}_{11} \cdot \text{H}_2\text{O}$, after proton exchange, based on the (200) peak at 11.8° ¹¹⁰. $\text{K}_2\text{Ti}_6\text{O}_{13}$ was reported with the use of KOH instead of NaOH in the hydrothermal treatment¹¹¹.

Acid washing with 0.1M HNO_3 converts the sodium titanate to phase pure anatase titania with no damage to the nanotube products¹⁰⁹. The acid wash treatment causes proton exchange to occur, but in some cases also causes the film to detach from the titanium metal surface¹¹⁰. Annealing at 300-550°C for 2 hours leads to conversion of the hydrogen titanate to anatase titania¹¹⁰.

If the titanium metal is pre-treated by coating it with a dilute layer of titania nanoparticles, the morphology remains similar but the composition is slightly different. An oriented film of titania nanotubes has been reportedly produced by reacting the pre-coated titanium metal with 10M NaOH at 150°C for 6-10 hours⁶³. At reaction times of less than 6 hours, sheets which have not yet wrapped into nanotubes are seen amongst the nanotube product. It is suggested that the nanotube product in this case is $\text{H}_2\text{Ti}_3\text{O}_7$. Using HRTEM, Tian et al report that the tubes have an outer diameter of 12nm, an inner diameter of 3.7nm, and an interlayer spacing of 0.78nm⁶³. An array of vertically aligned

columnar structures with 60nm width was reported after the growth of pre-coated titanium metal in 10M NaOH at 150-170°C for 20 hours¹¹². The surface area of this structure was measured at $35 \pm 10 \text{ m}^2/\text{g}$, lower than the $55 \text{ m}^2/\text{g}$ of P25. With only a DIW wash and then annealing to 450°C for 5 hours, the final product was TiO₂ as characterized by XRD¹¹².

2.4: Use of High Aspect Ratio Titania In Dye Sensitized Solar Cells

High aspect ratio nanostructures, such as nanorods or nanotubes, are becoming popular as a likely way to increase the efficiency of DSSC's. The hypothesis for the increased efficiency is based on the nanostructures increasing the speed of electron transfer through the titania film, increasing light scattering and possibly increasing the surface area and dye adsorption¹¹³⁻¹¹⁶. Titania nanoparticle films have an electron diffusion coefficient that is more than two times less than that in bulk single crystal titania¹¹⁵, and the hope is that this can be increased greatly by designing a better titania film microstructure.

The microstructures that have been designed so far fall into three categories: amorphous nanowires, composite films of nanorods and spherical nanoparticles, and aligned nanotube arrays. The high aspect ratio structures were produced in many different ways including the hydrothermal treatment discussed above¹¹⁷⁻¹¹⁹, oriented attachment¹¹³, using anodic alumina membranes¹²⁰ or by anodization^{116,121}. Table 2.4.1 demonstrates some examples of the solar cell characteristics with each type of microstructure. In general, both the amorphous nanorods and the composite microstructures have good efficiency, in the range of 7%, while the aligned nanotube

Table 2.4.1: Characteristics of High Aspect Ratio DSSC's

	Titania NR's ¹¹⁹	Titania NR's ¹¹⁴	20wt% NR Composite ¹¹⁵	NR and NP Composite ¹²²	Aligned NT's ¹¹⁶	Aligned NT's ¹²¹
I _{SC} (mA/cm ²)	12.8	13.4	24	13.97	9.0	7.87
V _{OC} (V)	0.78	0.748	0.61	0.73	0.61	0.75
FF	0.75	0.703	0.55	0.70	0.55	0.49
Efficiency (%)	7.5	7.06	8.6	7.12	3.0	2.9
Film Thickness (μm)	14.4	16	14		5.7	0.36
Surface Area (m ² /g)		40		100		

cells have much lower efficiency, around 3%, at this stage of research. The aligned nanotube microstructure has the disadvantage of being difficult to produce in thick layers and the nanotubes themselves are polycrystalline. The fill factor in these cells is low due to an uncharacterized insulating layer that forms during anodization between the titanium and the nanotubes, which increases the series resistance. The crystallite size has been reported to be on the order of 30-50nm, similar to the size of a P25 particle, and this causes the electron transport time in the nanotube microstructure to be similar to that in the nanoparticle films, as measured by intensity modulated photocurrent spectroscopy¹¹⁶. Both Zhu et al and Mor et al conclude that there are fewer recombination sites on the nanotube array than in a nanoparticle film as shown by the longer electron lifetimes observed in the nanotube array. Although these cells show a decreased fill factor and no gain in their electron diffusion rate, the lower recombination and improved light harvesting may allow for thicker films to produce higher efficiencies as the anodization process is improved further.

As shown above, the amorphous nanorod cells have good efficiency, mostly due to their high short circuit current, which is linked to high dye adsorption, high surface area, and low recombination. The surface area of these films ranges dramatically from 117.8m²/g in some to 40m²/g in others^{114,119}. It is difficult to measure this accurately as it changes with annealing temperature and time because the morphology of the hydrothermally grown nanorods is variable. Even though the surface area is low and the pore volume remains high, dye adsorption in the films, measured by sodium hydroxide desorption, is observed to be greater than that in the nanoparticle coatings¹¹⁴. The open circuit voltage and the short circuit current, when plotted in relation to thickness, can be a

measure of the recombination effects in the titania film. If recombination in the coating is high, V_{OC} will drop steeply and the I_{SC} will plateau as the thickness increases. When recombination is low, the I_{SC} continues increasing with thickness because the increased dye adsorption in the thicker coating produces higher currents, which are not hindered by increased recombination effects. In comparison to nanoparticle films, the V_{OC} in the nanorods decreases less steeply¹¹⁹ and the I_{SC} continues increasing with thickness, showing that recombination is hindered in the nanorod coatings. The increase in the I_{SC} in general over that in nanoparticle cells may be due to better conduction, increased dye adsorption or better light harvesting due to increased light scattering¹¹⁴. The fill factor, which is indirectly proportional to the series resistance in the cell, increases in the nanorod films, most likely due to the lower recombination. Ohsaki et al suggest that the lower recombination is due to the increased electron lifetime measured in the nanorod films which is three times greater than that in the nanoparticle films. They attribute an increase in V_{OC} to a negative shift in the Fermi level caused by increased electron density in the nanorods¹¹⁷. Some reports have shown lower V_{OC} and lower I_{SC} in the nanorod cells^{117,118}.

Composite films tend to use nanoparticles as the major phase with a 10-15wt % addition of nanorods. Figure 2.4.1 illustrates SEM images of different composites. The nanorods act as light scattering centers and help maintain the high surface area of the coatings^{115,120,122}. The biggest improvement in these cells is from increased dye adsorption, because of its dependence on surface area and light harvesting efficiency. The I_{SC} tends to increase, but still plateaus as the recombination is still high since the charge transport is still mainly contained in the major phase of nanoparticles¹¹⁵. Tan et al

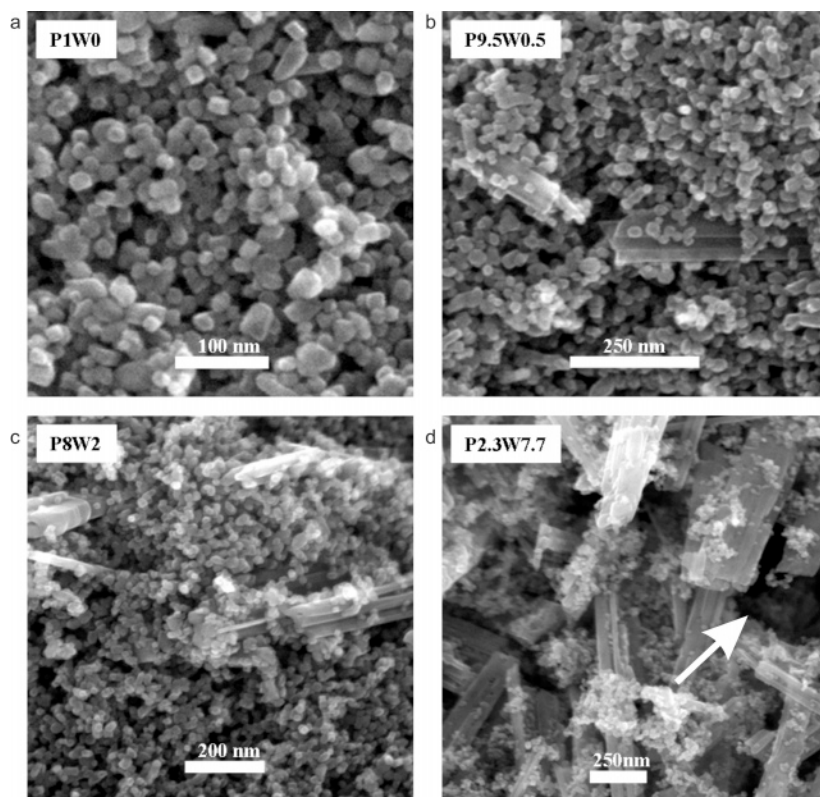


Figure 2.4.1. SEM images of a) nanoparticles film, b) 5wt% nanorod film, c) 20wt% nanorod film and d) 77wt% nanorod film¹¹⁵.

reported that if the weight percent of nanorods is increased from 20% to 77%, the I_{SC} is diminished due to the decreased dye adsorption, but continues increasing with thickness. This illustrates that recombination is greatly lessened in the nanorods, but the decreased surface area keeps the better conduction from raising the overall efficiency.

It is apparent that high aspect ratio nanostructures could have a future in dye sensitized solar cells if the conduction advantage could be coupled to the high surface area available in nanoparticle coatings. Current research in this area does show that in all examples of the amorphous nanorods and composite microstructures, the efficiency was increased over those made with common spherical nanoparticle films.

CHAPTER 3: METHOD OF ATTACK

The objectives of this research were to produce dye sensitized solar cells with commercially available components and compare these with cells made with specifically designed titanium dioxide layers. Within this objective, it was necessary to (1) produce uniform coatings of commercially available titanium dioxide nanoparticles, (2) construct DSSC's with efficiencies high enough to see comparative differences, (3) develop titania layers of high aspect ratio nanoparticles by hydrothermal reaction, (4) characterize the titania nanostructures, and (5) build DSSC's with the designed titania layers.

The design and construction of DSSC's has become relatively uniform across the literature, and so the first goal was to follow and complete this process in our laboratory such that 2-4% cells could be made reproducibly. The titanium dioxide coating was the focus of the research with a control film consisting of dispersed P25 (Degussa) nanoparticles deposited by doctor blading. High aspect ratio titania nanostructures have begun to be used in DSSC's recently^{115,117,122}, and their ability to maintain high surface area while increasing the speed of electron transfer creates the opportunity for higher efficiency solar cells. Hydrothermal systems were used to produce low temperature DSSC's, for less expensive commercialization and flexible substrate possibilities. Characterizing the hydrothermal reaction system and its products, and using geometric modeling of the DSSC's, allows for a more complete understanding of the effect of the titania structure on the efficiency of the solar cell.

CHAPTER 4: EXPERIMENTAL PROCEDURES

4.1 Dye Sensitized Solar Cells

Dye sensitized solar cells were produced and tested in order to optimize the efficiency and reproducibility. In this section, the materials used and the methodology of building and testing the cells will be discussed. The final cell design was used in all future work unless stated otherwise.

4.1.1: Materials

The untreated electrodes were received from Flexitec, Brazil, and consisted of microscope slides coated in fluorine doped tin oxide (FTO) with a $5-10\Omega/\square$ sheet resistance. Recently, the supplier was changed to Hartford Glass, IN and the thickness of the glass increased to 2.3mm. To produce the platinum electrodes, two methods were used. The first utilized Pt-Catalyst T/SP from Solaronix, which was doctor bladed onto an FTO slide with Scotch tape used as a barrier for the edges and to maintain thickness. It was then heated to 110°C for 10 minutes, and 400°C for 30 minutes and appeared as a uniform, transparent gray layer. These will be referred to as “catalytic platinum” electrodes. Platinum was also sputtered onto the FTO slides, as it adhered better to the transparent conductive oxide than to plain glass, although the conductivity of the TCO is unnecessary in this case. This type of electrode has a mirror finish and is referred to as a “sputtered platinum” electrode. The electrolyte used in the initial control cells was Iodalyte AN-50, also from Solaronix, which is an iodide based electrolyte in an acetonitrile solvent. Further work used a prepared electrolyte in a mixed acetonitrile

(CH₃CN) / methoxypropionitrile (MPN) solvent with a recipe of: 5mL CH₃CN, 5mL MPN, 0.07mL 4-tertbutylpyridine, 0.67g LiI and 0.127g I₂. This electrolyte worked comparably to that previously bought from Solaronix. In some experiments, cells were tested with less volatile electrolytes by using ionic liquids as the reduction-oxidation couple and solvent in order to reduce sealing issues. The preparation of these electrolytes involved the simple stirring of the appropriate amounts of the chosen chemicals. Most electrolytes used an imidazolium iodide (Ionic Liquids Technologies GmbH & Co. KG) mixed with 4-tert-butylpyridine and guanidinium thiocyanate. Table 4.1.1 illustrates some of the tested combinations that were found in the research literature. To produce the dye solution, 20mg of Ru-535 (Solaronix) was dissolved in 100mL of ethanol by stirring for 2-3hours. The dye was kept in a sealed plastic bottle to minimize the absorption of water as it causes the dye to degrade. The dye was normally used for 2-3 weeks before replacing with a new dye solution.

Titanium dioxide nanoparticles, product name P25, were purchased from Degussa and were dispersed in an aqueous solution for general coating purposes. Initially, 0.4mL of acetylacetone and 5mL of distilled deionized water (DIW) were mixed together, and then 12g of P25 and 15mL DIW were slowly added in until the mixture became a uniform slurry. In some cases, a mortar and pestle were used to grind the P25 while mixing with water to lessen the amount of aggregates, but this led to the loss of much of the powder. In most cases, the mixing was done using a stirring rod in a vial. After the titania was well dispersed in the solution, 0.2mL of a surfactant, Triton X-100, was added to help minimize cracking in the final coating. 4g of the slurry is then removed and diluted with 0.5mL DIW for coating thinner films. The original version of this recipe

Table 4.1.1. Ionic Liquid and Nanoparticle Electrolytes

	1 ¹²³	2 ¹²⁴	2* ¹²⁴	5 ¹²⁵	8P ¹²⁶	8H ¹²⁶
Lithium iodide	0.1M	---	0.5M	0.1g	0.1	0.1
Iodine	0.1M	0.5M	0.5M	0.019g	0.05M	0.05M
4-tertbutylpyridine	---	----	---	---	0.5M	0.5M
N-methylbenzimidazole	0.45M	0.45M	0.45M	---	---	---
1-methyl-3-propylimidazolium iodide	13	13	13	---	0.3M	---
1-methyl-3-ethylimidazolium dicyanamides	7	---	---	---	---	---
1-methyl-3-hexylimidazolium iodide	---	---	---	---	---	0.3M
Guanidinium thiocyanate	---	---	---	---	---	---
3-methoxypropionitrile	---	7	7	50mL	Solvent	Solvent
Poly(ethylene oxide) MW=2000000	---	---	---	0.264g	---	---
Fumed silica nanoparticles	---	5wt%, 3vol%	5wt%, 3vol%	---	---	---
Titanium dioxide 20-25nm particles	---	----	---	0.0383g	---	---

In the above table, the numbers with no units are meant to be volume ratios, such that in the first recipe, the ionic liquids were used as solvent in a 13:7 volume ratio.

utilized the work of Nazeeruddin, et al, and throughout the research, this dispersion was changed slightly for different coating thicknesses and tailored to the deposition method³².

Each solar cell has at least a stripe of mesoporous titania, colored purple in figures 4.1.1 and 4.1.2. This layer consists of the P25 dispersion deposited by doctor blading or spray coating; however, for most cells, a sol-gel barrier layer was also included between the mesoporous titania and the FTO to reduce direct contact between the FTO and the electrolyte. The titania sol, made with 3mL titanium isopropoxide (TIP), 2.5mL acetic acid, and 38mL 1-butanol, was prepared by first mixing the 1-butanol and acetic acid, and then slowly adding the TIP with stirring. The solution was stirred for at least 10 minutes before deposition, and could only be used for 24 hours before gelation begins to occur. For deposition, the FTO substrates were cut into approximately 25mm squares, with 3-4mm of one edge covered with Scotch tape to leave room for a contact. The FTO square was placed face-up onto the spin coater chuck with double-sided tape and seven drops of sol were dropped onto it. The spin coating was done at 3000rpm for 40 seconds (Spincoater Model P6700, Specialty Coating Systems). After drying in air, the tape was removed and the FTO/sol-gel substrate was heated at 150°C for 30 minutes with a 5°/min ramp.

After the FTO/sol-gel substrates cooled, they were broken in half again to form 12.5 x 25mm pieces onto which the mesoporous titania coatings were deposited. Scotch tape was placed on the edges to maintain uncoated contacts as shown in figure 4.1.1 and 4.1.2. For the spray coating deposition, the P25 dispersion discussed above was placed into a small glass jar with a nozzle that connected to the spray gun, which was attached to a nitrogen gas tank. The FTO substrates were taped on the edges for contact templating

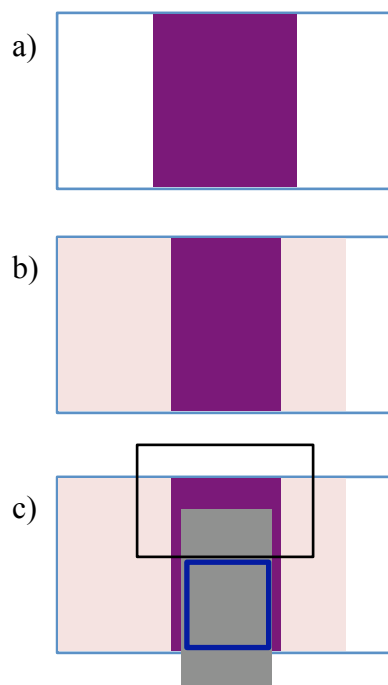


Figure 4.1.1. Illustration of the building of a DSSC by the binder clip method: a) depiction of titanium dioxide (purple) coating on FTO glass, b) addition of Scotch tape (pink) to protect the FTO from excess electrolyte, and c) the (gray) platinum electrode is placed gently and the black box portrays where the binder clip is used to hold the cell together. The active area of the cell is shown as a blue box in c.

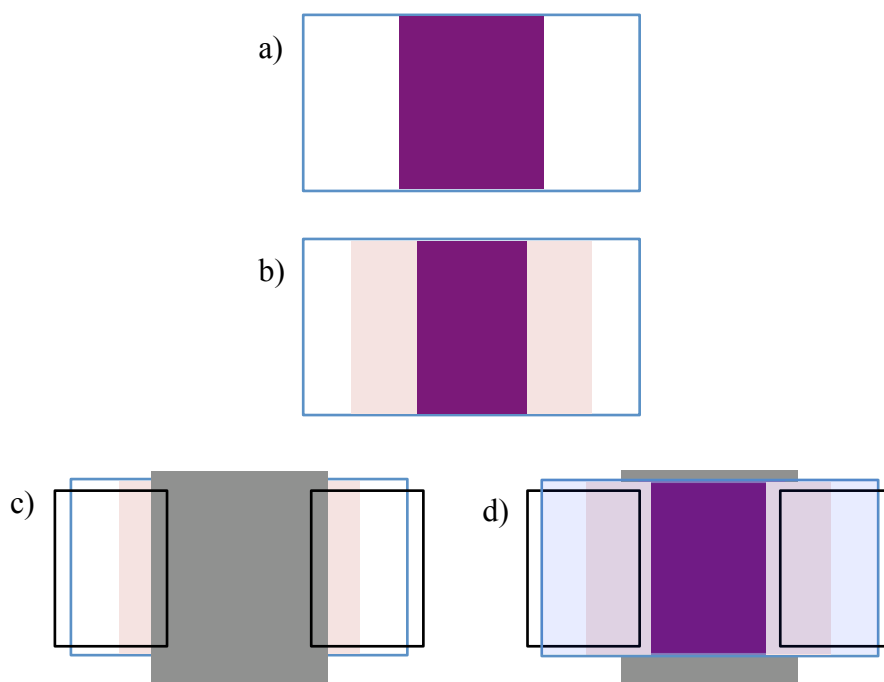


Figure 4.1.2: This schematic demonstrates the building of a hot melt sealant DSSC. The TiO_2 coating is shown in a, b) describes the hot melt sealant (pink) placement, and c) and d) illustrate where the binder clips (black squares) are attached as the cells go into the oven for heat treatment, platinum facedown and titania facedown, respectively. After heating, the binder clips are removed.

and then attached to dark colored paper that acted as a large substrate for easy mobility. The substrates were then hung vertically for even spraying. To spray, the gun was held approximately 6 inches away and aimed directly at the substrates. The nitrogen regulator was set at 30psi for a constant, low-pressure spray. 2-4 coats of spray were applied to the FTO substrates until they appeared to be a light white color. After spraying, the substrates were dried horizontally in air. After removal of the tape, sintering was done at 500°C with a 5°/min ramp for 30 minutes, as was done for all mesoporous titania coatings.

Doctor blading was a more common deposition method in this research and was used unless otherwise stated. Uniform coatings could be made rapidly and reproducibly. Again, Scotch tape was used as a coating template and to maintain the appropriate thickness. More layers of Scotch tape were added to increase the thickness if desired; however, unless otherwise stated, cells were made with one layer of tape. The tape was also connected to a large substrate below the glass pieces to immobilize them during deposition. A stirring rod was used to deposit 2-3 drops of P25 dispersion on the FTO or FTO/sol-gel substrates. Then a plain glass microscope slide (Fisher) was used to pull the dispersion evenly across the substrate, with pressure against the taped edges to produce a uniform thickness. The substrates were allowed to dry in air for up to 24 hours, and were then heat treated at 500°C with a 5°/min ramp for 30 minutes.

After heating of the coated substrates, they were immediately placed into petri dishes and covered with the dye solution where they remained, covered, for 12-24 hours. Putting the substrates into the dye while they were still warm from the furnace helped to keep water

away from the surface. As the substrate was also protected from water adsorption in the dye solution, it was kept there until just before the cell was built.

4.1.2: Building DSSC's

Two different methods of building a cell were commonly used, depending on whether the testing would be long term or short term. Here, three methods are discussed as the Amosil sealing method was later replaced by the hot melt sealing method.

Binder Clip Method: This method has the advantage of producing higher efficiencies as the interlayer distance between the platinum electrode and the titania coating is minimized, but it is a short term method as the electrolyte evaporates rapidly since there is no sealant protecting it from air. The titania coating is deposited and sintered, and then tape is used to cover the edge of the FTO completely on one side and partially on the other so that room for a contact remains. The tape acts as a barrier between the electrolyte and the FTO as a connection between these two results in leakage current and lower efficiency, as shown in figure 4.1.1b. The electrolyte solution is dropped onto the titania section of the substrate, and then the platinum electrode is carefully placed onto the electrolyte/titania. The size of the platinum electrode is minimized for low cost, and can be reused in these cells. The binder clip is added last, pressing together the two glass substrates. It is this pressure from the clip that minimizes the thickness of the electrolyte layer. The steps involved in production of this type of cell are shown in figure 4.1.1.

Amosil Sealing Method: The first attempt to produce a sealed cell so that long-term cell experiments could be undertaken utilized Amosil 4 sealant (Solaronix). Amosil

4 is an epoxy resin sealant in which the two Amosil products were mixed together and then rapidly placed onto the glass substrate near the edges of the titania coating. A small spatula was used for mixing and depositing the epoxy in narrow lines. Two holes were left in the outline so that the cell would fill with electrolyte via capillary forces. The platinum substrate was placed above the titania substrate and these were pressed gently together as the Amosil 4 sealant created a seal between the two electrodes. The space between the electrodes was large, in the range of 2-4mm, which lowered the efficiency, and the sealant was quite messy when the electrolyte was added.

Hot Melt Sealant Method: Another product from Solaronix, SX1170-25 or SX1170-60, was used as the next generation sealing method in this research. A 25 or 60 μ m transparent film that seals with slight heat, this method was neat, simple and created a small interlayer distance, although the binder clip method produced the least distance between electrodes. Small strips of sealant were cut, shown in pink in figure 4.1.2, and placed on the outside edges of the titania coating. Then the platinum was placed to cover approximately half the width of the strips. Binder clips were used to hold the cell together as it was heated to 110°C for 15 minutes. The binder clips were removed after a short cooling period and at this point, the substrates were completely sealed to one another. The electrolyte was added by pipetting a drop onto the substrate surface that was then pulled through the opening of the cell by capillary forces. For longer term sealing, hot glue was used to seal these top and bottom edges to slow volatilization of the electrolyte.

4.1.3: Solar Cell Characterization Methods

The titania coatings, both sol-gel and mesoporous, were characterized before the cell build for thickness and uniformity. Profilometry (Tencor, Alpha-step 200) was used to measure the thickness and the uniformity of the P25 mesoporous coatings. In this method, a small needle runs across the glass substrate and measures the thickness of the step from the glass to the titania layer. The thickness can be measured up to almost 2000 μm in from the edge. As the sol-gel barrier layer is much thinner, on the order of nanometers, it was characterized using ellipsometry (Jobin Yvon Horiba UVISEL). The thickness and crystallization with temperature was measured with this equipment.

After the cell build was completed, the cells were moved immediately into the electrical characterization lab so that as little electrolyte as possible was lost to volatilization. If the binder clip method was used, the cells were built in the characterization lab. The cells were placed on a small table with a fixed height such that the light output from the 300W Xenon solar simulator (Newport, Oriel 91160A) reaching the cell was 90W/m² as measured by an irradiance meter (Daystar, Solaqua) as shown in figure 4.1.3. The platinum side was face-up so that the light passed through the back of the titania electrode. When the titanium substrates from the hydrothermal growth system were used to build cells, the cells were tested with the FTO/catalyzed platinum substrate facedown since the Ti metal is opaque. Alligator clips on the platinum edge and the FTO edge connected the cells to the voltage source (HP 4140B pA meter/voltage source). A LabView program ran both the solar simulator and the electrical characterization equipment. The program set -0.3 to 1.0 volts on the cell with a step size of 10mV, and collected the output current in the dark and under illumination.

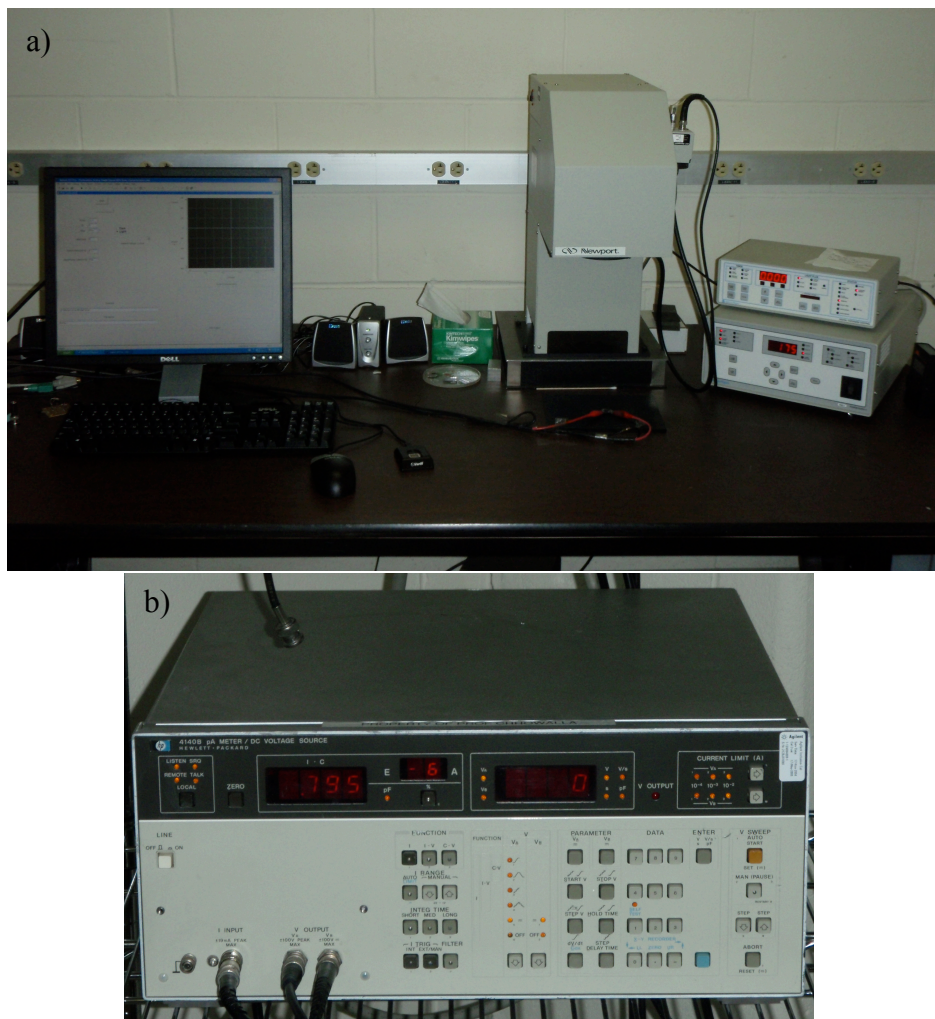


Figure 4.1.3. Images of a) Newport solar simulator and computer, and b) the voltage source.

The output was saved into two separate files, one with the current and voltage data at each point and one with the calculated solar characteristics results, including efficiency, fill factor, etc. This data was then transferred to excel and the characteristics were recalculated for accuracy. If long-term experiments were done, the cells were kept in a sealed bag until the next test was run.

4.2: Hydrothermal Growth of Nanostructures

The initial hydrothermal growth solutions were a combination of a basic solution and titanium dioxide nanoparticles (P25). The basic solution consisted of the appropriate amount of either potassium hydroxide (KOH) or sodium hydroxide (NaOH) pellets (Sigma Aldrich) dissolved in DIW, with stirring, to form the desired concentration. The titanium dioxide powder, commonly 0.5g, was added to the solution while stirring and then the suspension was transferred to the Teflon beaker that sits inside the Parr reactor. The stainless steel reactor was sealed tightly by screwing on the lid, and fastening with 6 small screws at the top. The solution was heated to 110°C to 175°C in a small oven in the laboratory that was set to run automatically for the appropriate number of hours, up to 24. At reaction times greater than 24 hours, the system had to be shut off manually. After the reaction was completed, the reactor stayed in the oven until it had cooled to at least 50°C, which was approximately 2 hours after heating was completed, but was then removed promptly as the products changed over time. For the hydrothermal growth systems that were done on a titanium metal substrate, the 0.127in thick Ti metal sheet (Sigma Aldrich) was cut to size, approximately 25 x 40mm, with scissors. A small round circle of Teflon that was made to fit the Teflon beaker was used that had a slit across the

top where the Ti metal sat so that it was at an angle to the solution. This setup is portrayed in figure 4.2.1. Then the basic solution with or without added TiO_2 was carefully poured into the beaker and the Parr reactor was sealed and heated as usual.

The post-treatment processes of the powder varied based on the experiment being completed. When the reactor was cooled and opened, the supernatant of basic solution was pipetted out carefully so as not to disturb the powder cake that had settled to the bottom during cooling. This supernatant was often disposed of as waste, but was kept when necessary for characterization of the reaction system. In these cases, it was put into a scintillation vial and labeled carefully. The powder was removed by adding 50mL DIW and then was transferred to a beaker. If an acid wash was done, 2mL hydrochloric acid (HCl) was added to this system. For both acid and water washes, the powder/DIW dispersion was stirred overnight. Similar treatments were done with the titanium metal substrates, but in these cases the supernatant and remaining powder were disposed of as waste, unless necessary for characterization. The Ti metal was placed in a beaker of 50mL DIW with or without the addition of 2mL of HCl, depending upon the experiment being conducted, and left to sit overnight without stirring. In the case of both the Ti metal or the powder, the washes were often done more than once. The Ti metal could be easily transferred from one beaker to another, but the powder product had to be allowed to settle, and then the supernatant was pipetted out and new solution was added. The number of washes was dependent on the experiment although if none is indicated, only one DIW wash occurred. After the washing stages, the Ti metal and the powder product were often heat treated to 500°C for 30 minutes at a ramp of 5°C per minute. The post-

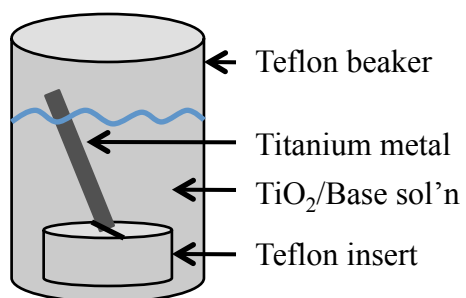


Figure 4.2.1. Schematic of the Teflon beaker placed inside the Parr reactor for hydrothermal reactions on a titanium metal substrate.

treatment heating process varied by experiment, and others will be mentioned in the results section. The products of these experiments were labeled based on the reactant (powder or sheet metal) and the date completed. For example, the sample H090606 was a hydrothermal experiment run with TiO_2 powder on September 6, 2006. If Ti metal were used in place of the powder, the sample name would be Ti090606. Since there were numerous washing steps that were characterized, most names were appended based on their chronology. H090606A was the powder cake as it was removed from the reactor, H090606B was after one acid wash and H090606C was after two acid washes. These are clearly marked in any further discussion.

4.3: Characterization of Hydrothermal Products

4.3.1: X-Ray Diffraction (XRD)

XRD is useful in determining the composition of the products grown by hydrothermal methods. In regards to the powder products, after washing, the powders were dried in air at room temperature before characterization. As there were only small amounts of these powders, a conventional sample holder could not be used. A strip of double-sided tape was placed in the middle of the top half of a large microscope slide (50x75mm). The powder was then gently placed onto the tape and pressed down with another glass slide. This produced a strip of powder on a glass slide that was directly placed into the x-ray diffractometer (Siemens D500). The titanium metal products were tested in a similar fashion, as the metal substrates were not large enough to fit into the machine on their own; they were taped to a large glass slide and then tested. XRD testing was done for 38 minutes on each sample with a dwell time of 0.5 seconds and a step size

of 0.03° . The background of the resulting data was removed using the Materials Data Jade 8 software and the pattern was transferred to Microsoft Excel for graphing purposes.

4.3.2: Scanning Electron Microscopy (SEM)

SEM uses electrons to produce an image of the surface of a sample. Most images were taken using a Zeiss (DSM 982 Gemini) microscope at Rutgers University. The FEI/Philips XL30 Field Emission Scanning Electron Microscope at Princeton University was used for a few samples, as marked. The powder samples were either doctor bladed onto a glass slide while in suspension or dropped onto carbon tape after drying. Carbon tape was used to stick the samples onto the aluminum SEM studs. Gold coating was done on some samples as the titanate growth charged even at low voltages. The titanium metal samples were cut with scissors to small sample sizes and adhered to the carbon tape on the studs. SEM was regularly taken at 5-10kV with a working distance of 12mm. On some samples, energy dispersive x-ray spectroscopy (Princeton Gamma Tech) was used in conjunction with the SEM to determine the elements in the product. Image maps were taken using the Imix software in conjunction with the EDS.

4.3.3: Transmission Electron Microscopy (TEM)

Powder samples were easily prepared for the TEM by grinding with a mortar and pestle under ethanol. A small drop of the suspension was then placed directly onto a copper grid that sat on filter paper. After the ethanol dried, the sample went directly into the microscope. Samples in suspension were taken from the hydrothermal reaction solution or the washing treatments and dropped onto the copper grids with no pre-

treatment. When the hydrothermal growth on titanium metal substrates was characterized by TEM, the coating was scraped off of the Ti metal into a mortar by razor blade. Then the ethanol was added and the steps were completed as above. All TEM images were taken at 200kV with the TopCon EM-002B Transmission Electron Microscope at Rutgers University. The negatives were developed as directed and dried overnight. Diffraction patterns were collected in conjunction with the images.

CHAPTER 5: DYE SENSITIZED SOLAR CELLS

5.1: Results of Dye Sensitized Solar Cells

The initial studies on DSSC's used the P25 dispersion discussed above and tended to have high variability. A variety of coating methods, annealing temperatures, and sealing methods were tested, and the parameters and characteristics of a set of such cells are shown in table 5.1.1. These cells were useful to the research as a method of finding the most favorable design for a solar cell, based on efficiency and ease of production. This section will discuss the variety of cell design variables that were studied, such as annealing temperature and thickness, and then will focus on the two main testing variables, the titania coating and the electrolyte. In the figures, the following abbreviations were made:

I_{SC}	Short circuit current (often given with respect to area)
V_{OC}	Open circuit voltage
PP	Peak power point
I_{PP}	Current at the peak power point (often given with respect to area)
V_{PP}	Voltage at the peak power point
FF	Fill factor

5.1.1: Cell Design Tests

Tables 5.1.2 and 5.1.3 illustrate different types of cells that were tested in order to optimize the cell construction process. In table 5.1.2, the main variable tested was the width of the titania coating that varied from 0.5cm to 1cm. It was found that thinner strips of titania perform better. The increase in efficiency from those in table 5.1.1 to 5.1.2 was largely due to the change from catalytic platinum to sputtered platinum electrodes. This distinct increase can also be seen in table 5.1.3 where the variables

Table 5.1.1. Characteristics of Initial DSSC's

Sample	Date	I _{sc} (mA)	V _{oc} (V)	V _{pp} (V)	I _{pp} (mA)	PP (mW)	Fill Factor (%)	Efficiency (%)	Sol'n Aged (days)	Temp (°C)	Layers P25	Summary of cells 12.2005.xls
A	12/20/05	0.282	0.71	0.39	0.19	7.41E-05	37.01	0.07	4	100	1	
B	12/20/05	1.530	0.54	0.29	0.99	0.000287	34.75	0.29	4	100	1	
C	12/20/05	0.721	0.64	0.38	0.47	0.000177	38.70	0.18	4	100	1	
D	12/20/05	0.599	0.67	0.37	0.46	0.00017	42.41	0.17	4	100	1	
E	12/20/05	1.800	0.62	0.38	1.33	0.000504	45.29	0.50	4	400	1	
F	12/20/05	0.953	0.69	0.36	0.49	0.000176	26.83	0.18	4	400	1	
2L1	12/20/05	1.292	0.49	0.32	0.84	0.000269	42.46	0.27	4	520	2	1 layer tape, coated P25 twice
2L2	12/20/05	1.154	0.5	0.32	0.74	0.000237	41.04	0.24	4	520	2	1 layer tape, coated P25 twice
3L1	12/20/05	0.236	0.66	0.27	0.11	3E-05	19.07	0.03	4	520	3	1 layer tape, coated P25 3x
3L2	12/20/05	0.723	0.51	0.31	0.41	0.000126	34.47	0.13	4	520	3	1 layer tape, coated P25 3x
Old 1	12/20/05	1.720	0.59	0.35	1.223	0.000428	42.18	0.43	4	520	1	
Old 2	12/20/05	1.770	0.58	0.34	1.25	0.000424	41.40	0.42	4	520	1	
US 1	12/20/05	1.230	0.57	0.34	0.89	0.000302	43.16	0.30	0	520	1	ultrasonicate P25
US 2	12/20/05	1.760	0.59	0.35	1.19	0.000418	40.11	0.42	0	520	1	ultrasonicate P25
New	12/20/05	0.935	0.62	0.36	0.56	0.000202	34.78	0.20	0	520	1	
450 1	12/20/05	1.134	0.64	0.39	0.75	0.000291	40.30	0.29	0	450	1	
450 2	12/20/05	2.130	0.53	0.32	1.47	0.000471	41.67	0.47	0	450	1	
520 3	12/20/05	1.355	0.58	0.36	0.89	0.000322	40.77	0.32	0	520	1	
520 1	12/20/05	0.522	0.66	0.38	0.29	0.000109	31.99	0.11	0	520	1	
520 2	12/20/05	1.130	0.58	0.37	0.76	0.000283	42.91	0.28	0	520	1	
520 thick	12/20/05	1.510	0.55	0.32	0.87	0.000278	33.52	0.28	0	520	2	2 layers of tape, 1 coating P25

AAA Cells Summary.xls

Table 5.1.2. Binder Clip Cells with Sputtered Pt Electrodes

Date	Sample	SolGel	TiO2	Platinum	Electrolyte	Sealant Method	Efficiency (%)	Isc (mA)	Current Density (mA/cm ²)	Voc (V)	FF (%)	Area (cm ²)	Notes
6/12/06	B	none	doc blade P25	sputtered	AN-50	binder clip method	2.23	0.68	5.64	0.67	58.66	0.12	thin strip titania
6/12/06	C	none	doc blade P25	sputtered	AN-50	binder clip method	1.60	1.82	4.33	0.69	53.49	0.42	thick strip titania
6/12/06	D	none	doc blade P25	sputtered	AN-50	binder clip method	2.82	1.27	7.03	0.70	57.31	0.18	thin strip titania
6/12/06	E	none	doc blade P25	sputtered	AN-50	binder clip method	1.14	1.52	3.04	0.68	55.04	0.50	thick strip titania
6/12/06	F	none	doc blade P25	sputtered	AN-50	binder clip method	1.28	0.71	3.38	0.68	55.72	0.21	thin strip titania
6/12/06	I	none	doc blade P25	sputtered	AN-50	binder clip method	0.36	0.30	1.21	0.63	46.91	0.25	thin strip titania

AAA Cells Summary.xls

Table 5.1.3. Sealing Method and Pt Electrode Comparison

Date	Sample	SolGel	TiO2	Platinum	Electrolyte	Sealant Method	Efficiency (%)	Isc (mA)	Current Density (mA/cm ²)	Voc (V)	FF (%)	Area (cm ²)
6/22/06	BC1	none	doc blade P25	sputtered	AN-50	binder clip method	0.30	0.86	4.30	0.23	30.40	0.20
6/22/06	T1	none	doc blade P25	sputtered	AN-50	teflon liner	0.01	0.01	0.02	0.63	43.45	0.36
6/22/06	T2	none	doc blade P25	sputtered	AN-50	teflon liner	0.45	0.25	1.05	0.68	62.34	0.24
6/22/06	T3	none	doc blade P25	sputtered	AN-50	teflon liner	0.33	0.34	0.94	0.68	51.12	0.36
6/22/06	T4	none	doc blade P25	sputtered	AN-50	teflon liner	0.70	0.58	2.42	0.63	45.61	0.24
6/26/06	A	none	doc blade P25	Pt gel/FTO	AN-50	SX and kapton tape	0.31	1.31	0.89	0.66	52.28	1.47
6/26/06	B	none	doc blade P25	sputtered	AN-50	SX and kapton tape	0.99	4.00	3.16	0.63	49.52	1.27
6/26/06	C	none	doc blade P25	Pt gel/FTO	AN-50	SX and kapton tape	0.01	0.04	0.04	0.65	54.66	1.08
6/26/06	D	none	doc blade P25	sputtered	AN-50	SX and kapton tape	0.01	0.00	0.01	0.62	66.50	0.29

tested are the sealing methods and the platinum coating. Although this chart illustrates that hot melt sealing (SX and kapton tape) produces the most efficient cells, due to greater variability in the cells, the binder clip method continued to be used as it showed higher efficiencies than the other sealing methods in most tests.

As discussed in Section 4.1, two layers of titania were often used. The sol-gel coating on the FTO substrate acts as a barrier to recombination. Table 5.1.4 illustrates the testing of cells with sol-gel and mesoporous layers in two different combinations. Table 5.1.5 improves upon this data by interweaving the type of platinum utilized. In this data, six cells of each type were tested, with four sets that include barrier and non-barrier layers and sputtered versus catalytic platinum electrodes.

Cells were also tested to determine the variability within a given set of cells and the possibility of using different metal electrodes. Figure 5.1.1 demonstrates the graph and resulting data of one reproducibility test. For metal electrodes, thin layers of gold and aluminum were evaporated onto glass slides to test the efficiency of using different metals for the back contact. Figure 5.1.2 demonstrates that the platinum electrodes work better than those of gold, and the aluminum electrodes are not shown in the graph as these cells short circuited in every case.

In improving the cell, it was noticed that not only do the materials cause changes to the efficiency, but also the geometry of the cell construction. The efficiency is shown as a function of thickness in figure 5.1.3. Figure 5.1.4 demonstrates different ways of coating the titania onto the FTO and in figure 5.1.5, the differences in the cell characteristics based upon these geometric changes are illustrated.

Table 5.1.4. Comparison of Additional Layers of TiO₂

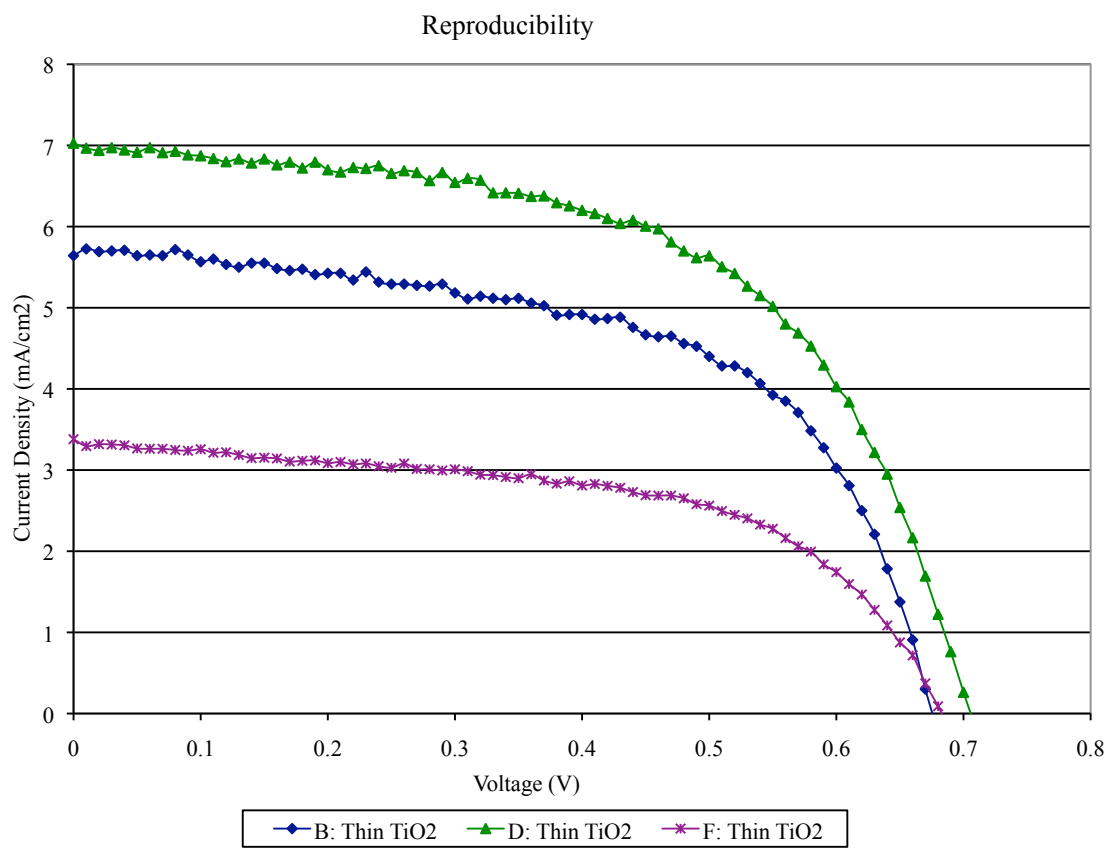
AAA Cells Summary.xls

Date	Sample	TiO ₂	Platinum	Electrolyte	Sealant Method	Efficiency (%)	Isc (mA)	Current Density	Voc (V)	FF (%)	Active Area (cm ²)
06/16/06	A	Sol - P25	sputtered	AN-50	binder clip method	1.14	1.401	3.336	0.67	51.16	0.42
06/16/06	A	Sol - P25 - Sol	sputtered	AN-50	binder clip method	0.00	0.002	0.004	0.49	25.06	0.36
06/16/06	B	Sol - P25	sputtered	AN-50	binder clip method	1.13	1.700	3.036	0.68	54.95	0.56
06/16/06	B	Sol - P25 - Sol	sputtered	AN-50	binder clip method	0.00	0.001	0.002	0.65	18.97	0.42

Table 5.1.5. Barrier Layer and Platinum Electrode Comparison

	I_{sc} (mA/cm ²)	V_{oc} (V)	PP (mW/cm ²)	V_{pp} (V)	I_{pp} (mA/cm ²)	FF	Efficiency
B/CPt 1	1.92	0.67	0.7798	0.49	1.59143	60.75%	0.87%
B/CPt 2	1.45	0.66	0.5672	0.49	1.16	59.37%	0.63%
B/CPt 3	1.33	0.66	0.2996	0.34	0.88	34.01%	0.33%
B/CPt 4	1.73	0.65	0.6712	0.47	1.43	59.69%	0.75%
B/CPt 5	1.51	0.66	0.5736	0.48	1.20	57.56%	0.64%
B/CPt 6	1.59	0.65	0.6370	0.49	1.30	61.67%	0.71%
NB/ SPt 1	2.70	0.68	0.9656	0.47	2.05	52.59%	1.07%
NB/ SPt 2	2.30	0.66	0.8568	0.46	1.86	56.44%	0.95%
NB/ SPt 3	1.84	0.67	0.6722	0.49	1.37	54.63%	0.75%
NB/ SPt 4	2.07	0.66	0.7264	0.44	1.65	53.27%	0.81%
NB/ SPt 5	1.40	0.65	0.4932	0.45	1.10	54.10%	0.55%
NB/ SPt 6	1.81	0.69	0.6647	0.47	1.41	53.10%	0.74%
B/SPt 1	1.84	0.66	0.7967	0.50	1.59	65.74%	0.89%
B/SPt 2	1.40	0.63	0.6020	0.49	1.23	68.35%	0.67%
B/SPt 3	1.02	0.66	0.4670	0.52	0.90	69.09%	0.52%
B/SPt 4	1.20	0.65	0.5167	0.52	0.99	66.31%	0.57%
B/SPt 5	0.01	0.01	0.0001	0.01	0.01	38.34%	0.00%
B/SPt 6 (SC)	0.00	0.51	0.0000	0.17	0.00	19.86%	0.00%
NB/CPt 1	0.76	0.62	0.3038	0.49	0.62	64.26%	0.34%
NB/CPt 2	0.49	0.60	0.1777	0.45	0.39	60.31%	0.20%
NB/CPt 3	0.87	0.63	0.3683	0.51	0.72	67.32%	0.41%
NB/CPt 4	0.95	0.63	0.3800	0.51	0.75	63.60%	0.42%
NB/CPt 5	1.37	0.67	0.5630	0.51	1.10	61.42%	0.63%
NB/CPt 6	1.12	0.65	0.4528	0.47	0.96	62.29%	0.50%

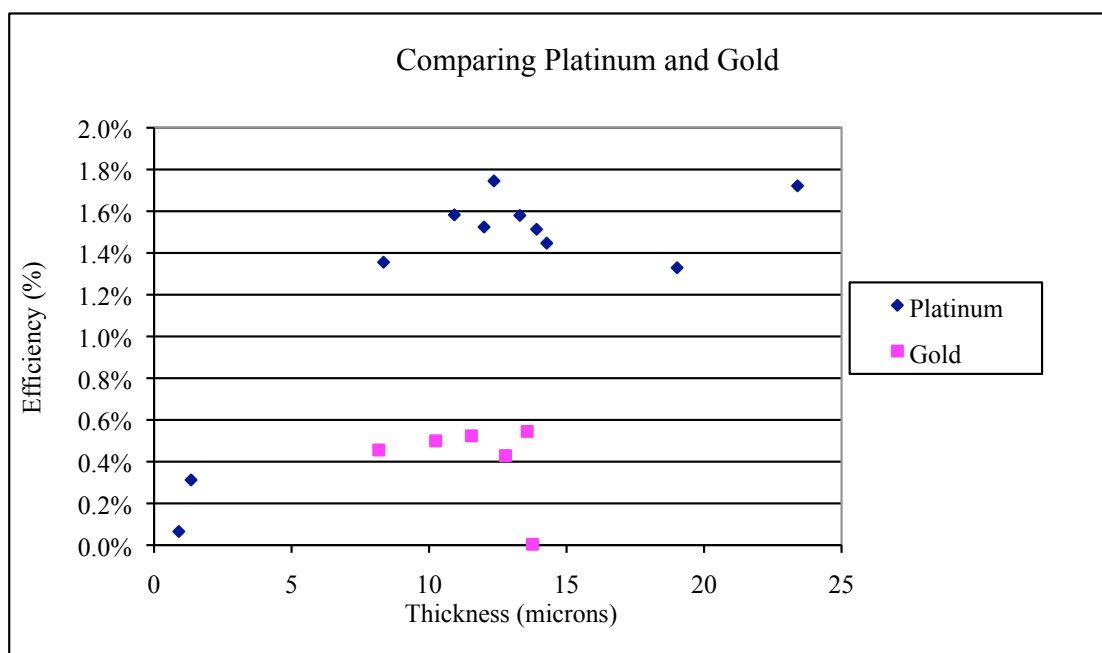
(Barrier and Pt Disproven Oct07/all cells.xls)



	Area (cm ²)	I _{SC} (mA/cm ²)	V _{OC} (V)	Fill Factor %	Efficiency %
B	0.12	5.64	0.68	58.1	2.23
D	0.18	7.03	0.71	56.5	2.82
F	0.21	3.38	0.69	54.9	1.28

(061206 – all data.xls)

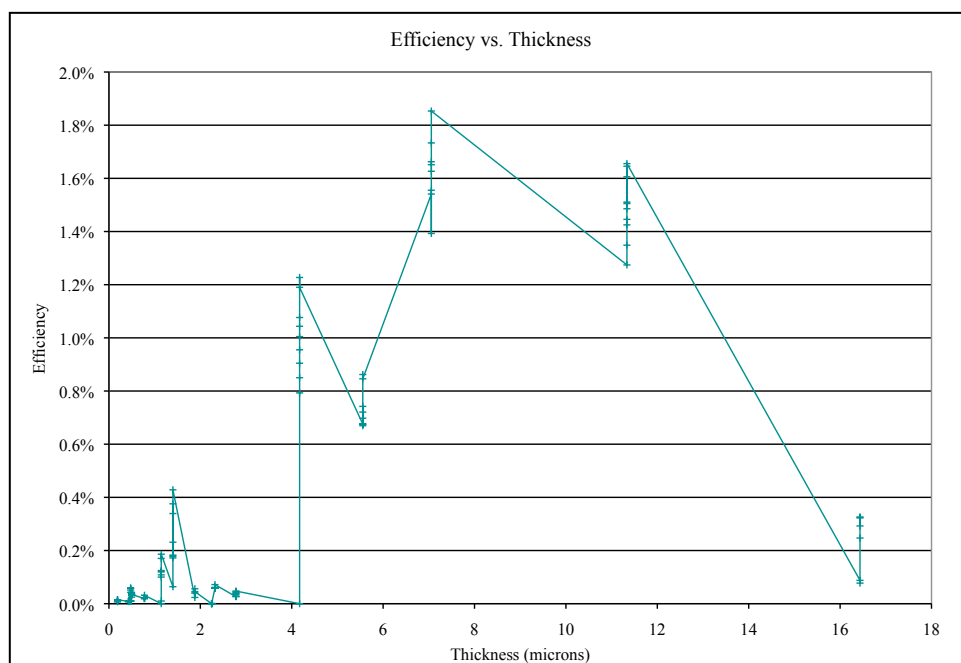
Figure 5.1.1: Three different cells with similar construction were used to test the reproducibility of the cell builds. The efficiencies varied, illustrating that the cells are not optimized.



Platinum Electrode			Gold Electrode		
Label	Thickness (μm)	Best Eff	Label	Thickness	Best Eff
6	0.9	0.065%	1	8.17	0.456%
0	1.345	0.312%	2	10.24	0.500%
7	8.345	1.356%	3	11.54	0.524%
8	10.92	1.583%	4	12.78	0.429%
2	12	1.524%	5	13.57	0.545%
1	12.36	1.745%	6	13.76	0.004%
4	13.3	1.580%			
3	13.91	1.513%			
9	14.28	1.447%			
11	19.02	1.329%			
5	23.4	1.722%			

(Gold Electrode Data.xls)

Figure 5.1.2. Comparing thickness and different electrodes illustrates that using platinum produces high efficiency cells.



(thickness graphs.xls)

Figure 5.1.3. The data resulting a set of spray coated cells illustrates that a thickness in the range of 8-12 μ m is optimum. The approximately 8 points at each thickness are due to different tests of the same cells showing efficiency variability as well.

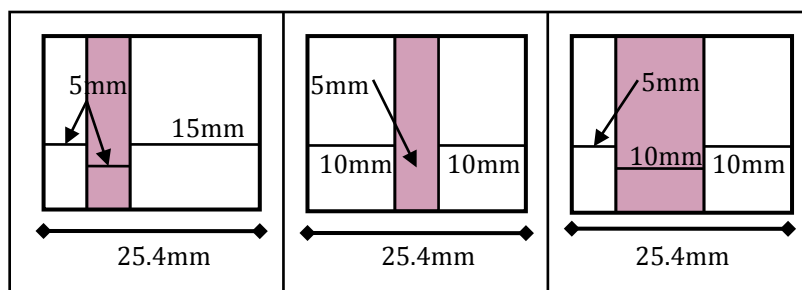
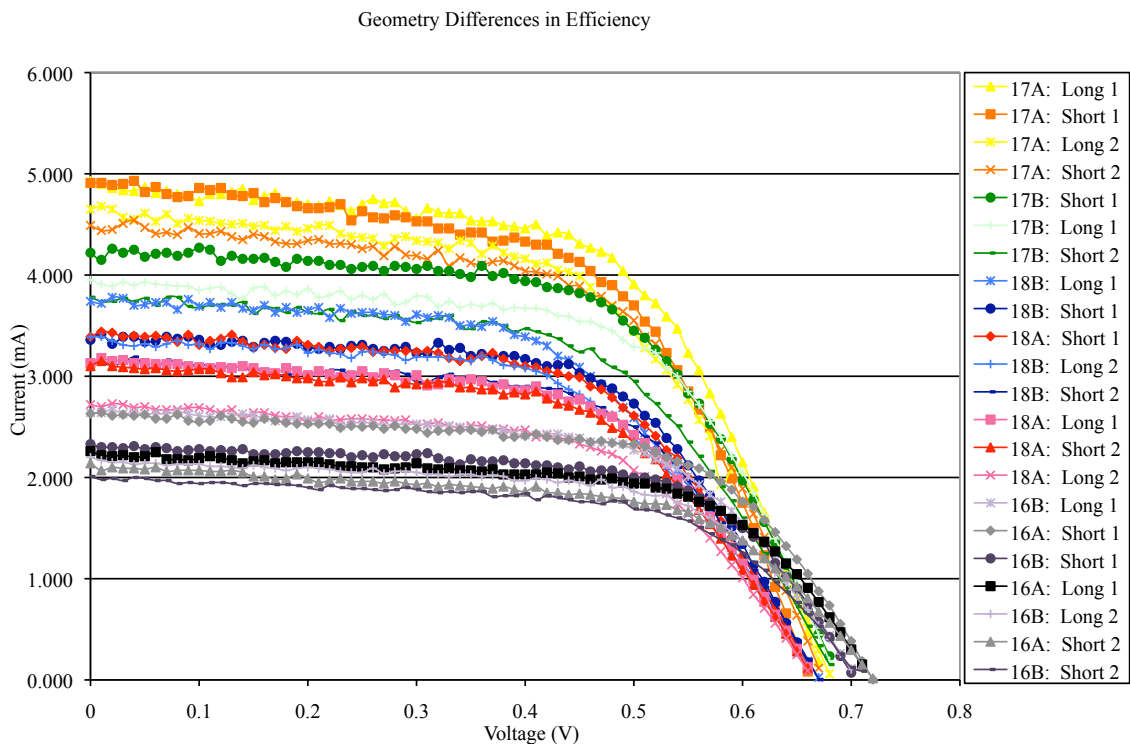


Figure 5.1.4. Different geometries that were tested as portrayed in figure 5.1.5.



(class data with graphs.xls)

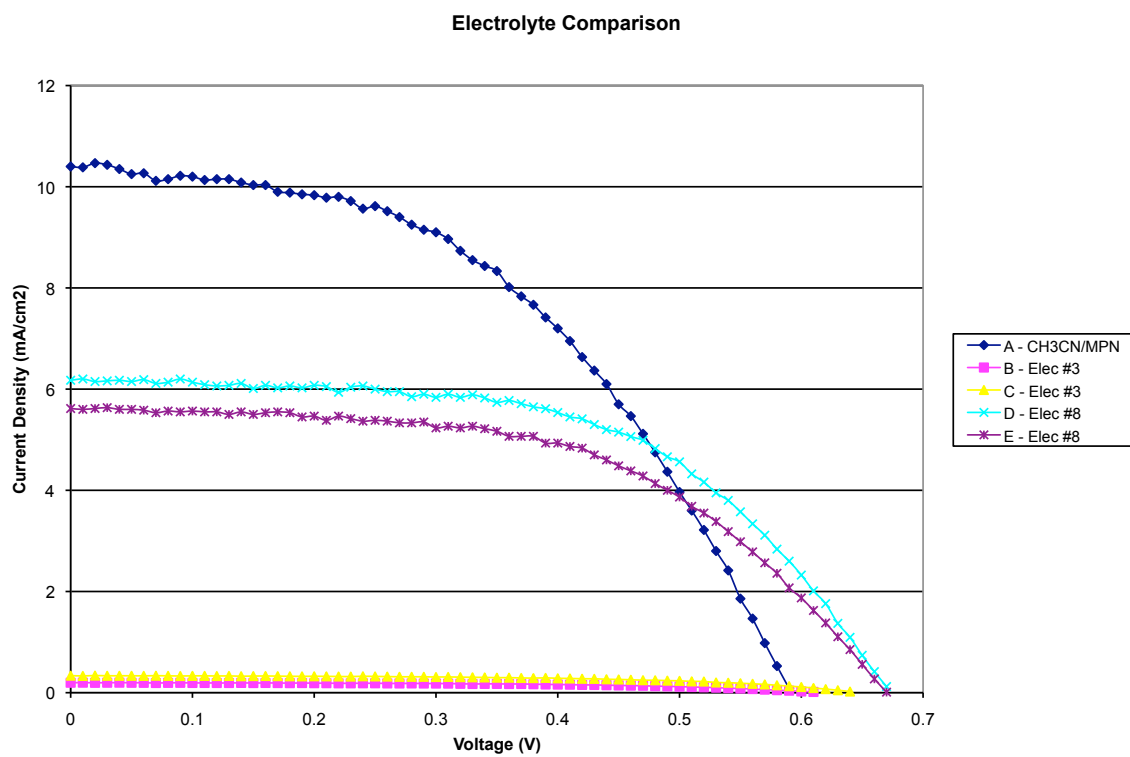
Figure 5.1.5. A set of six cells was produced by spray coating. The graph here illustrates the changes in efficiency when the distance from the contact to the titania is increased 3x from 5mm (short) to 15mm(long).

5.1.2: Electrolytes

Different electrolytes change the efficiency of the cell based mostly on their ionic conductivity, but they also affect the cell based on their volatility. Ionic liquid electrolytes were tested in comparison to volatile electrolytes, and tests over longer time frames were done with both types of electrolyte. A direct comparison test between two formulations of ionic liquid electrolytes (3 and 8M, from table 4.1.1) with a volatile electrolyte is shown in figure 5.1.6. Figure 5.1.7 illustrates rapid evaporation of a volatile electrolyte and how this decreases the efficiency in a binder clip cell. The tests shown here were taken directly after one another with an approximate time between measurements of one minute. An illustration of the ability of ionic liquid electrolytes to maintain the cell's efficiency over time is shown in figure 5.1.8. Figure 5.1.9 demonstrates cells made with a battery separator that is dipped in the ionic liquid electrolyte and then placed on top of the titania; finally, the platinum electrode is pressed down and the binder clip sealing method is used. Only small variations between tests were seen.

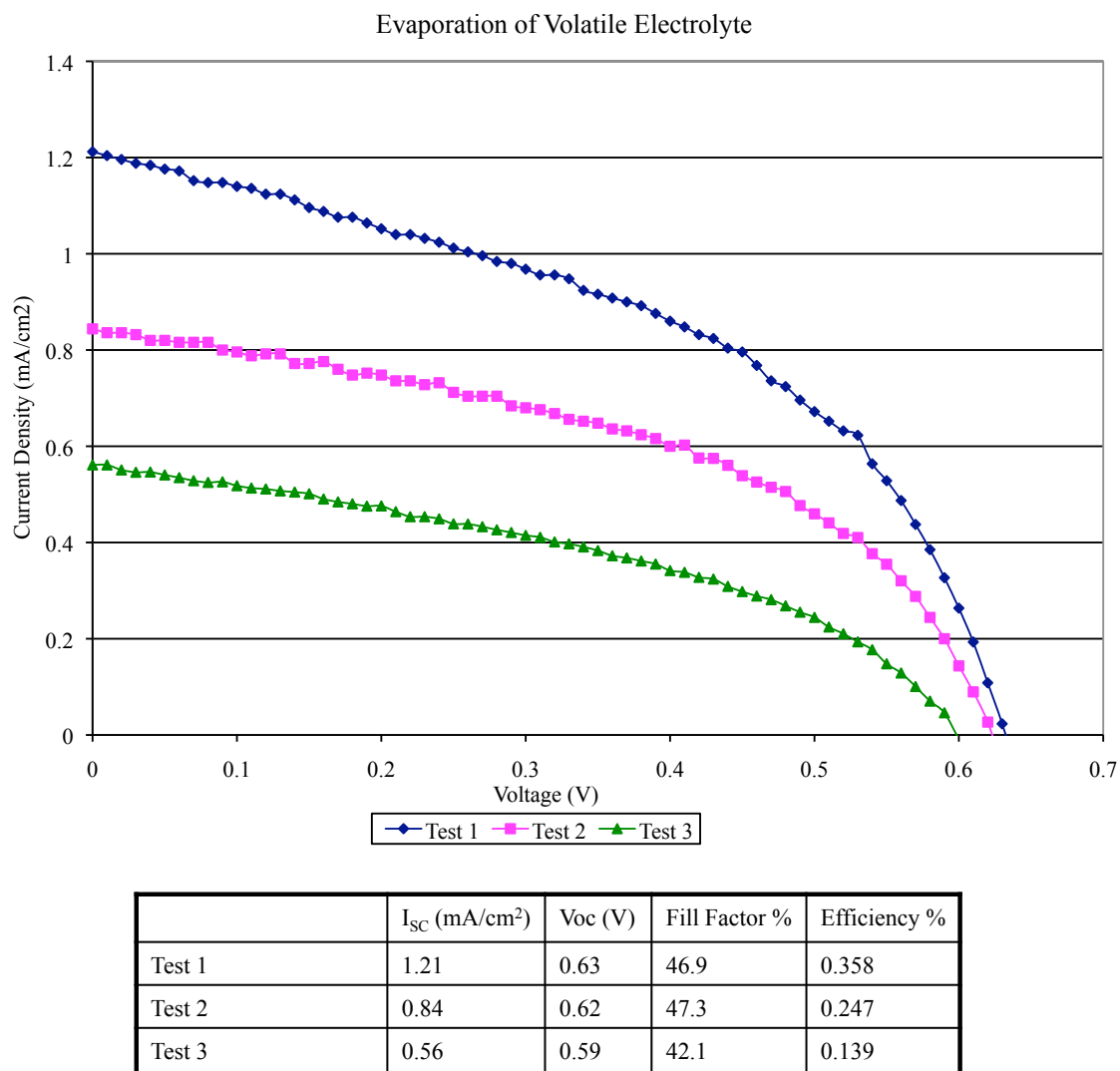
5.1.3: Titania

The mesoporous titania coatings that were used were either doctor bladed or spray coated onto the cells. The doctor bladed coatings have a specific surface area similar to that of the P25 nanoparticles at approximately $55\text{m}^2/\text{g}$. Figure 5.1.10 illustrates FESEM images of the two different types of coatings. When similar cell designs were used, the spray coated cells had higher efficiency. However, the spray coated cells had increased variability when compared to the doctor bladed films. Another variation on the coating



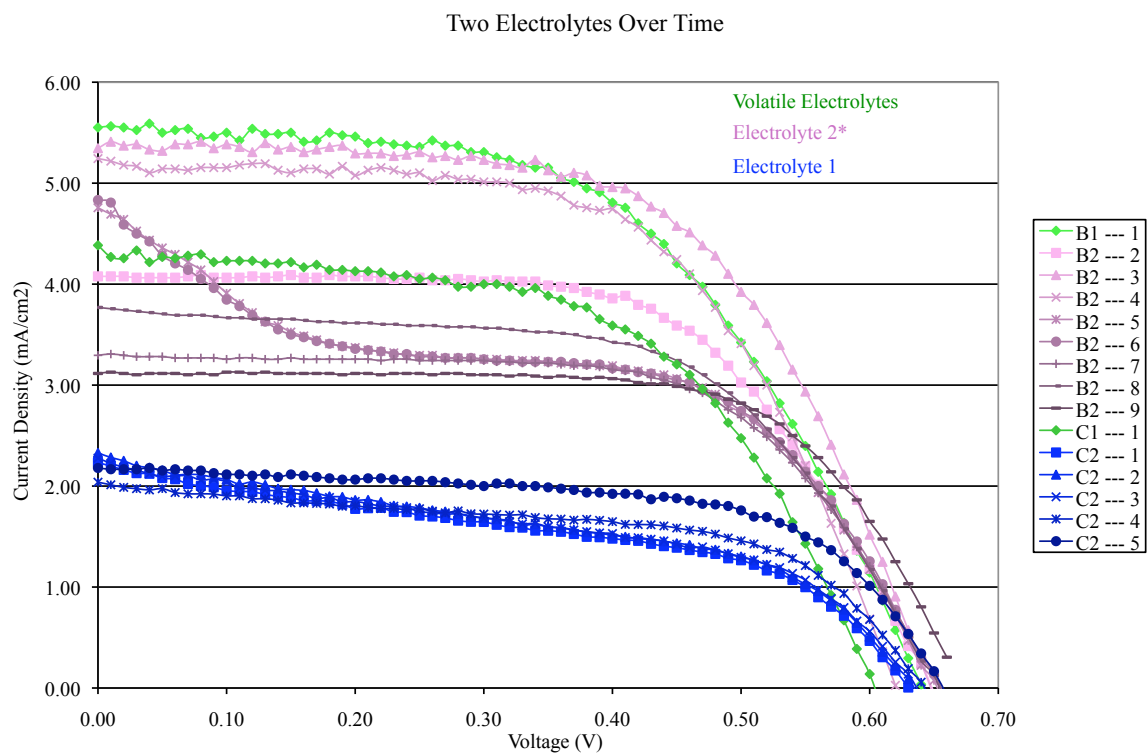
(030707 Electrolyte.xls)

Figure 5.1.6. Two formulations of ionic liquid electrolyte were tested and compared to the volatile MPN/CH₃CN electrolyte.



(061206 – all data.xls)

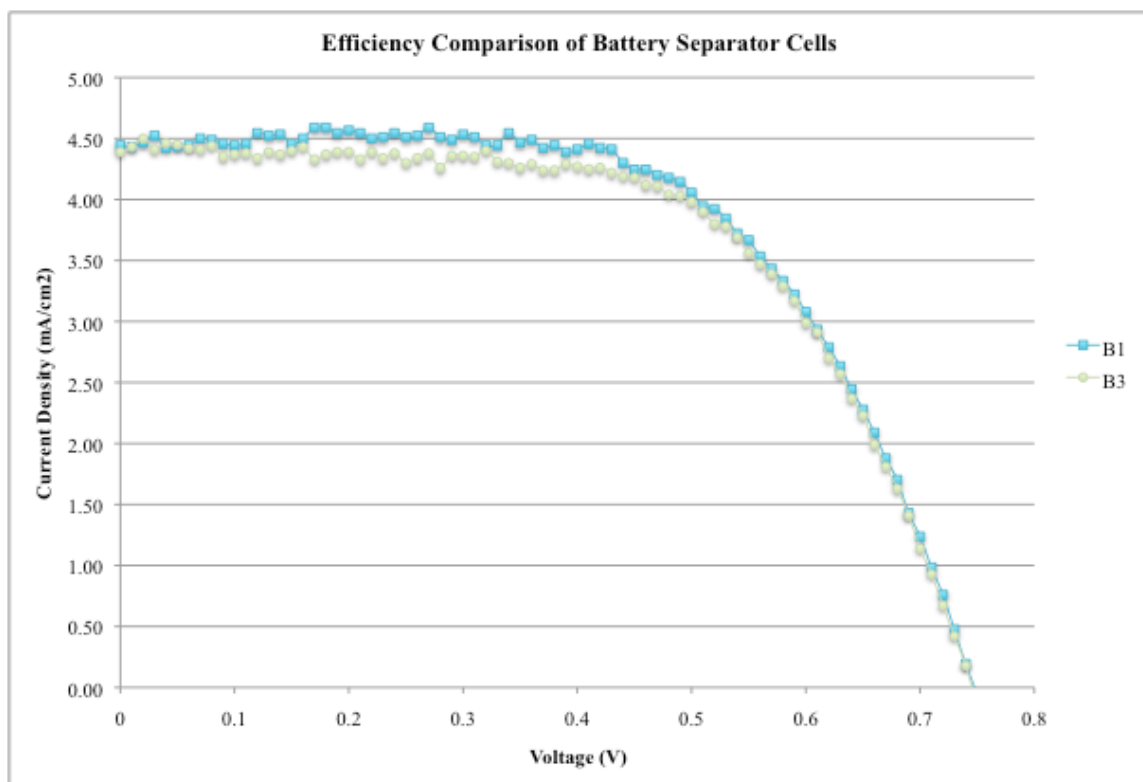
Figure 5.1.7. Evaporation of a volatile electrolyte within a cell occurs rapidly and greatly decreases the efficiency of the cell. This cell was made using the binder clip method, and such long-term tests only succeeded when better sealing methods were used.



	Isc (mA/cm ²)	Voc (V)	PP (mW/cm ²)	Vpp (V)	Ipp (mA/cm ²)	FF	Efficiency	Area (cm ²)	Electrolyte
B1 --- 1	5.55	0.64	1.9501	0.41	4.76	54.89%	2.17%	0.78	ACN/MPN
B2 --- 1	4.08	0.64	1.6277	0.46	3.54	62.38%	1.81%	0.78	2*
B2 --- 2	5.35	0.64	2.0759	0.46	4.51	60.67%	2.31%	0.78	2*
B2 --- 3	5.24	0.62	1.9169	0.42	4.56	58.96%	2.13%	0.78	2*
B2 --- 5	4.76	0.65	1.3979	0.47	2.97	45.22%	1.55%	0.78	2*
B2 --- 6	4.83	0.65	1.3918	0.46	3.03	44.30%	1.55%	0.78	2*
B2 --- 7	3.29	0.65	1.3738	0.47	2.92	64.15%	1.53%	0.78	2*
B2 --- 8	3.77	0.65	1.4626	0.46	3.18	59.70%	1.63%	0.78	2*
B2 --- 9	3.12	0.66	1.4103	0.50	2.82	68.59%	1.57%	0.78	2*
C1 --- 1	4.38	0.60	1.4664	0.43	3.41	55.74%	1.63%	0.78	ACN/MPN
C2 --- 1	2.23	0.63	0.6375	0.48	1.33	45.31%	0.71%	0.78	1
C2 --- 2	2.33	0.63	0.6572	0.48	1.37	44.81%	0.73%	0.78	1
C2 --- 3	2.28	0.63	0.6568	0.47	1.40	45.79%	0.73%	0.78	1
C2 --- 4	2.04	0.64	0.7317	0.48	1.52	56.08%	0.81%	0.78	1
C2 --- 5	2.18	0.65	0.8833	0.49	1.80	62.35%	0.98%	0.78	1

(all cells.xls)

Figure 5.1.8. Demonstration of two sets of ionic liquid electrolytes and their solar cell characteristics as the time from the cell build increases. Volatile electrolyte cells were tested once for comparison.



(cell comparison 110508.xls)

Figure 5.1.9. B1 and B3 are reproducible cells tested with battery electrolyte spacer and binder clip sealing method.

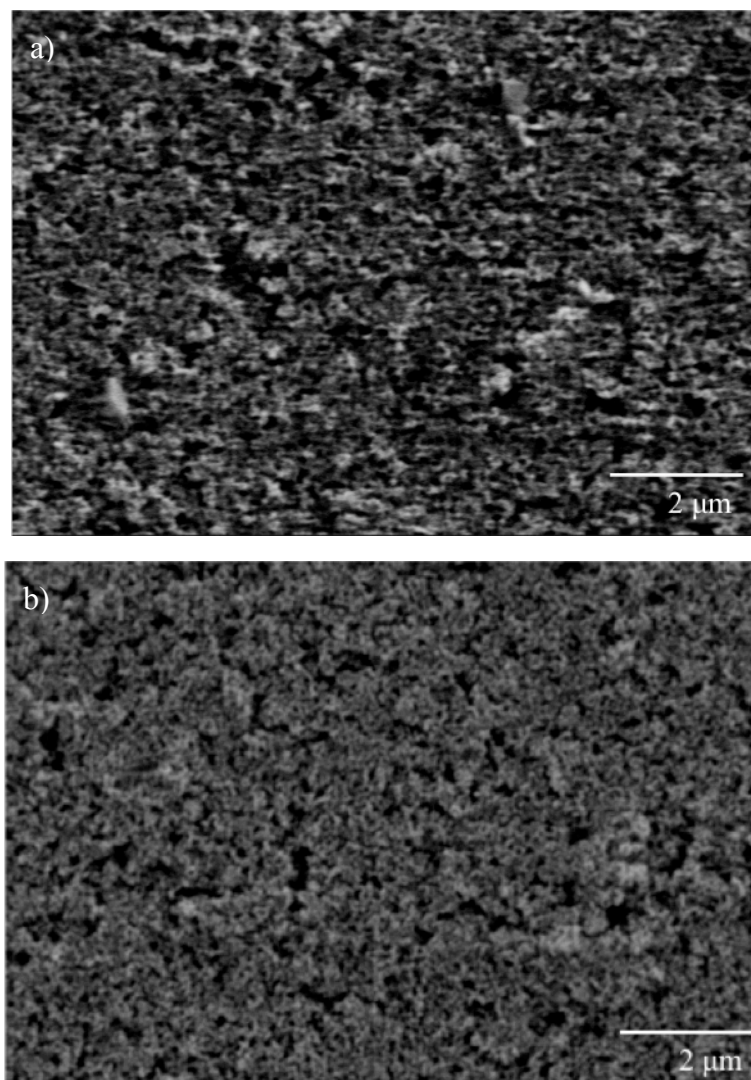


Figure 5.1.10. FESEM images of a) doctor bladed and b) spray coated titania.

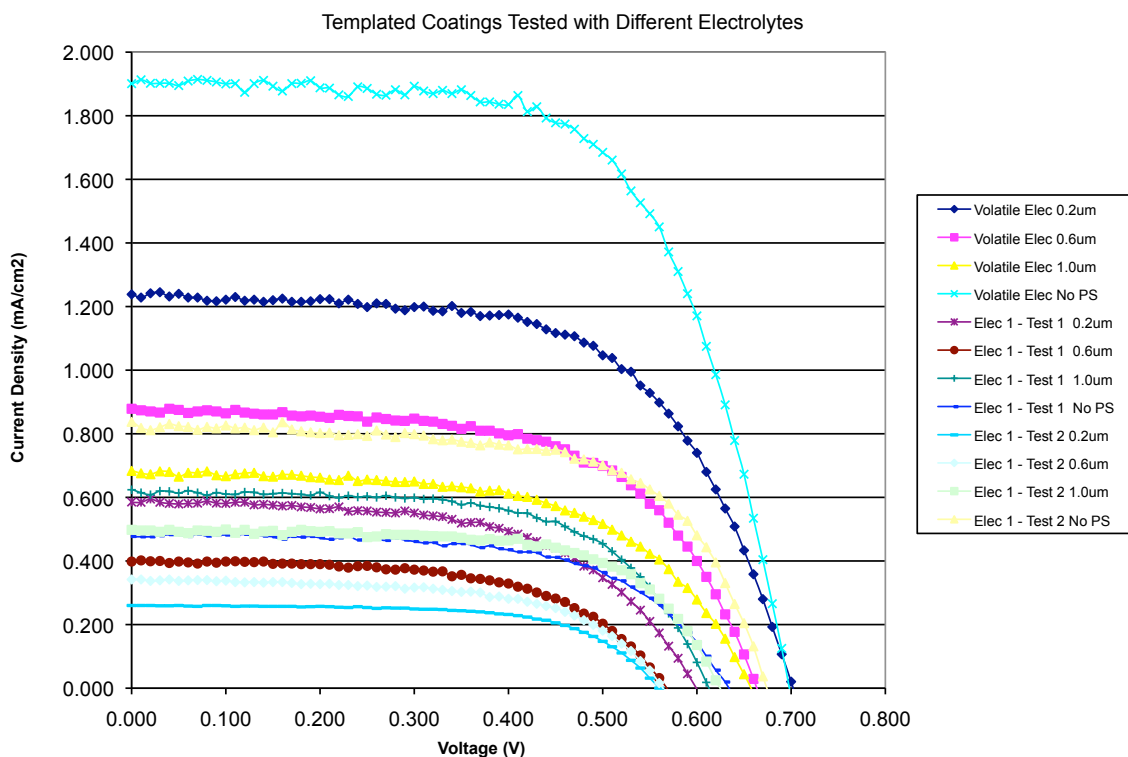
of titania used polystyrene (PS) spheres as templates. The PS spheres were added into the P25 dispersion with slight changes to the recipe such that the doctor blading deposition still produced uniform coatings. Figure 5.1.11 demonstrates the changes in the cell that occur when the PS sphere size varies from 0.2 μ m to 1.0 μ m as compared to those cells made with no PS templating. Figure 5.1.12 contains a FESEM image of templated titania coatings.

5.2: Discussion of Dye Sensitized Solar Cells

5.2.1: Comparison of Efficiency

It is apparent from the results shown in Section 5.1 that there are many variables that affect the efficiency of DSSC's. Most of the variables are easy to control such as annealing temperature and type of electrolyte, but some include a great deal of human error, including the sealing of the cells and the coating of the titania. These more difficult to control variables are the reason DSSC's tend to have some variability, as was shown in figure 5.1.1 where three control cells were made and tested. In this case, the IV curves of two of the cells differed by 20% and the third cell was 54% less efficient. With experience and improved construction methods, the cells have become more reproducible.

Using an ionic liquid electrolyte instead of iodide in a volatile solvent improved the reproducibility greatly, although it lowers the initial efficiency. This comparison can be seen in figure 5.2.1 where sealed cells actually increase in efficiency over 7 days while the binder clipped cells drop dramatically to zero efficiency. When the evaporation of the volatile electrolyte is tested, shown in figure 5.1.7, the efficiency decreases rapidly,



(all templated cells.xls AND AAA Cells Summary.xls)

			Area (cm ²)	Isc (mA/cm ²)	Voc (V)	PP (mW/cm ²)	Vpp (V)	Ipp (mA/cm ²)	FF	Efficiency
9/12/07	Volatile Elec	0.2um	0.6	1.23	0.69	0.52	0.50	1.04	61.25%	0.58%
9/12/07		0.6um	0.84	0.87	0.65	0.34	0.49	0.70	60.29%	0.38%
9/12/07		1.0um	0.66	0.68	0.64	0.25	0.48	0.53	58.69%	0.28%
9/12/07		No PS	0.99	1.91	0.68	0.83	0.50	1.66	63.82%	0.92%
9/12/07	Elec 1 - Test 1	0.2um	1.1	0.59	0.59	0.20	0.42	0.47	57.59%	0.22%
9/12/07		0.6um	1.1	0.40	0.56	0.13	0.40	0.33	59.03%	0.15%
9/12/07		1.0um	0.96	0.62	0.61	0.24	0.45	0.52	61.95%	0.26%
9/12/07		No PS	0.88	0.48	0.63	0.19	0.46	0.40	61.72%	0.21%
9/12/07	Elec 1 - Test 2	0.2um	1.1	0.26	0.56	0.09	0.44	0.21	64.56%	0.10%
9/12/07		0.6um	1.1	0.34	0.56	0.12	0.41	0.28	60.17%	0.13%
9/12/07		1.0um	0.96	0.50	0.62	0.20	0.48	0.42	64.95%	0.22%
9/12/07		No PS	0.88	0.84	0.67	0.35	0.52	0.68	62.76%	0.39%

Figure 5.1.11. Comparison of templated cells when different electrolytes are tested. Electrolyte 1 is an ionic liquid electrolyte version, while the volatile electrolyte used an acetonitrile/methoxypropionitrile solvent.

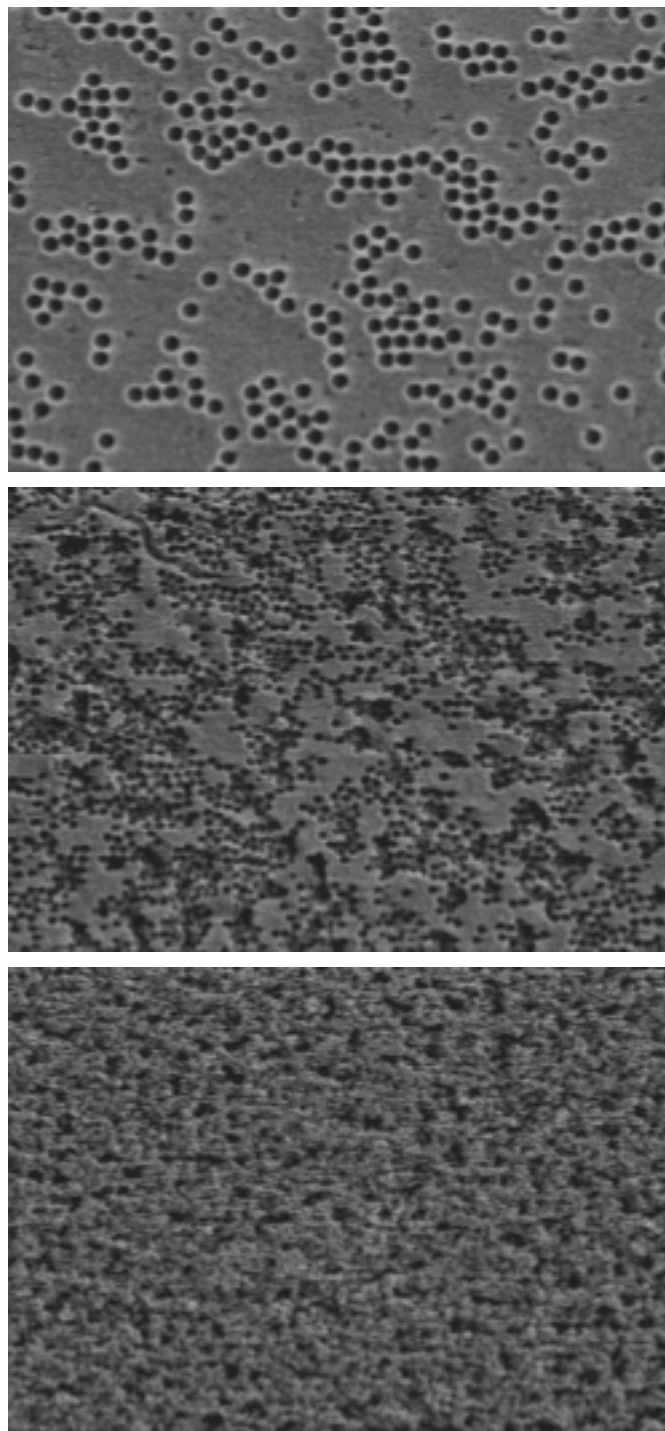
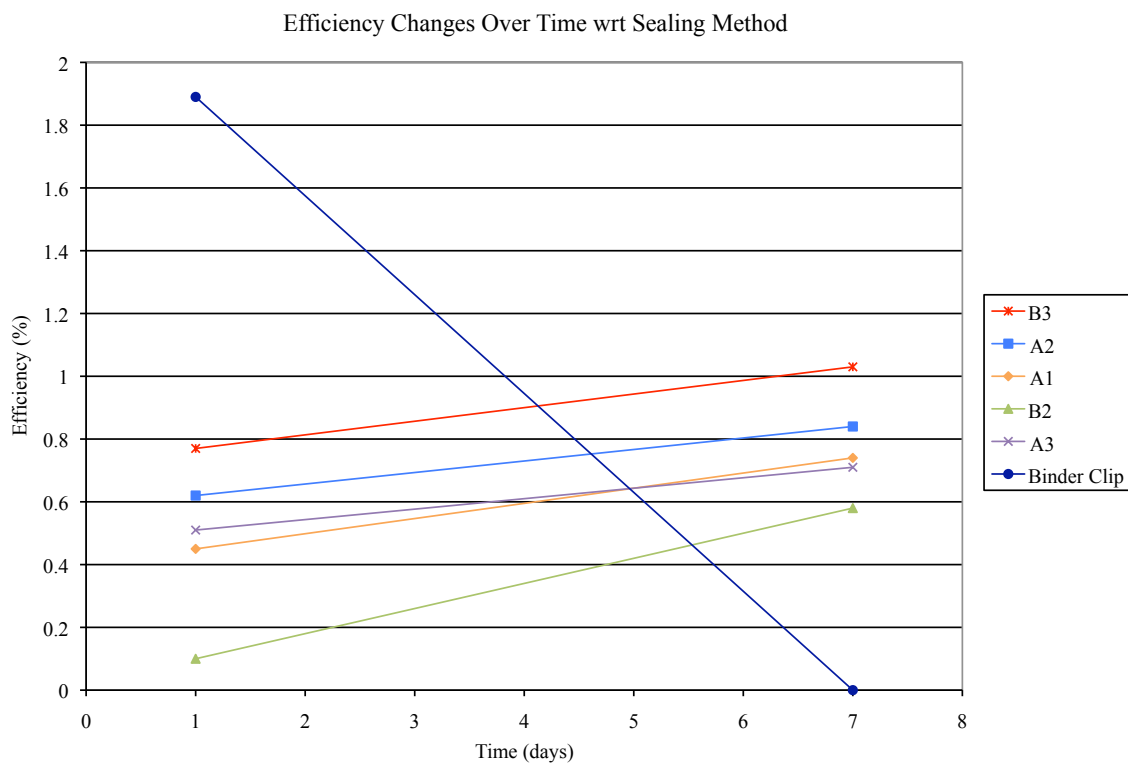


Figure 5.1.12. FESEM images of templated titania films made with 1 μm , 0.6 μm and 0.2 μm polystyrene particles.



(time tests.xls)

Figure 5.2.1. The hot melt sealed cells actually increase in efficiency over a week's time while the binder clipped cells decrease steeply to zero efficiency.

by 31% and 44% after each approximately 30-second interval.

Changes in the barrier layer and electrode materials were also tested to maximize the efficiency of the DSSC's. While it appears that the sol-gel barrier layer increases the efficiency in most cases, table 5.1.4 illustrates that using a second sol-gel barrier layer above the mesoporous titania decreases the efficiency greatly. This remarkable drop in efficiency demonstrates how important the pore volume in the mesoporous P25 layer is to producing effective currents. The double barrier layer, sol-P25-sol, design causes low efficiencies because the second layer of sol-gel fills in the pores in the P25 coating, decreasing the surface area. Since only a monolayer of dye is able to chemisorb to the titania, the output current is lowered. The type of platinum electrode that is utilized also strongly affects the advantages of the barrier layer. The graphs in figure 5.2.2 demonstrate the different results that occur when the barrier layer is used with catalytic or sputtered platinum electrodes. The cells in the sputtered platinum with a barrier layer group that short circuited were not calculated into the average in 5.2.2b as it was believed that their lack of current output was not due to the design but to mechanical problems with the cell construction. It is uncertain why the type of platinum electrode affects the importance of the sol-gel layer. With a barrier layer, the catalytic and sputtered platinum cells produce similar efficiencies, with a difference of only 1.5%. However, when a barrier layer is used in conjunction with the sputtered platinum electrode, the efficiency decreases by 20%. For the catalytic platinum cells, the efficiency increases by 56% with the addition of a barrier layer. The sputtered platinum layer is hypothesized to work more efficiently due to its reflective property that increases the amount of photons impinging on the dye, and because it has a lower resistivity than the FTO substrate

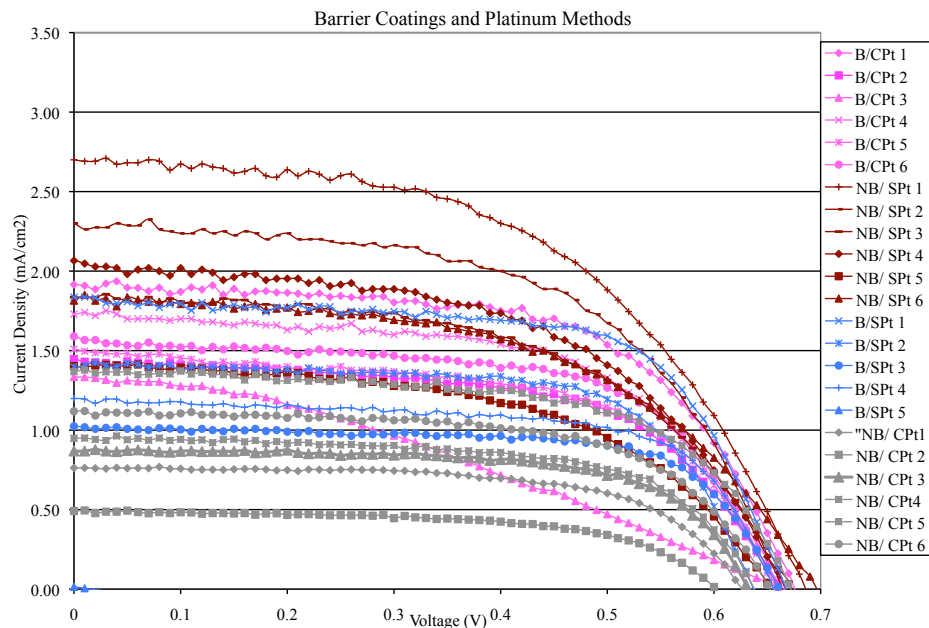
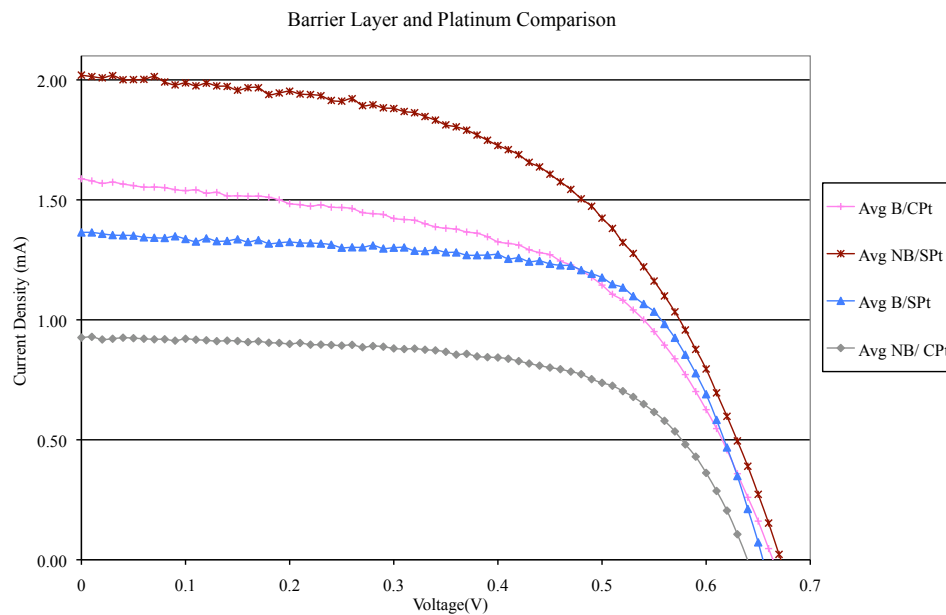


Figure 5.2.2a. Barrier coatings and types of platinum are compared in detail.



(092707.xls, 101107 Grp2 Test 1.xls, Barrier and Pt Disproven Oct07.xls)

Figure 5.2.2b. Graph demonstrates the average current for each group of cells, excluding any which short-circuited. This illustrates that the cells with a sputtered platinum layer and no barrier layer have the highest efficiency.

through which the catalytic platinum conducts.

In section 2.1, it was hypothesized that different electrodes would produce lower efficiencies than those found with platinum. This idea was tested with both gold and aluminum electrodes, replacing the platinum in the cell construction. Both metals were evaporated, separately, onto glass substrates. It was found that the platinum works 63% better than gold electrodes and that the gold dissolves rapidly, within 1 minute, in the acetonitrile and methoxypropionitrile electrolyte. The evaporated aluminum is more resistant to the solvent, but every cell tested with this electrode produced a short circuit.

5.2.2: Titania

There were three types of mesoporous titania coatings that were utilized in the different types of cells constructed: spray coated, doctor bladed and templated. Spray coating tended to result in non-reproducible coatings due to variables, such as specific distance from the substrate and pressure induced onto the spray gun trigger, that were difficult to standardize. This type of coating also caused the cells to short more often until a barrier layer coating was routinely added to the cell construction. This was most likely due to the increased porosity in these films which, while increasing the amount of dye adhering to the titania, also allowed a pathway for the electrolyte to reach the FTO electrode. Doctor blading was a more reproducible method, with repeatable thickness in the range of 15-20 μm . The disadvantages to this coating technique include edges that are up to 10 μm thicker than the rest of the coating and lower efficiency. However, due to its reproducible nature, doctor blading was the most commonly used deposition technique in this research. Templating of the titania coating produces very different pore structures

than those found in either spray coating or doctor blading. This technique and the cells produced have been published in the Journal of the American Ceramic Society¹²⁷. The improvement of the cell's efficiency with this technique is highly dependent on the type of electrolyte utilized, as will be discussed in section 5.2.3.

5.2.3: Electrolytes and Titania Interaction

The type of electrolyte and titania coating that should be chosen for use in an optimized DSSC is based on the ability of the electrolyte to penetrate throughout the pores of the titania coating. There are, however, some competing factors. If the titania film contains a network of very small pores, a viscous ionic liquid electrolyte may not be able to penetrate to all dye molecules. However, if larger pores are created for effortless passing of the electrolyte, the number of dye molecules adsorbed onto the titania film would decrease with the surface area, lowering the current output of the cell. Early DSSC researchers took little of this precise optimization of the pore structure into account because with the use of high ionic conductivity, low viscosity electrolytes, there was little chance of the liquid not reaching every pore in the networked film. However, as it was realized that the conditions for the use of a solar cell require better sealing methods, electrolytes with higher viscosity and solid state properties became more popular. No longer could it be assumed that the electrolyte reached into all corners of the mesoporous titania. In this research, the pore structure was to graduate from disorganized mesopores in the standard P25 coatings, to organized meso- and micropores in the templated PS coatings, and finally organized pores with a designed size made with nanotubes. Figure 5.2.3 illustrates schematics of each type of coating. Although the

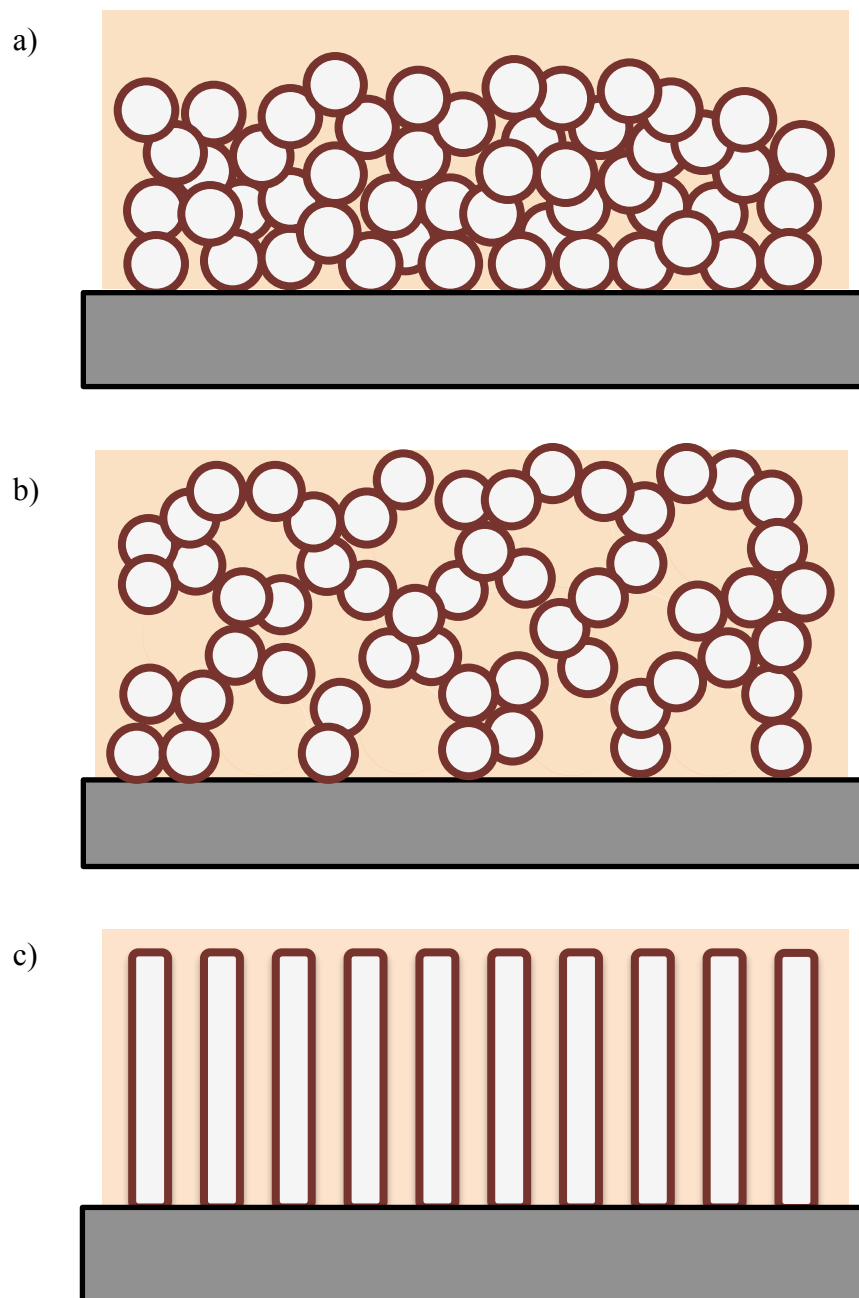


Figure 5.2.3. Schematic of titania coatings made with a) spherical nanoparticles, b) nanoparticles templated with polystyrene spheres, and c) nanorods.

final structure was not achieved as such, these different porosity types can be discussed in terms of geometric concerns for the amount of adsorbed dye and the penetration of the electrolyte. An optimal roughness factor is 1000, as this was the factor of the titania coating used in Grätzel's high efficiency DSSC's³. For a cell with a geometric area of 1cm by 1cm, this roughness factor calculates to a surface area of 0.1m². Table 5.2.1 shows the calculations for this idealized coating, including the area of the ruthenium based dye molecules and how many moles of dye molecules are adsorbed to the surface of a coating with the given surface area. Table 5.2.2 illustrates the calculation modeling done to demonstrate the geometric size of nanorods necessary for the coating to maintain the same surface area as that made with spherical nanoparticles. The calculated diameter of the nanorods is 16.8nm if they are spaced 8.4nm apart and 24.2nm if the space is decreased to 6nm. The nanorod coating allows greater penetration of the ionic liquid electrolyte because channels form through which the electrolyte can easily pass. Although only 8nm wide, the spacing allows for two dye molecules with 4nm of remaining space for electrolyte. The 6nm spacing only allows for 2nm of electrolyte, which may cause clogging. The use of these channels should increase the completeness and speed of penetration of the electrolyte when used in contrast to a microstructure with a series of winding pathways.

The templated coatings have a similar theoretical surface area to that of the spherical nanoparticle coatings; however, if all other dimensions remain the same, their surface area is decreased somewhat due to the large macropores that are inserted into the microstructure (figure 5.1.12). This can also be seen in table 5.2.3 in which the specific surface area increases as the polystyrene spheres decrease in size. Figure 5.2.4

Table 5.2.1 Optimal Spherical Nanoparticle TiO₂ Coating

Roughness Factor (RF)	Gratzel, M. <i>J Photochem Photobio C-Photochem Rev</i> 2003, 4, 145-153.	1000
Geometric Area (GA)		1cm x 1cm
Surface Area (SA)	= RF*GA	0.1m ²
Dye Molecule Area (RuA)	Rutheniumbipyridal with 2nm diameter, widest area	3.14*10 ⁻⁸ m ²
Number Dye Molecules on Rough Surface	= SA / RuA	3.18*10 ¹⁶ molecules
Mols of Dye per Area	= 1 / (RuA * Avogadro's No.)	5.29*10 ⁻⁷ mols/m ²
Mols of Dye on Rough Surface	= SA / (RuA * Avogadro's No.)	5.29*10 ⁻⁸ mols

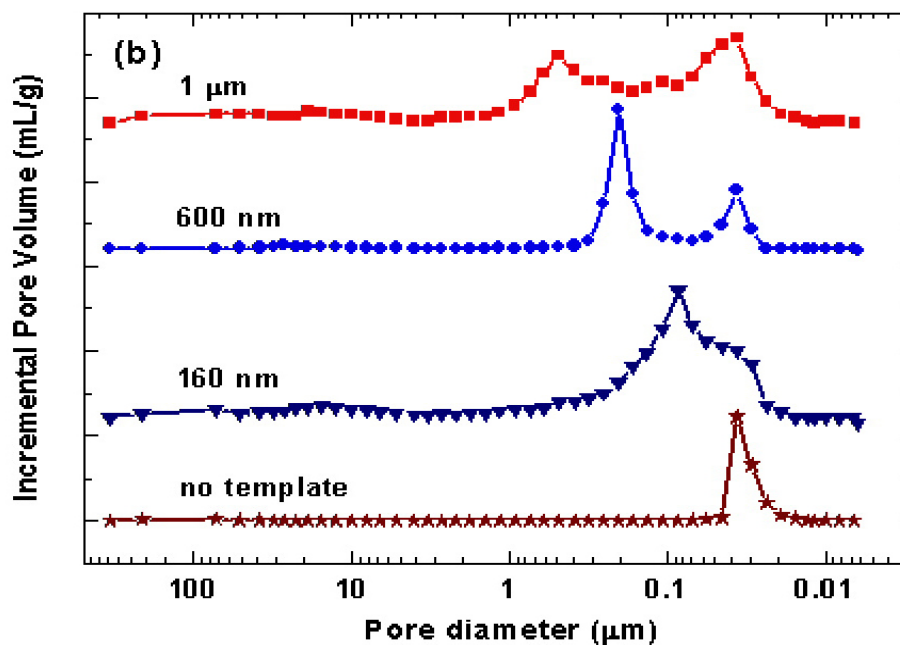
Table 5.2.2. Modeled Nanorod Coating with SA = Spherical Coating

Optimal Surface Area	$2\pi rhN + GA$	0.1 m ²
Fixed Nanorod Height		12 μm
Number of Nanorods (N)	GA/L^2	
Unit Cell Length (L)	3r	
Nanorod Radius (r)	$= (0.22\pi h * GA) / (SA - GA)$	8.4 nm
Nanorod Diameter	2r	16.8 nm
Angle before Contact with Nearest Neighbor (1 nanorod tilts)	$= \tan^{-1}(r/h)$	0.04°
Angle before Contact with Nearest Neighbor (2 nanorods tilt)	$= \tan^{-1}(r/2h)$	0.02°
Unit Cell Length (L)	2.5r	
Nanorod Radius (r)	$= (0.32\pi h * GA) / (SA - GA)$	12.1 nm
Nanorod Diameter	2r	24.2 nm
Angle before Contact with Nearest Neighbor (1 nanorod tilts)	$= \tan^{-1}(r/h)$	0.06°
Angle before Contact with Nearest Neighbor (2 nanorods tilt)	$= \tan^{-1}(r/2h)$	0.03°

Table 5.2.3. Properties of templated coatings based on the diameter of the PS spheres.

PS Size (nm)	Specific Surface Area (m²/g)	Roughness Factor (/μm)	Porosity (%)
1000	33.2	53.7	61.5
600	60.1	69.7	71
300	119.1	148.1	70.4
160	137.2	197.1	65.8

(data by Jason Qi)



(data by Jason Qi)

Figure 5.2.4. Changes in pore volume and pore diameter with respect to polystyrene sphere size and compared to P25 coating with no templating.

demonstrates differences in pore volume and pore size with changes in the polystyrene sphere size. The effect of templating can be seen especially in efficiency data comparing different types of electrolytes, as shown in figure 5.1.11. These results demonstrate the time it takes for the ionic liquid electrolyte (Elec 1) to penetrate the pores of the titania coating as after the second test, the electrolyte had penetrated the coating fully and worked best in the higher surface area, disorganized mesoporous titania coating. Ionic liquid electrolytes improve efficiency over time due to slow penetration through the pores of the titania, while volatile electrolytes give high efficiency immediately and then decrease over time due to evaporation.

The highest efficiency cell made throughout this research was 5% and was tested in collaboration with Corning, Inc. This cell used spray coated titania, a sputtered platinum electrode and was sealed with 25 μ m hotmelt. Figure 5.2.5 illustrates the data from these cells and their efficiency in comparison with similar cells tested at Rutgers. This demonstrates that this research did produce high efficiency solar cells. However, cells in the range of 2-3% with doctor bladed coatings were reproduced with less variability than others. Therefore, the “control” type cell that was used as a comparison for nanotubes and further optimization tests was that produced with doctor bladed titania annealed to 500°C, the mixed acetonitrile/methoxypropionitrile electrolyte, as the cells were only tested in the short term, and sputtered platinum electrodes.

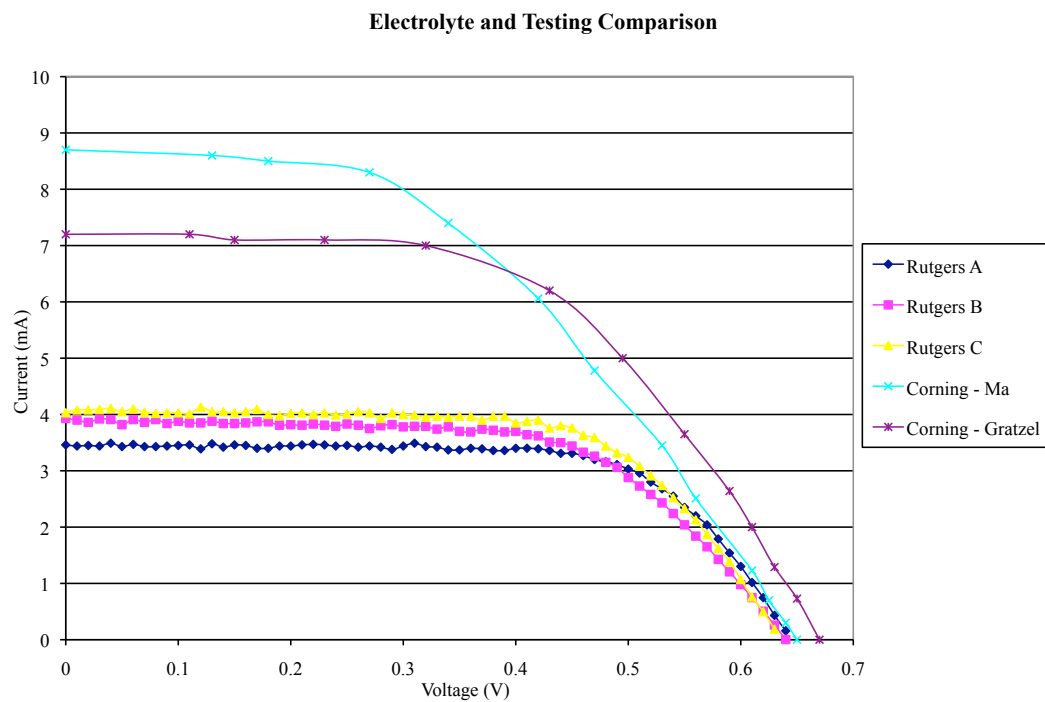


Figure 5.2.5. Testing was done in collaboration with Corning, Inc¹²⁸. and it was shown that the research cells were able to have greater efficiency with different electrolytes and testing equipment.

CHAPTER 6: HYDROTHERMAL REACTIONS

6.1: Results of Hydrothermal Reactions

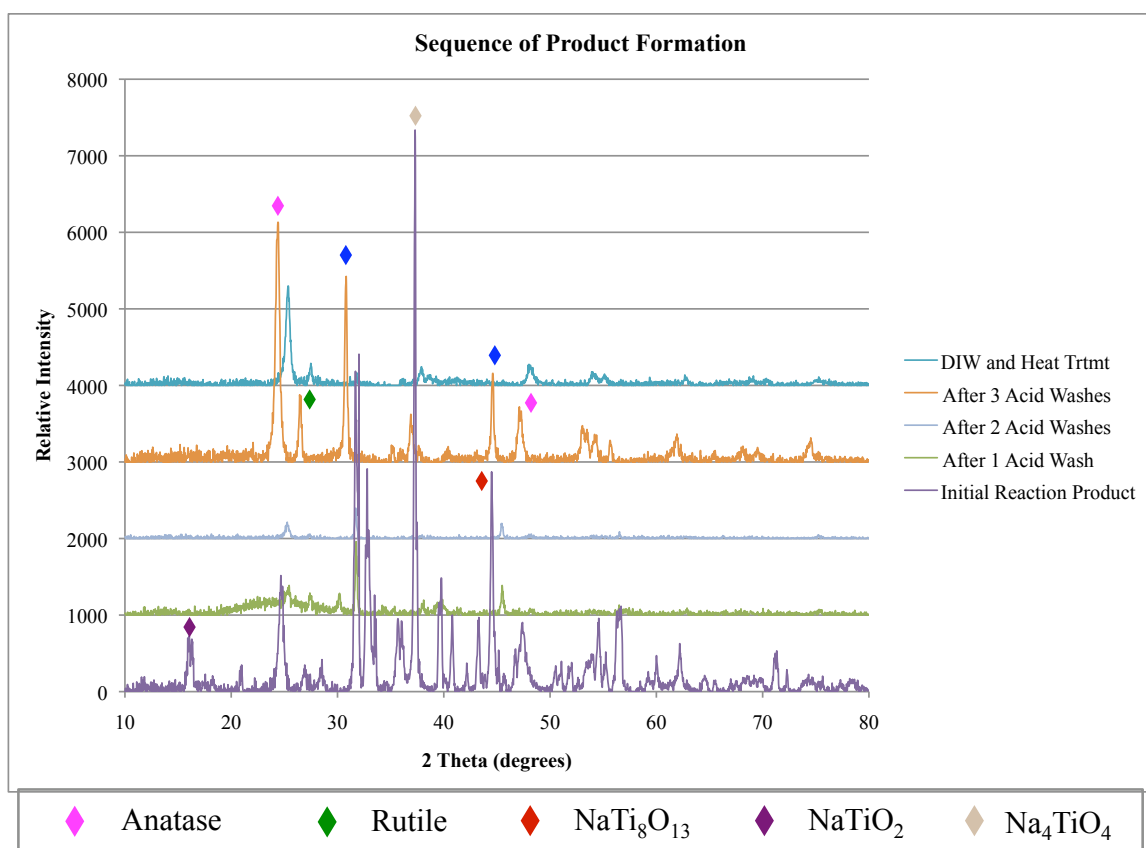
This section outlines the research conducted to produce high aspect ratio nanostructures by hydrothermal growth methods with the final objective being production of high surface area coatings. Two types of hydrothermal reactions were studied: those that were grown in solution with powders as the final product and those that were grown directly on titanium metal with coatings as the final product. The focus of this research was on the morphological and phase changes that occur throughout the reactions. The hydrothermal growth on titanium metal reactions were tested in order to remove the deposition step from the construction of the DSSC's using high aspect ratio nanostructures.

6.1.1: Solution Grown of High Aspect Ratio Nanostructures

Table 6.1.1 portrays a selection of samples made throughout 2006 showing the variables that were tested in the hydrothermal growth process. These include temperature and reaction time, amount and concentration of base, and type and amount of titania nanoparticles, which are all part of the hydrothermal reaction itself. Characterization was also done during and after the post treatment process to understand its effects. Figure 6.1.1 illustrates such a sequence of XRD patterns of sample H090606, showing that the composition varies greatly from the initial hydrothermal product to the final acid and water washed, heated titania product. The steps shown in this figure include the initial product, which is powder taken directly from the hydrothermal reactor, dried in air, and

Table 6.1.1: List of Hydrothermal Solution Samples

Sample	Temp (C)	Time (hrs)	Solution	Precursor	% Full	Rinse	Rinses w/ Acid	Rinses w/ DI	end pH
Amy 1 - S1	150	2	2.5N NaOH	solgel anatase					
Amy 1 - S2	150	2	10M NaOH	solgel anatase					
2.3	150	1	10M KOH	solgel anatase					
4.10 NaOH	200	12	2.5M NaOH	solgel anatase					
4.10 KOH	150	1	10M KOH	solgel anatase					
5PN1	100	6	5M NaOH	1.3g P25	15	EtOH			
5PN2	150	6	5M NaOH	1.3g P25	15	EtOH			
5PN3	200	6	5M NaOH	1.4g P25	15	EtOH			
H050406	120	30	10M NaOH	1.7g P25	100	HCl, DI	2	5	4
H081606	150	6	5M NaOH	1.5g P25	50	HCl, DI	2	3	
H082406	150	6	5M NaOH	5.0g P25	50	HCl, DI	3	3	
H082806	150	6	5M NaOH	3g P25	100	HCl, DI	2	3	
H083006	150	6	5M NaOH	1.5g S082906	50	HCl, DI	2	2	
H090506	150	6	5M NaOH	1.5g P25	50	HCl, DI	1	3,3	
H090606	150	6	5M NaOH	5.0g P25	50	HCl, DI	2	3	
H091806	150	6	5M NaOH	0.5g P25	50	HCl, DI	1	2	
PN091906	RT	0	5M NaOH	0.5g P25	---	HCl, DI	2	1	
H092606	90	6	5M NaOH	0.5g P25	50	HCl, DI	1	1	4.5
H101106	150	6	5M NaOH	0.5g P25	50	HNO3	2	0	
H102306	150	12	5M NaOH	0.5g P25	50	HNO3, DI	2	1	
H102406	150	18	5M NaOH	0.5g P25	50	HNO3	1	0	
H100206	150	6	5M NaOH	0.5g P25	50	HNO3	2	0	
H102506	150	12	5M NaOH	0.5g P25	50	DI	0	1	

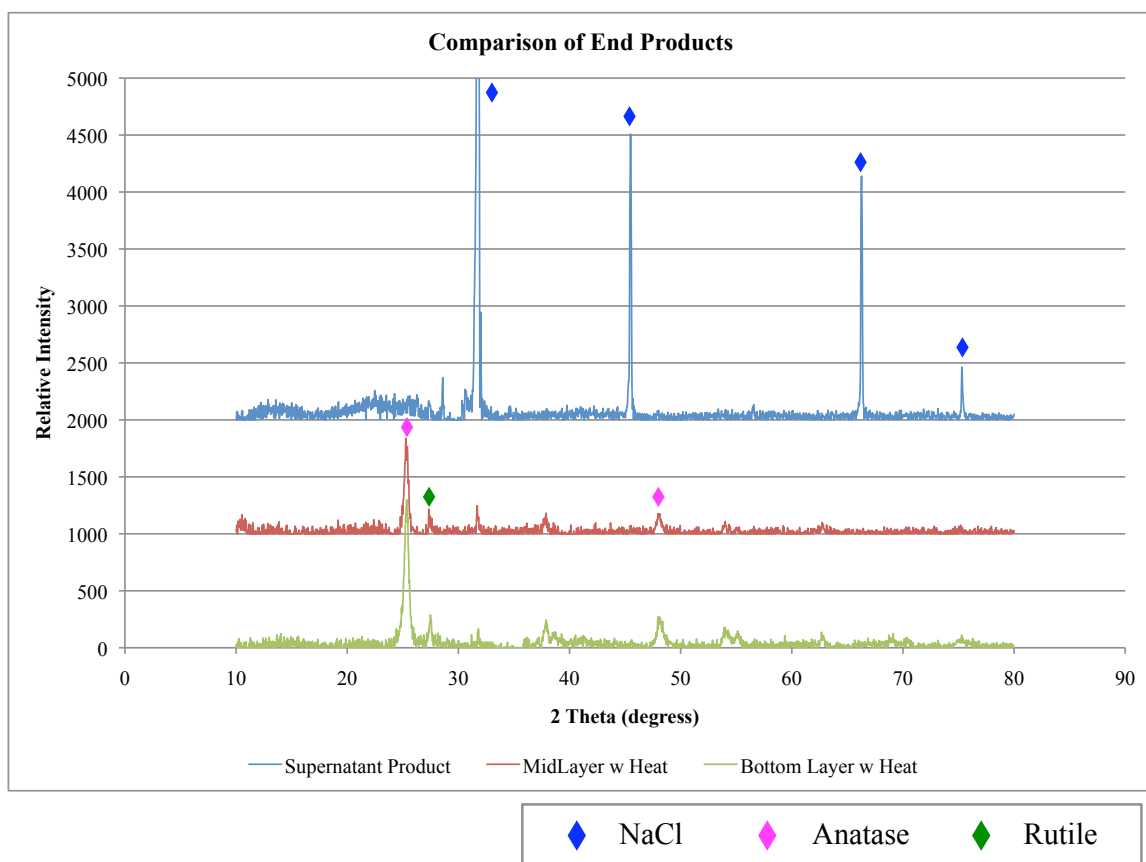


(H090606A.xls)

Figure 6.1.1. XRD data of solution growth products showing the sequence from initial material to final titania product. Sample H090606 was 5.0g P25 in 50mL 5M NaOH at 150C for 6 hours.

characterized. The next three stages consist of powder removed from the process after each acid wash. The final product is the powder remaining after the three acid washes are done, the acid is removed, and a DIW rinse is completed. In this case, the final product was not heated, although in many cases was annealed at 500°C for 30 minutes before being characterized. In the final solution, three different products were found. The first is simply the supernatant, dried in air. The other two products are white powders, one that fully precipitates, and one that remains dispersed in solution, creating a middle layer, most likely due to a smaller particle size. The XRD patterns of these different products can be seen in figure 6.1.2. It is obvious that the two white powders are of similar hydrothermal product composition while the supernatant contains simple salt from the reaction between the sodium hydroxide and hydrochloric acid. FESEM images in figure 6.1.3 illustrate the different nanostructures that form throughout the reaction sequence. The nanostructures appear to change from long needles to open ended nanotubes throughout the post treatment processes.

In order to optimize the different variables, the products of comparative reactions were characterized. The optimal temperature of 150°C was chosen based on morphology and composition after a system of reactions were run at 100, 150 and 200°C (samples 5PN1, 5PN2, 5PN3), with the XRD results shown in figure 6.1.4. FESEM images of the same samples, shown in figure 6.1.5, demonstrate that reactions done at temperatures below 150°C do not produce high aspect ratio nanostructures, but nanorods and nanofibers are found at 150°C and 200°C, respectively. Figure 6.1.6 reveals that changes in the hydrothermal reaction time, from 6 hours to 24 hours, have little effect on the initial composition of the material, illustrating that the reaction is complete at 6 hours. In



(H090606A.xls)

Figure 6.1.2. End products of the hydrothermal reaction include the supernatant after washing and two other powder products that appear to suspend at different equilibrium heights in the water wash.

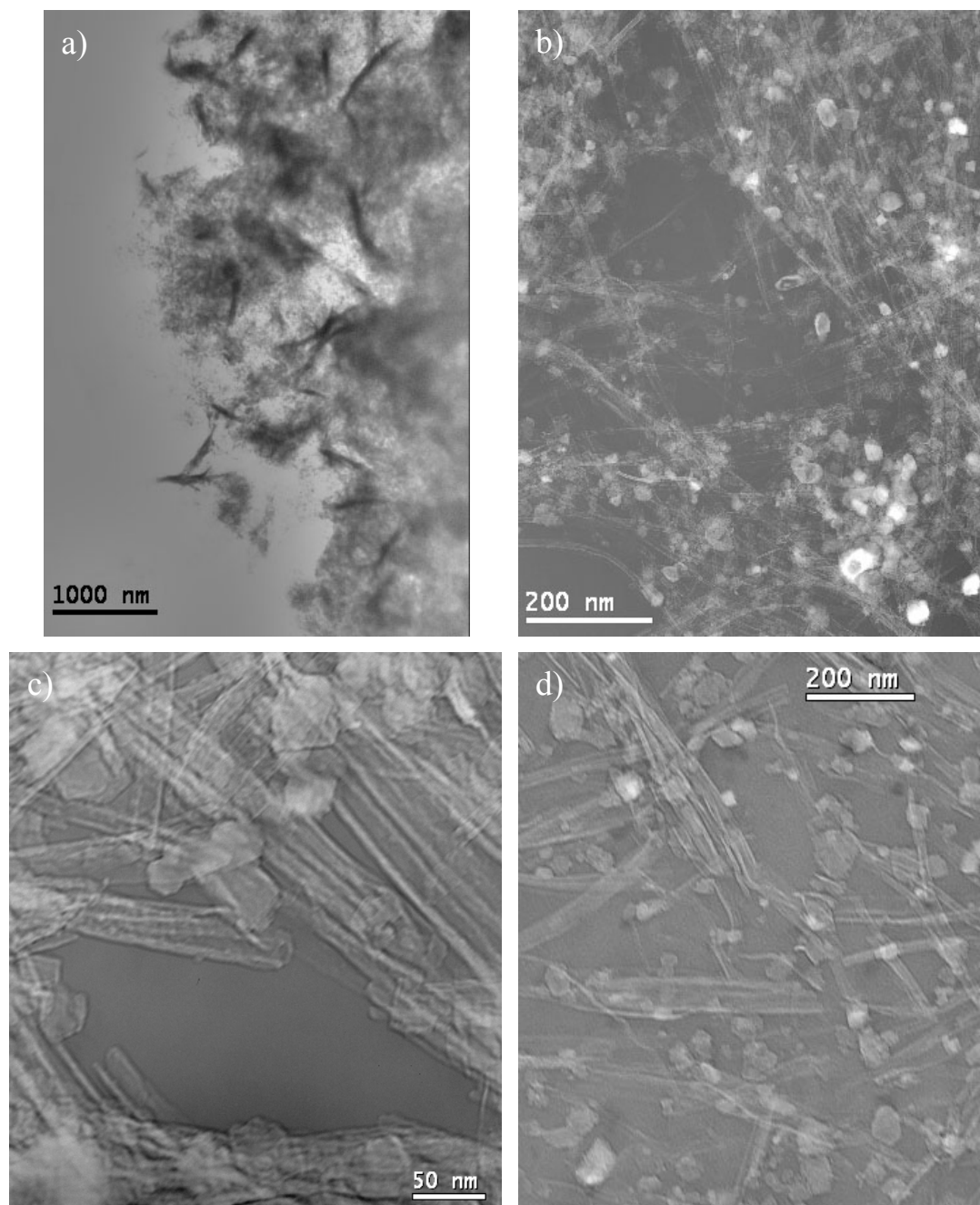
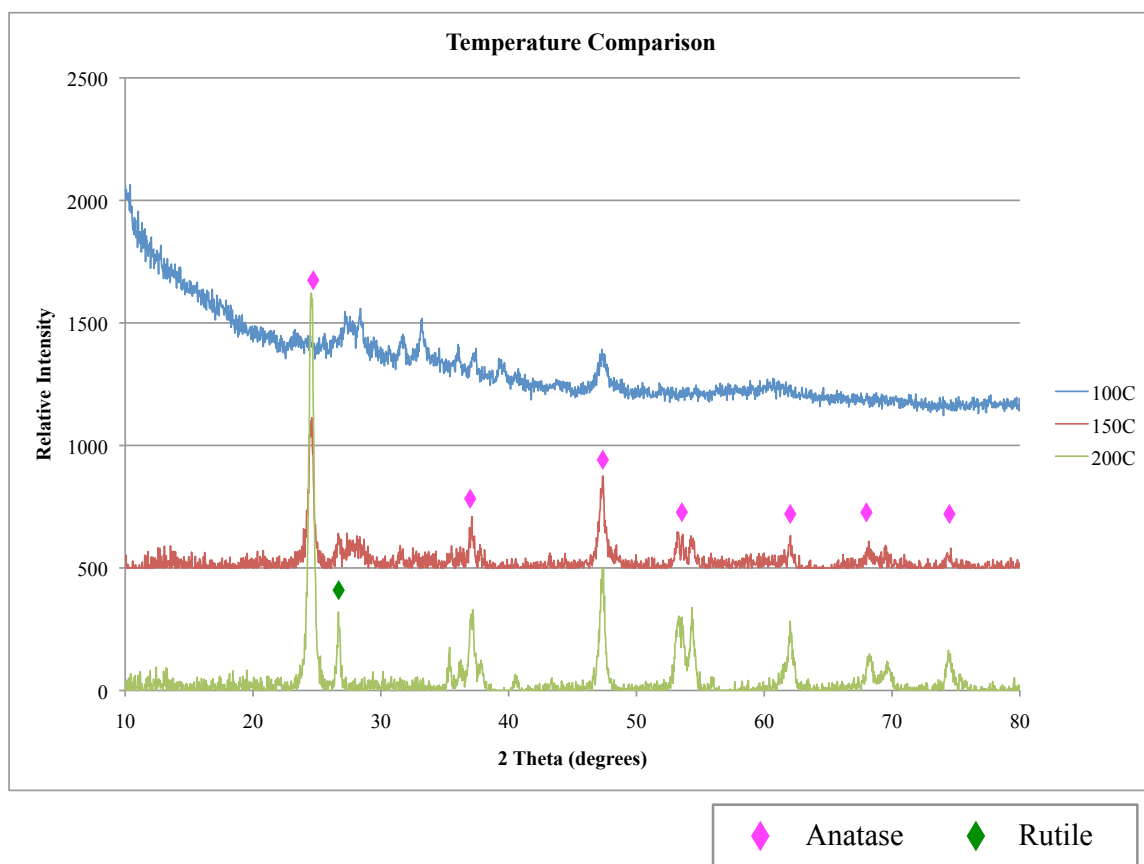


Figure 6.1.3. TEM images demonstrate the changes in the morphology due to the reaction sequence. a) Initial hydrothermal product, b) after 1 acid wash, c) end product still dispersed in solution, and d) completely precipitated final product.



(5PN Comparison.xls)

Figure 6.1.4. Comparison of composition of products formed at different temperatures.

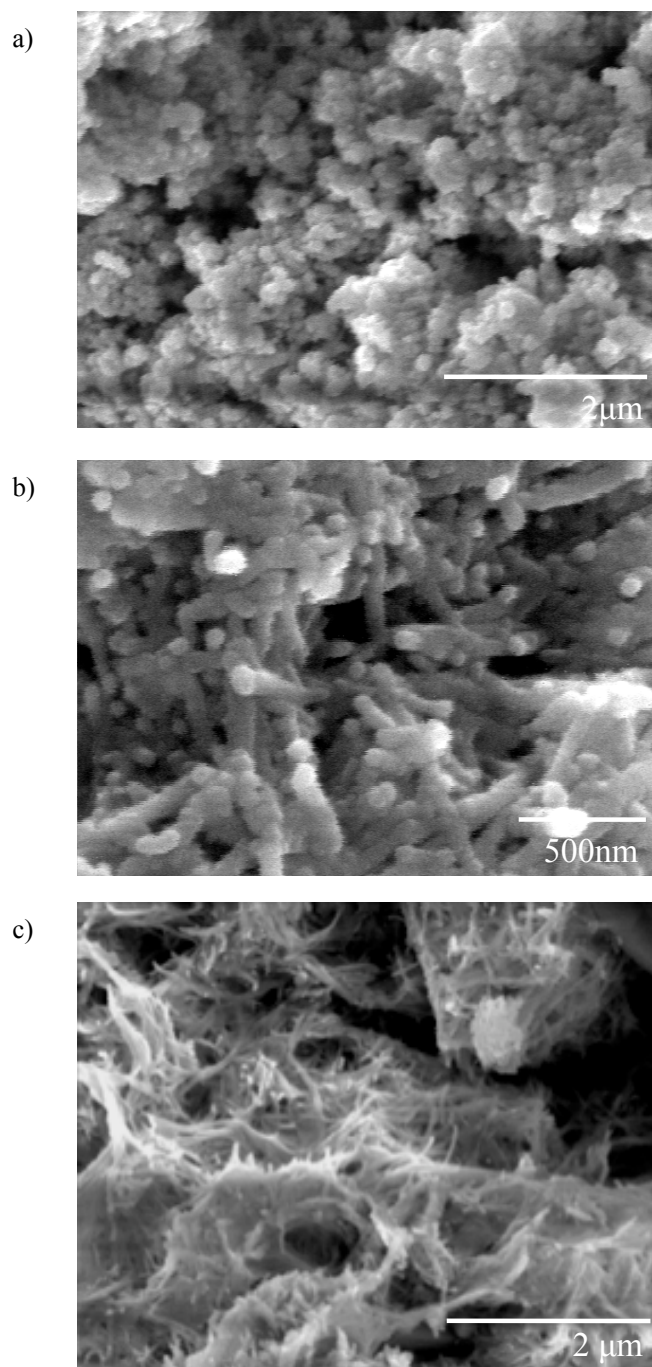
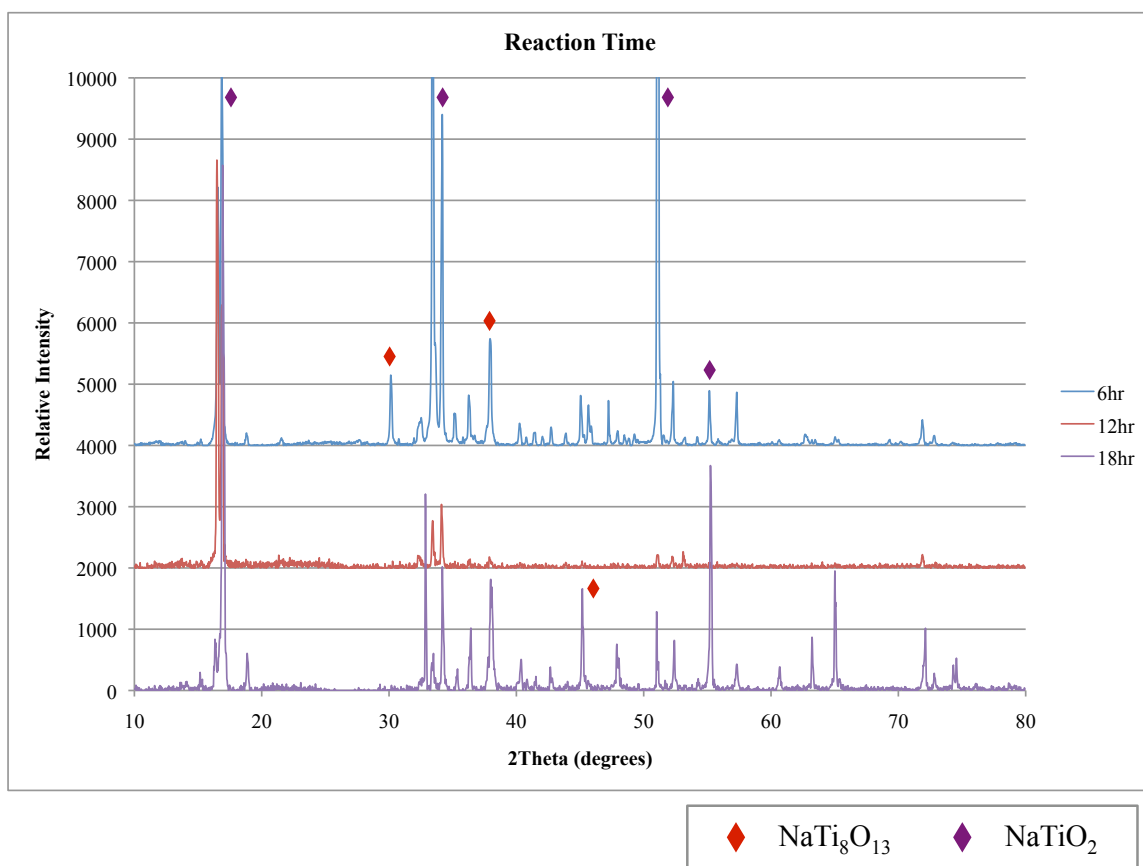


Figure 6.1.5. Images of the product morphology when the reaction temperature is a) 100°C, b) 150°C and c) 200°C.

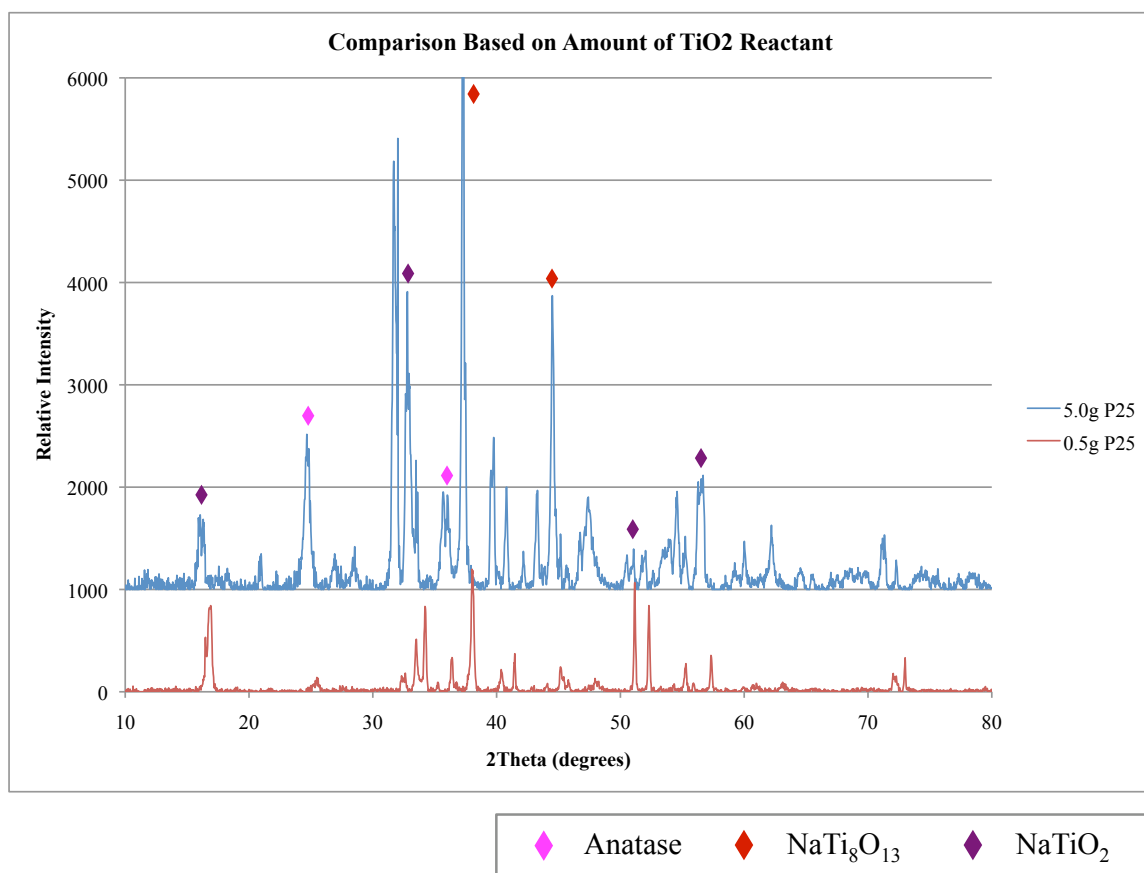


(Reaction Time Comparison.xls)

Figure 6.1.6. Changes in the reaction time cause only slight differences in the composition of the initial product when tested directly after the hydrothermal reaction.

regards to the reactant concentration, a large amount of the P25 reactant causes a greater concentration of unreacted particles to be found in the initial product, and the compositional variability is greater than in the product made with a smaller amount of P25. These differences can be seen in figure 6.1.7. The effect of the concentration of the base in the initial hydrothermal reaction is shown by FESEM images taken of two samples, one reacted in 2.5M NaOH and one reacted in 10M NaOH, in figure 6.1.8. The lower concentration of NaOH does not produce high aspect ratio nanostructures as higher concentrations do. Throughout the research, XRD patterns were taken of the final products to determine the effect of different hydrothermal reaction and post treatment conditions, and figure 6.1.9 illustrates a summary of these. The similarities in the composition of the final products, after post treatment processes, demonstrate that the final product composition is somewhat independent of the reaction variables.

By using TEM, the different structures formed throughout the hydrothermal reaction can be clearly seen. Figure 6.1.10 shows the quasi-spherical microstructure of the P25 nanoparticles (Degussa), which were used in all hydrothermal reactions, unless otherwise mentioned. The diffraction pattern illustrates the polycrystalline nature of the particles. TEM was done on samples taken directly out of the hydrothermal bath and a variety of structures are found before the post treatment processes take place. An image of one of the disordered variations is found in figure 6.1.11. The disordered structure is shown by the combination of spots and rings in the diffraction pattern. While these shapes can be found in the TEM images, nanotubes were more frequent, such as those seen in figure 6.1.12. The particles seen in conjunction with the nanotubes are assumed to be unreacted P25, as they appear quite similar to those seen in figure 6.1.10. The



(amount P25 added comparison.xlsx)

Figure 6.1.7. The initial product includes a larger concentration of unreacted particles as well as increased compositional variability when 5.0g P25 are used in the hydrothermal reaction as compared to 0.5g.

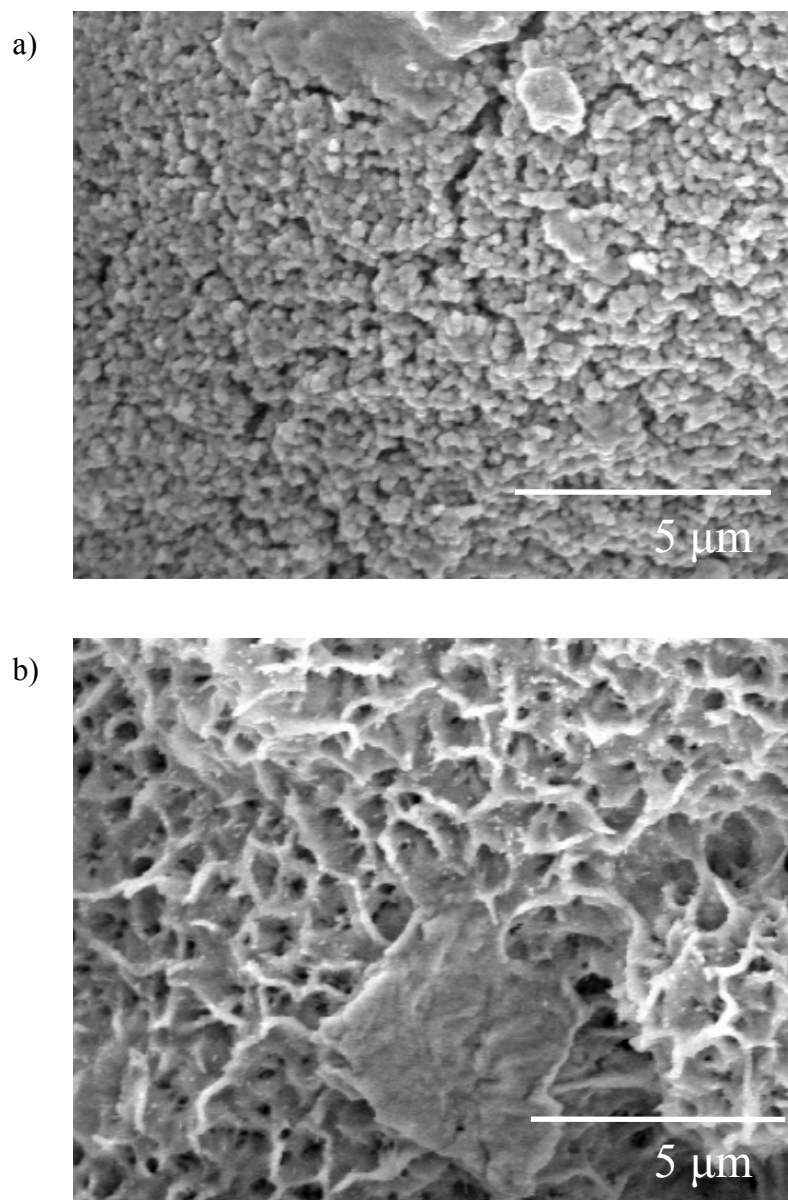
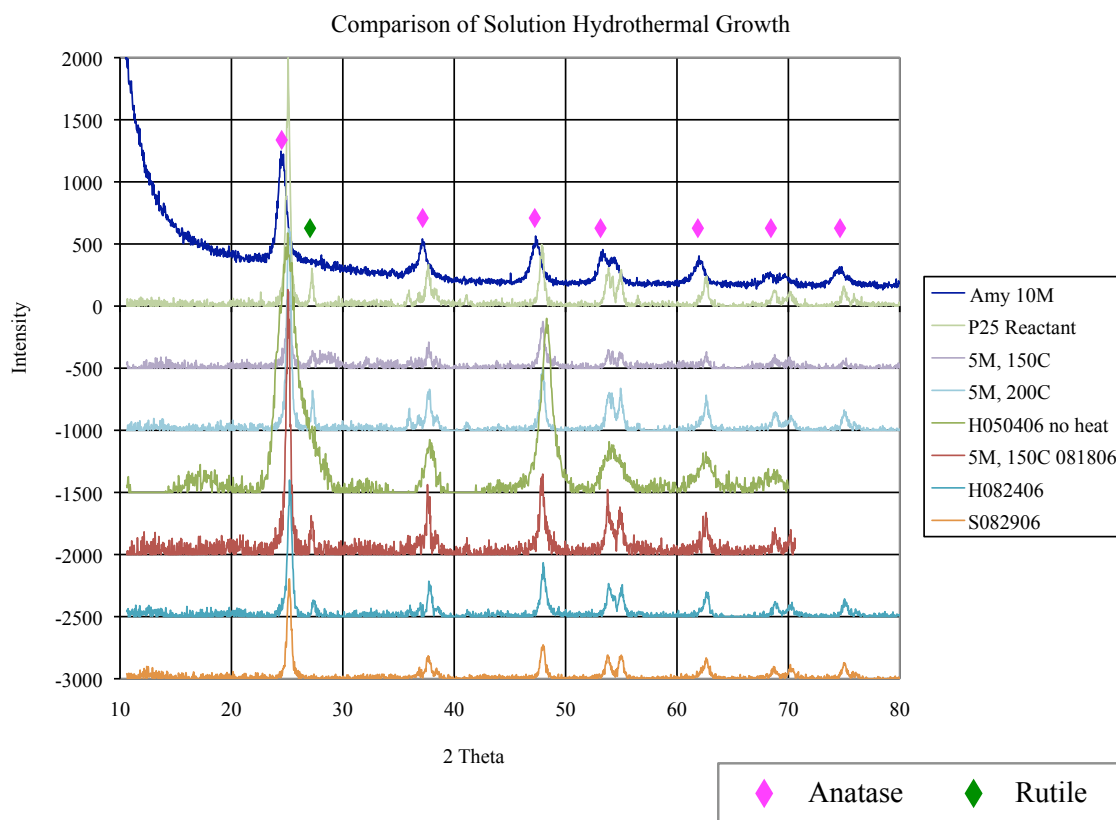


Figure 6.1.8. When the concentration of the NaOH solution is increased from a) 2.5M to b) 10M, a large increase in surface area is seen.



(091806 – JDS – Update on TiO₂ Nanotubes.ppt)

Figure 6.1.9. XRD data showing solution growth products to be titania.

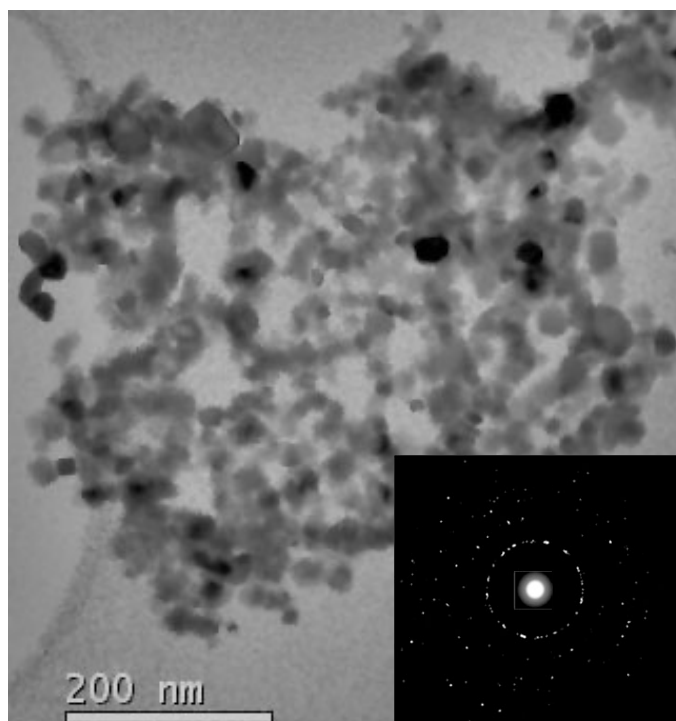


Figure 6.1.10. TEM image and diffraction pattern of commercially available P25 show morphology of reactant nanoparticles.

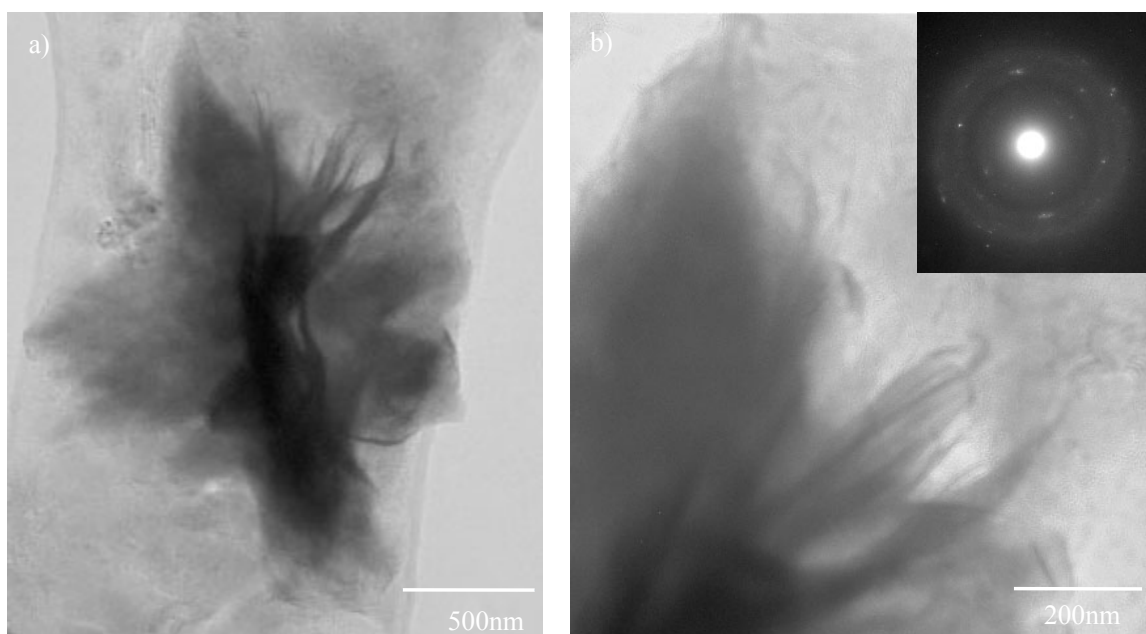


Figure 6.1.11. Disordered structures are seen after 6 hours at 150°C in 5M NaOH. TEM images show a) complete flower shape and b) magnified edge with diffraction pattern.

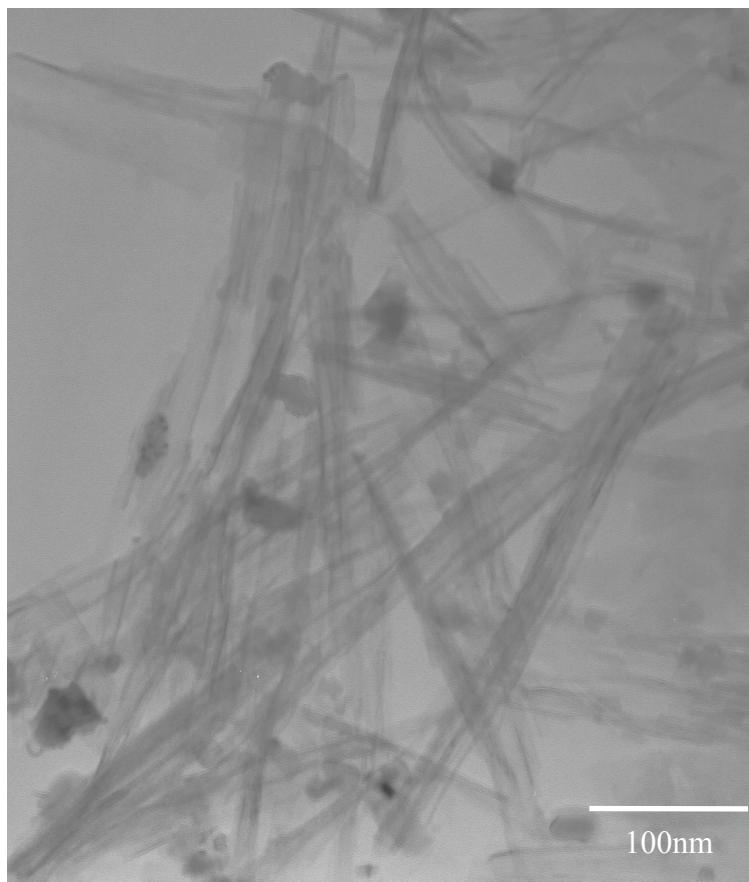


Figure 6.1.12. This TEM image shows nanotubes that form during the initial hydrothermal reaction, not in the acid wash phase.

nanotube morphology is maintained after acid washing with little changes to the structure, as the products after post treatment processing are shown in figure 6.1.13.

After the hydrothermal reaction was fully characterized, the next step was to test the nanostructure products in DSSC's. To do this, the products had to be deposited on FTO substrates. Figure 6.1.14 shows an initial test of deposition of the products done on a silicon wafer to simplify the characterization. In this image, it can be seen that the nanotubes hold up to the deposition treatment and create interesting secondary structures. More discussion on this area of work can be found in sections 6.1.3 and 6.2.3. To simplify cell construction, the ability to remove the deposition step completely was tested by producing high aspect ratio nanostructures grown directly on titanium metal, which will be discussed in the next section.

6.1.2: Nanostructures Grown on Substrates

Hydrothermal growth on titanium metal was done similarly to the solution growth system with the same variables being tested and using XRD and FESEM for characterization. A variety of samples were run to determine the optimal conditions to grow high aspect ratio nanostructures with minimal width and maximum height, which would give coatings with the highest surface area. It was found early on that very different microstructures could be produced, which were dependent on the base concentration, reaction time and whether additional titania nanoparticles were added to the solution. Table 6.1.2 contains a list of some of the tested samples that includes the structures formed as the three main variables were changed. It has been found that there are areas of each morphology within the variable window. For example, under 5M

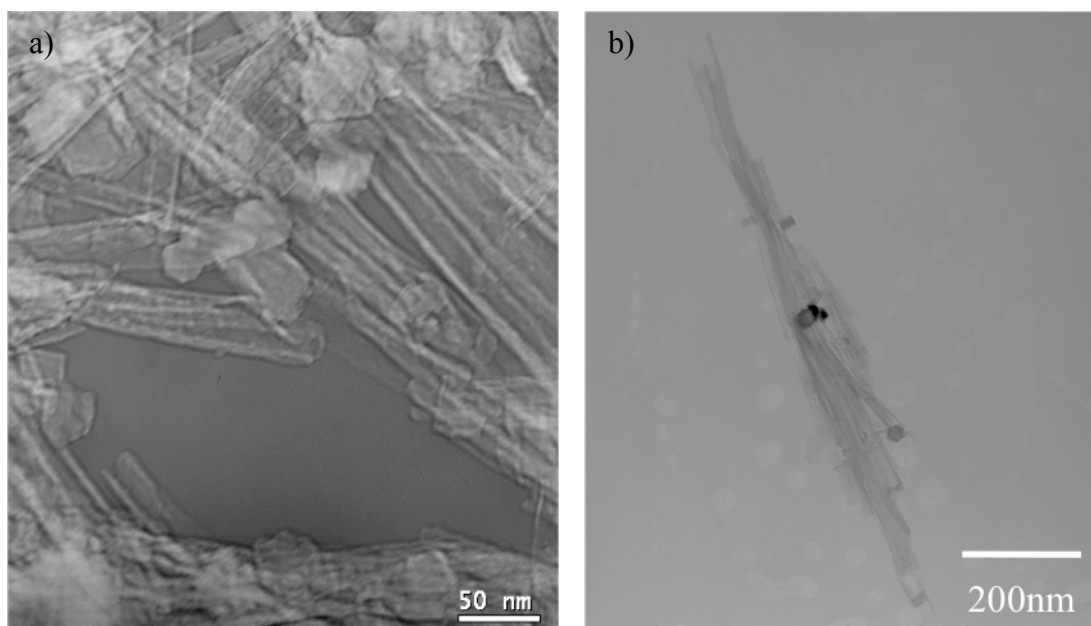


Figure 6.1.13. Open ended nanotubes form as an end product a) in sample H090606, after acid washing and aligned nanotubes are seen in b) sample H102306, after acid washing.

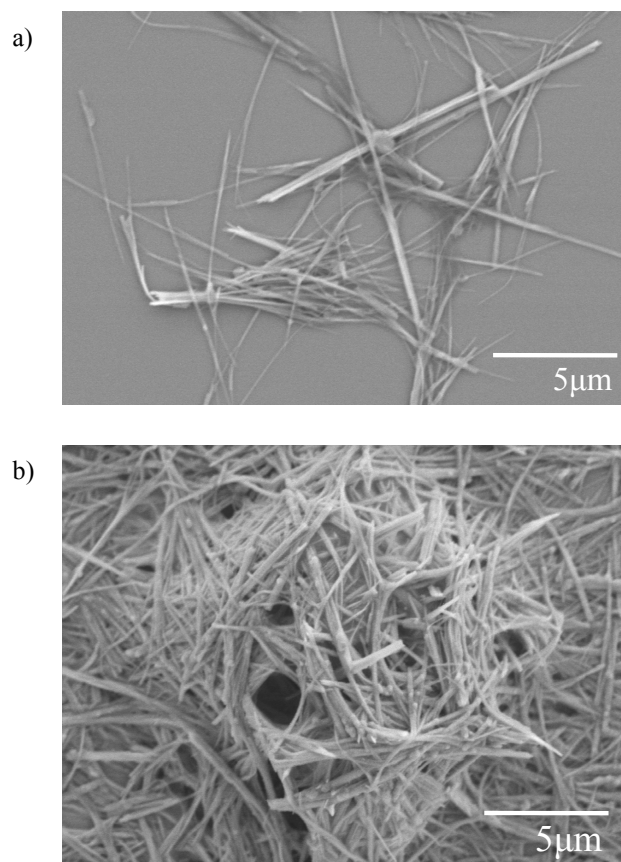


Figure 6.1.14. Deposition of high aspect ratio structures and the secondary structure that forms.

Table 6.1.2. Products Formed by Hydrothermal Growth on Titanium Metal

	1M	5M	10M
3hr, Ti metal	071808: Fibrous, belt-like	072108: 2-5 μ m platelets on wide fiber bkgd	041808: 5-10 μ m platelets on wide fiber bkgd
18hr, Ti metal	021708: Flat sheets, early platelet 070108: long thin fibers and some sheets	021508: 20-25 μ m platelets on thin fiber bkgd	021808: Flat sheets, early platelets 031308: 20 μ m platelets, wide thin ribbons
3hr, Ti + P25	070708: Fibrous, belt-like, clumps on bkgd	072208: thin fibers, some wide strips, clumps on bkgd	042508: long thin fibers mostly clumped together
18hr, Ti + P25	071608: Fibrous, belt-like, clumps on bkgd, some lg platelets	021408: thin fibers, mostly open web, some fibrous clumps	021608: long thin fibers very clumped together

NaOH, only the preliminary ruffle structures are formed.

The morphology of the products has been characterized with FESEM. Figure 6.1.15 illustrates the untreated titanium metal as it was most often used as a reactant in the hydrothermal reactions. Three types of reactions were run overall, those with untreated titanium metal in just sodium hydroxide, those with titanium metal in sodium hydroxide with additional titania nanoparticles, and those where the substrate is titania coated titanium metal in sodium hydroxide. The initial tests were done on the P25 coated onto titanium metal, which was then hydrothermally grown in NaOH, following the work of Tian, et al⁶³. Figure 6.1.16a shows images of these coatings where large platelet structures often form. To determine why platelets form instead of nanotubes or nanofibers as expected, reactions were then undertaken with no titania at all. These also produced platelets, as shown in figure 6.1.16b. Finally, additional P25 was added to the reaction solution and this led to a complete lack of platelets and instead led to nanofiber formation, seen in figure 6.1.16c. These figures were taken at different reaction conditions and the reaction conditions for each structure type is more carefully delineated below.

The samples depicted in figure 6.1.17 were hydrothermally grown at 150°C with only titanium metal and 50mL of the appropriate NaOH solution in the reactor. These images demonstrate the changes in the morphology as the reaction time is increased and the NaOH concentration is increased. In figure 6.1.18, similar hydrothermal reactions were run, but with 0.5g P25 added to the reaction. The differences in morphology demonstrate that no platelets form when additional TiO₂ nanopowder is in the system. Three different types of morphological structures were found in figures 6.1.17 and 6.1.18,

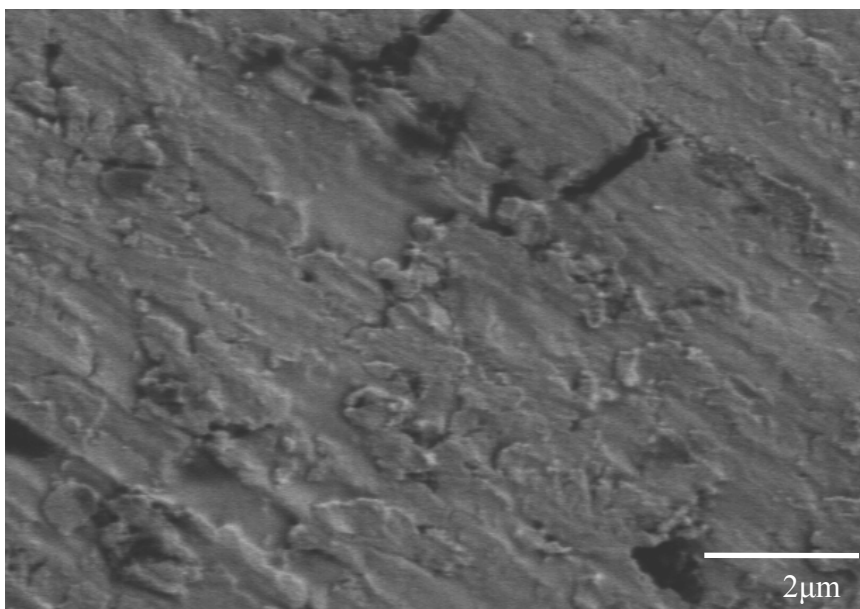
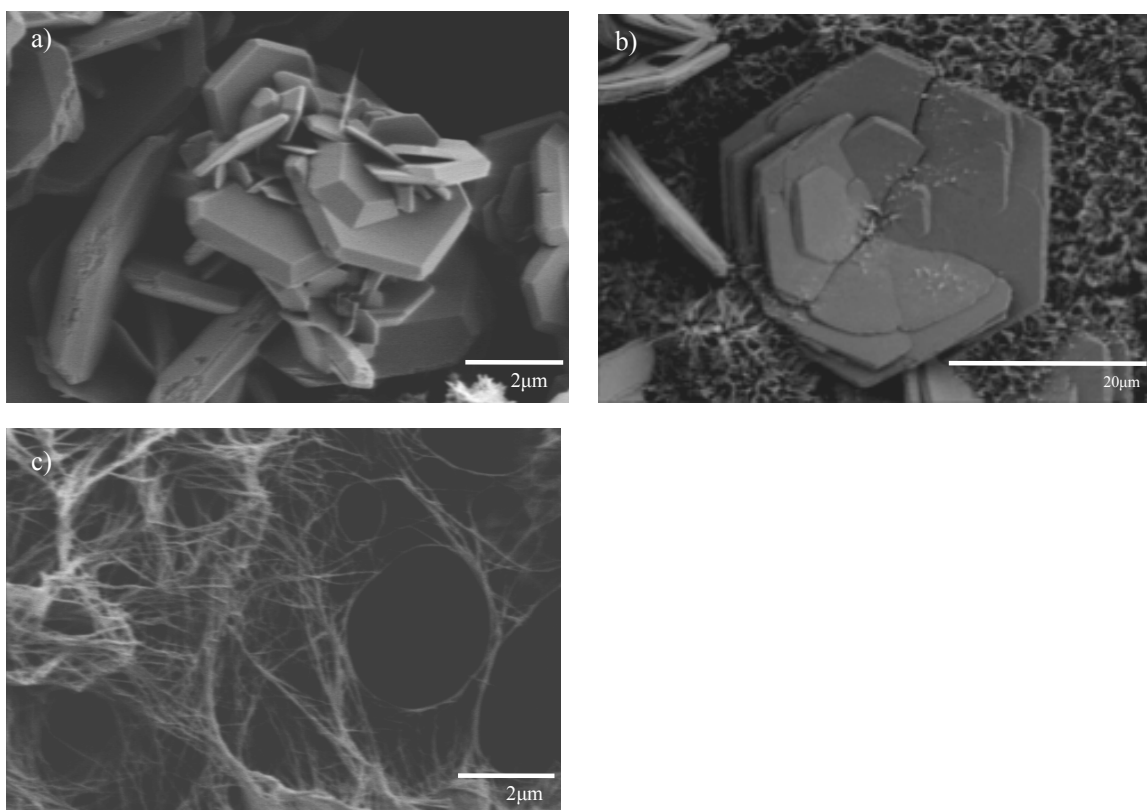


Figure 6.1.15. A FESEM image of the untreated titanium metal from Sigma Aldrich used in the hydrothermal reactions.



(TiO₂ and titanate on Ti metal.pptx)

Figure 6.1.16. FESEM images show the range of microstructures produced a) with TiO₂ film on Ti, b) untreated Ti and c) additional TiO₂ nanoparticles added to solution.

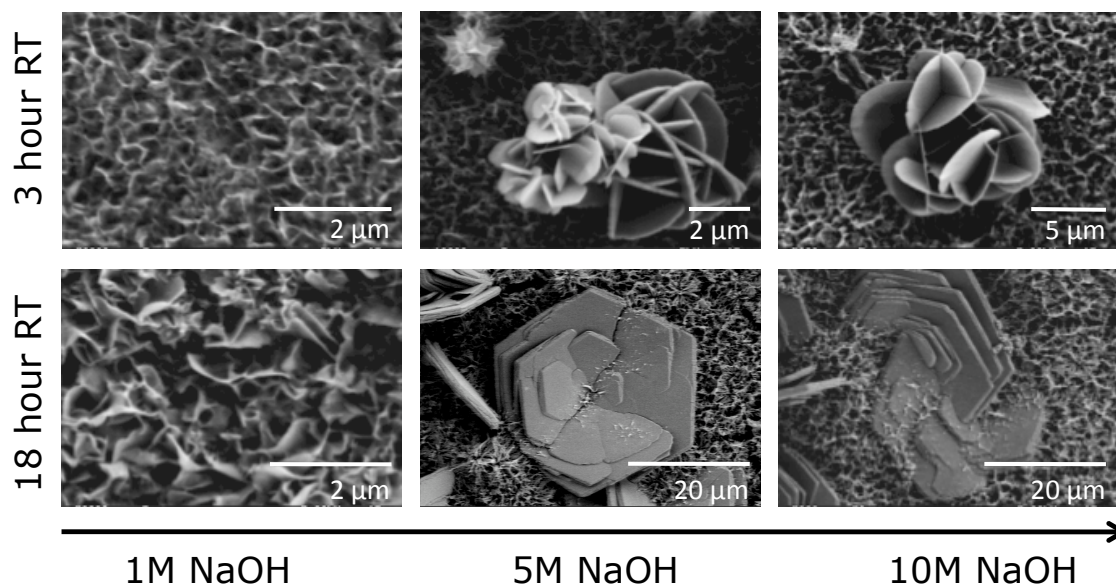


Figure 6.1.17. These images demonstrate the changes in the morphology with reaction time and NaOH concentration when no TiO_2 is added to the reaction.

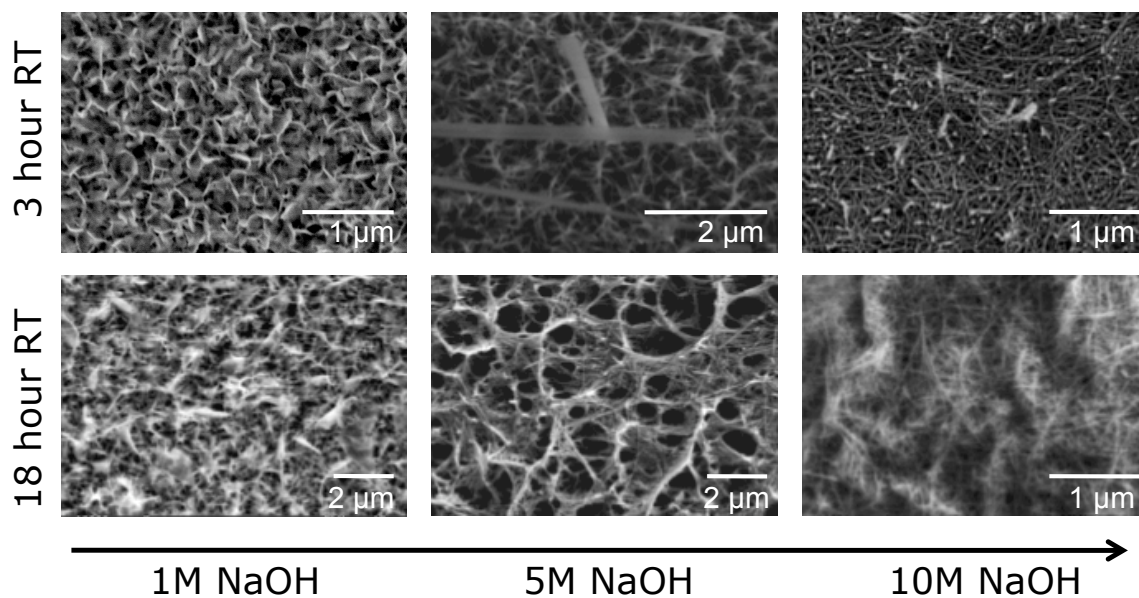


Figure 6.1.18. Nanofibers are formed when P25 is added to the hydrothermal reaction independent of reaction time or NaOH concentration. The size of the nanofibers is affected by NaOH concentration.

including preliminary ruffle forms, large platelets without additional TiO_2 and nanofibers when TiO_2 is added. The compositions for some of these samples were tested with XRD. In figure 6.1.19, the XRD results for the samples with a wide ribbon morphology formed at low reaction time or low NaOH concentration are shown. The platelet morphology is formed under a wider range of reaction conditions including 5-10M NaOH and reaction times from 12-24 hours, as long as no TiO_2 is added to the system. The compositional variability in these products is shown in figure 6.1.20. Figure 6.1.21 demonstrates the XRD patterns of the nanofibrous coatings, which appear to be titanium dioxide, and are formed when titania nanoparticles are added to the hydrothermal reaction system.

As the addition of TiO_2 was the necessary step to growing only high aspect ratio nanostructures, another method of adding titania was also tested. Spun sol-gel films, similar to those used as a barrier layer in DSSC's, were coated onto the titanium metal and this substrate was then hydrothermally reacted. Although some platelets could be found in these cases, it appears that as the thickness of the sol-gel layer increased, the amount of platelet formation decreased. An image of the hydrothermally reacted sol-gel is shown in figure 6.1.22a.

While it was shown in section 6.1.1 that the acid washing treatment did not degrade the nanotubes, it has been found that the reaction systems are quite different when Ti metal is added to the system. In this case, figure 6.1.23 illustrates that the acid washing causes a loss of the open microstructure although nanofibers can still be detected in the final product. For this reason, different washing steps were tested with the sol-gel hydrothermal coatings. A simple water wash was tested at an increased temperature of 80°C and for 3 days. The microstructure was maintained, as can be seen in

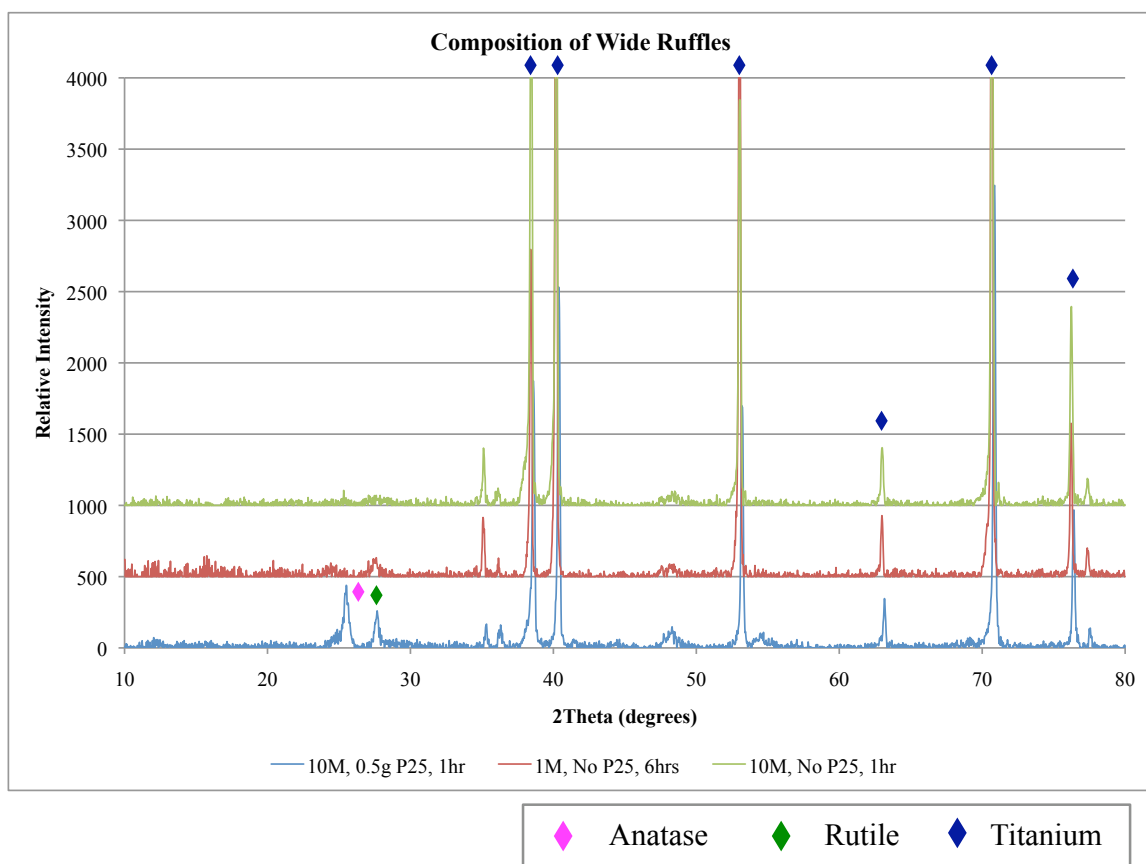


Figure 6.1.19. Hydrothermal reactions with short reaction times or low concentrations of NaOH result in preliminary thin ruffle-like structures with compositions seen here.

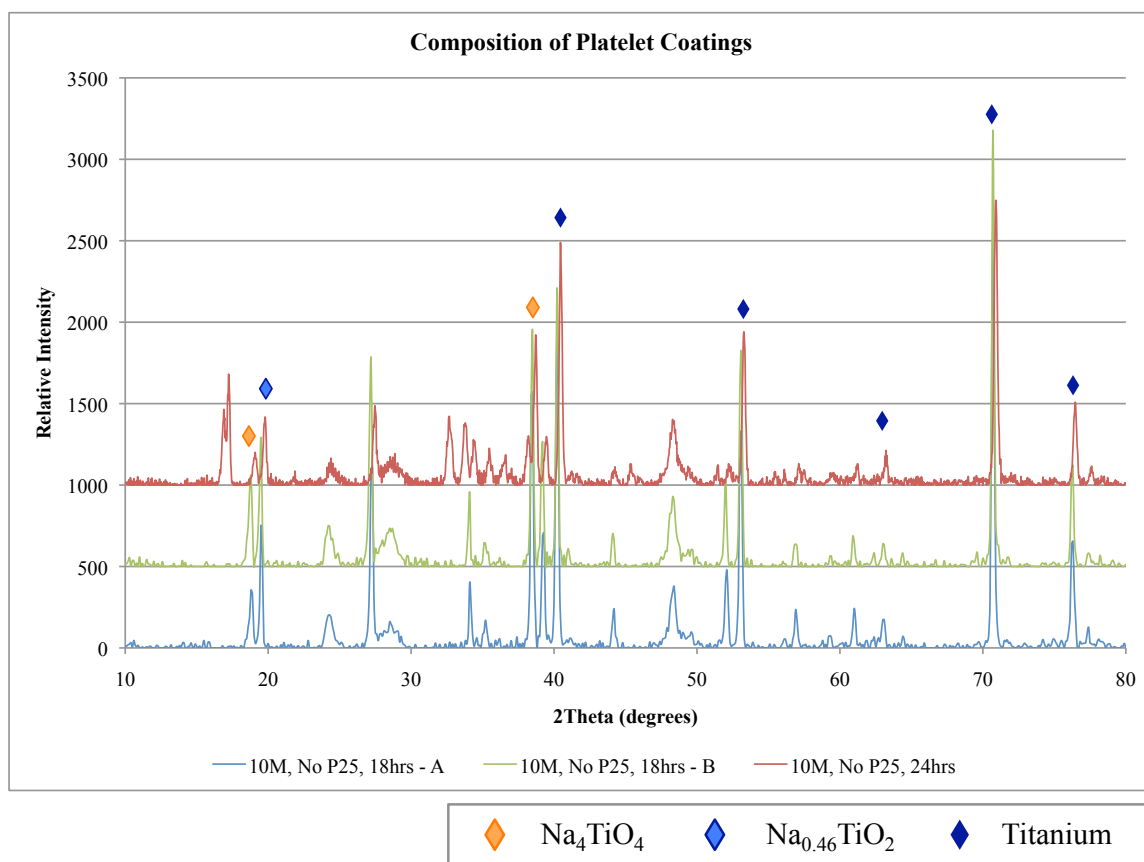


Figure 6.1.20. Platelets are formed when the hydrothermal reaction is done in 5-10M NaOH for longer times (12-24hrs) and when no TiO_2 is added. These XRD patterns demonstrate the compositions that these reaction conditions produce.

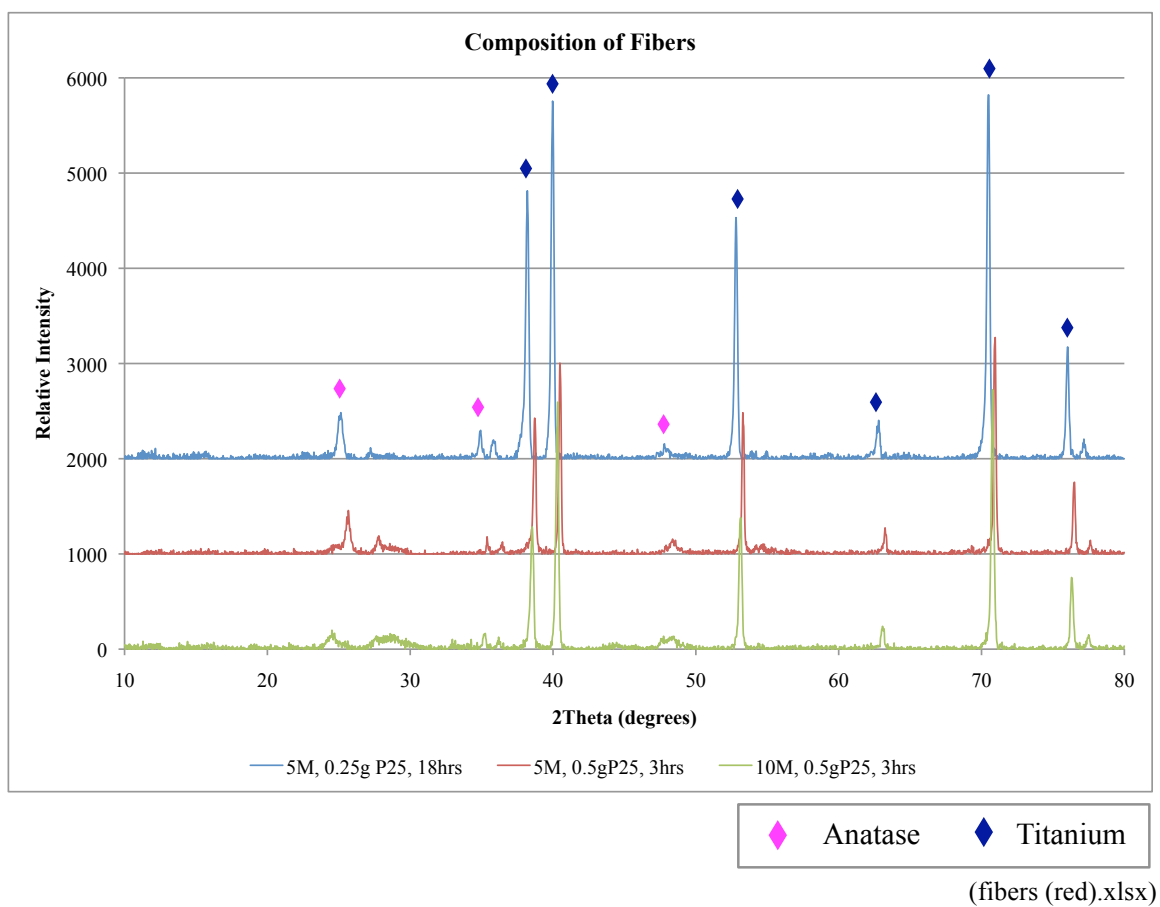


Figure 6.1.21. XRD patterns of titanium metal coatings consisting of nanofibers demonstrate that these nanostructures are titanium dioxide.

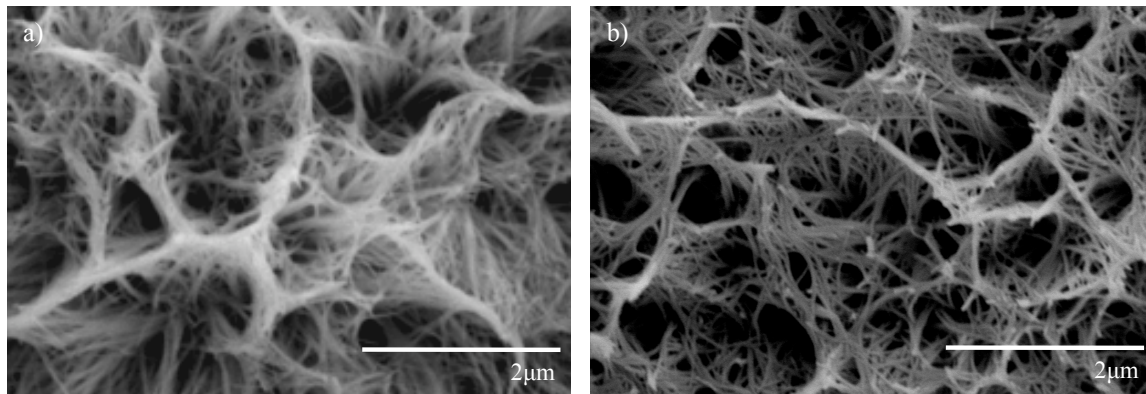


Figure 6.1.22. a) Sol-gel coated titanium metal hydrothermally grown produces high aspect ratio nanofibers with a high surface area. b) High surface area is maintained after aging in 80°C DIW for 3 days.

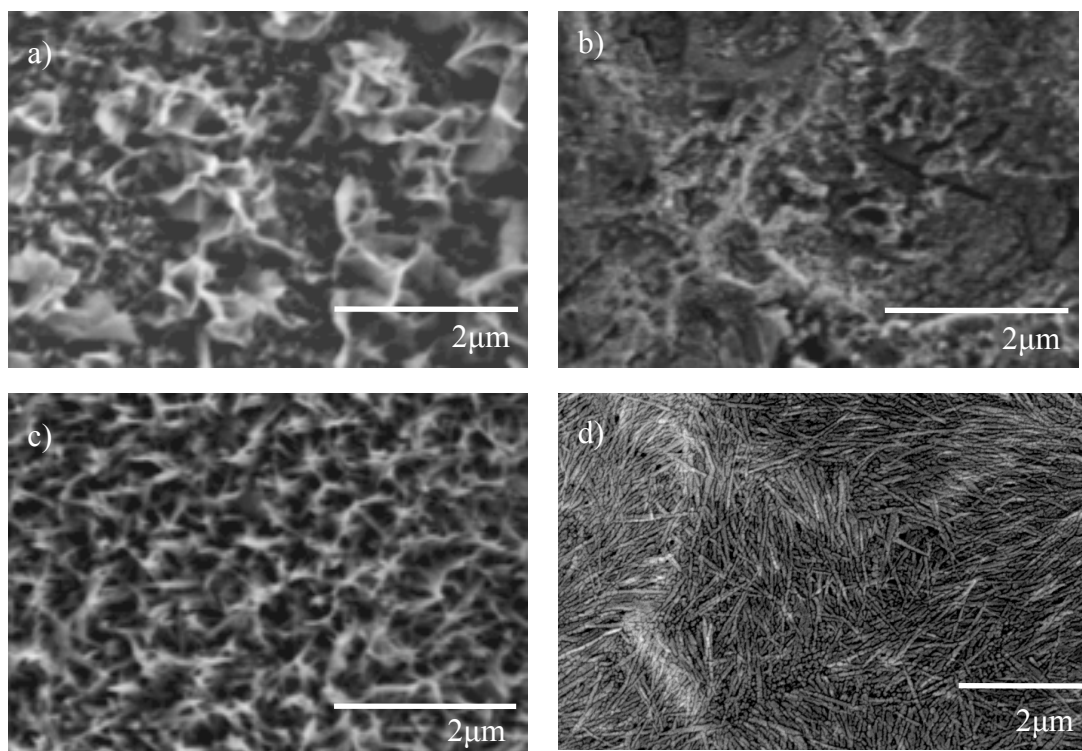


Figure 6.1.23. The post treatment process tends to degrade the open microstructure although the nanofibers are still visible. The samples in a) and c) were rinsed overnight in DIW while those in b) and d) are from the same hydrothermal reaction but were washed overnight in HCl. All samples were heated to 500°C for 1hr after the DIW/HCl wash.

figure 6.1.22b, but figure 6.1.24 shows the EDS where some Na remains in the product. XRD was also used to determine whether acid washing was a useful method for proton exchange; however, as can be seen in figure 6.1.25, in some cases the coatings are too thin and only the titanium metal peaks are visible.

6.1.3: Results of High Aspect Ratio Nanostructures in DSSC's

The objective of understanding the hydrothermal growth system is to be able to optimize the product for use in DSSC's. Initially, DSSC's were produced using the high aspect ratio powder products from the solution based hydrothermal growth process. The final products were used as prepared in the DIW rinse, which was then mixed with a surfactant solution, usually Pluronic P123 in ethanol. Spray coating was the chosen deposition method as doctor blading produced very non-uniform coatings. Even with spray coating, the hydrothermal product films were not as uniform as those produced with spherical P25 nanoparticles. Initial tests were run with sample H090606, which was the product of reacting 5.0g P25 in 5M NaOH at 150°C for 6 hours with a HCl post treatment wash. Figure 6.1.26 shows the low efficiency cells produced with these powders that were spray coated onto FTO/sol-gel substrates. More cells were produced to determine if the hydrothermal reaction conditions affect the efficiency of the solar cells. The results illustrated in figure 6.1.27 demonstrate that cells with very different efficiencies were produced by spray coating various hydrothermal product samples. The most efficient cells were prepared with samples that were reacted at low temperatures, and so the morphology of these samples, as discussed above, is spherical nanoparticles.

It was due to the difficulty of forming uniform films with the high aspect ratio

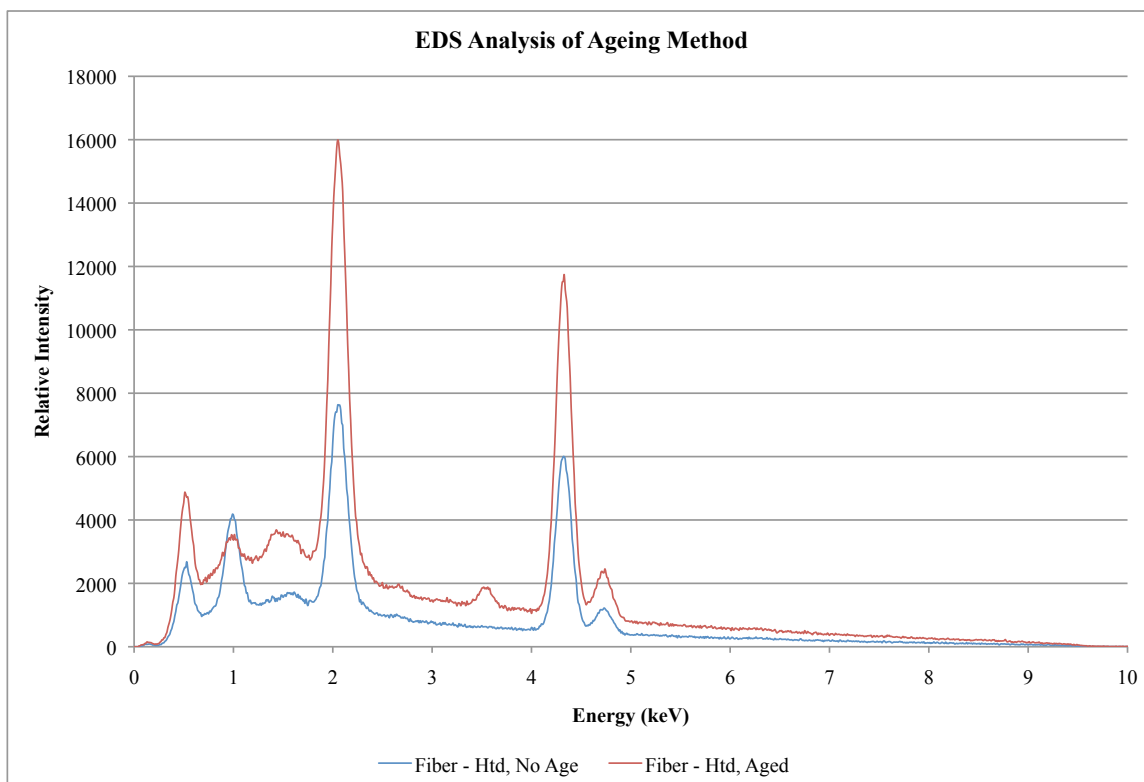
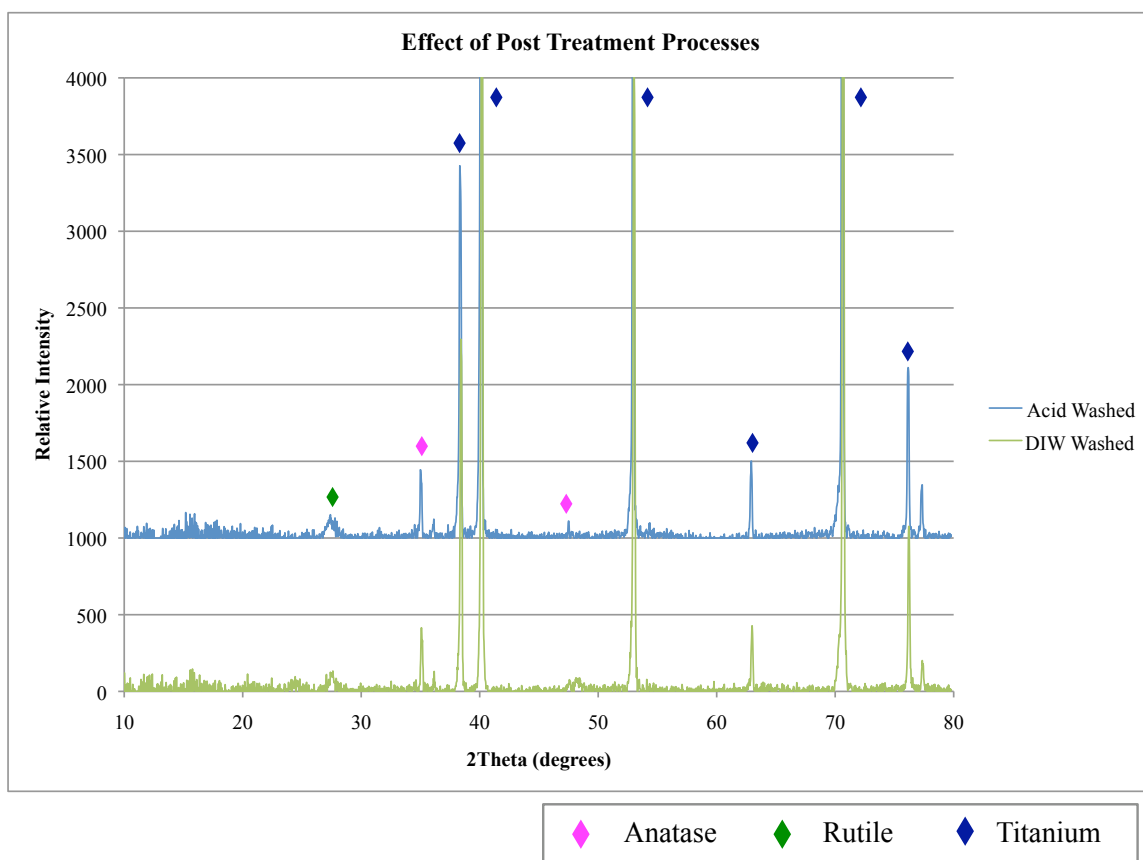


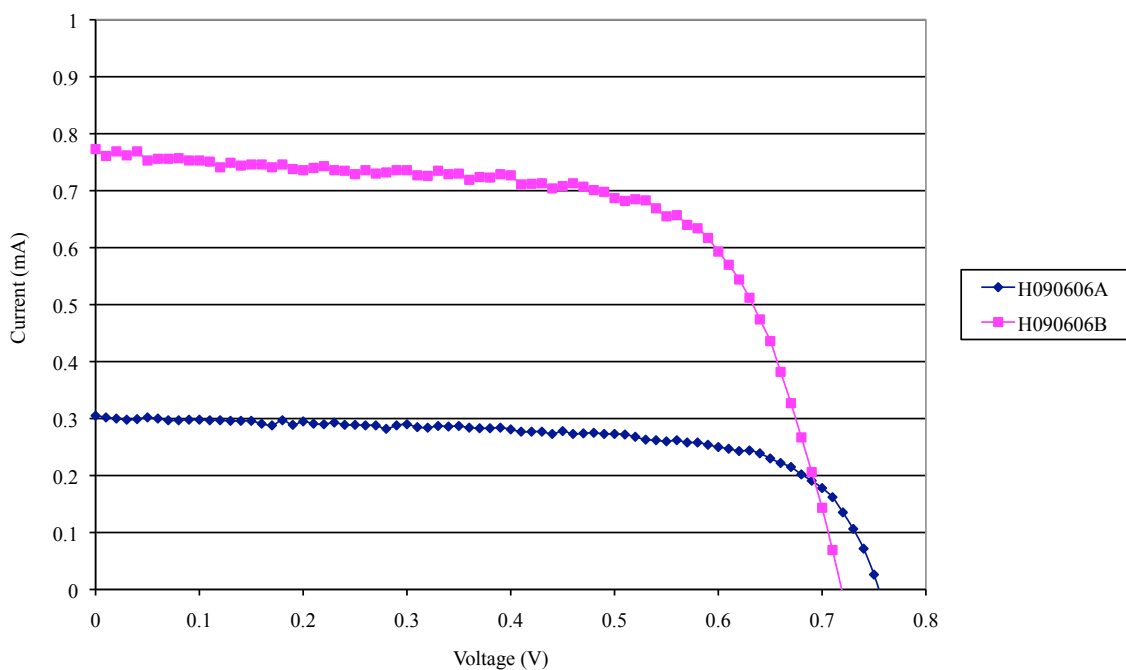
Figure 6.1.24. EDS analysis of the DIW aging method demonstrates that some sodium content remains, but that it is a promising method for proton exchange.



(ti metal titanate files.xls)

Figure 6.1.25. The thin coatings on the titanium metal make it difficult to take reliable XRD patterns. This is illustrated by the similarity between the acid washed and water rinsed coatings.

Photovoltaics with Nanotubes



	Area (cm ²)	Isc (mA/cm ²)	Voc (V)	PP (mW/cm ²)	Vpp (V)	Ipp (mA/cm ²)	FF	Efficiency
H090606 A	0.48	0.64	0.75	0.3203	0.63	0.51	67.20%	0.36%
H090606 B	0.48	1.61	0.71	0.7665	0.56	1.37	67.04%	0.85%

Figure 6.1.26. Early trial of high aspect ratio nanostructures used in a dye sensitized solar cell show that while energy is produced, the efficiency of the cells is quite low.

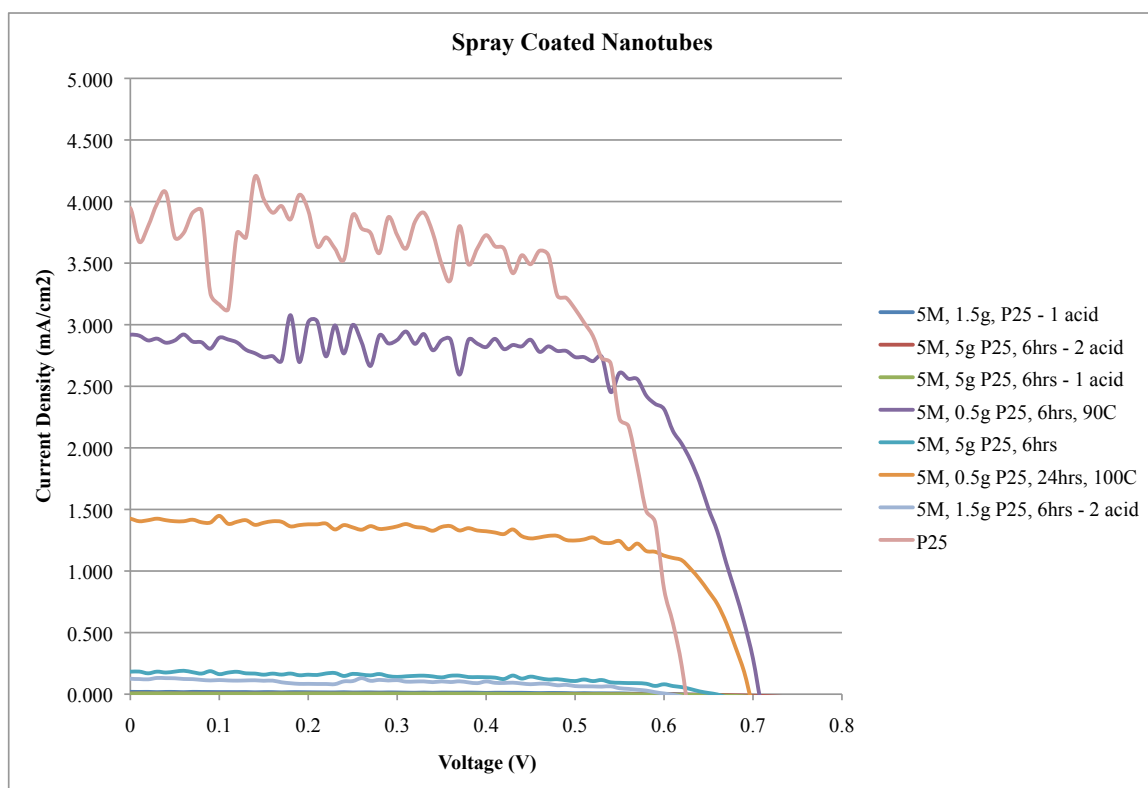


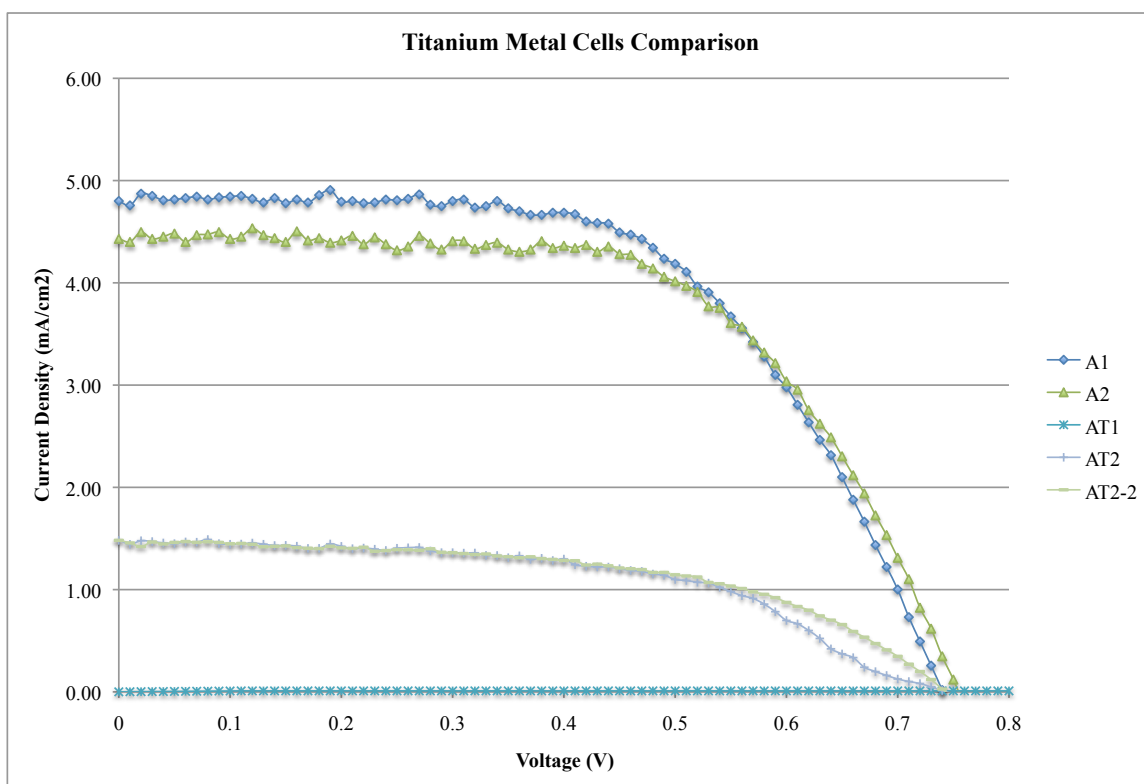
Figure 6.1.27. Spray coated cells were produced with a variety of different hydrothermally grown powder products. Few of these cells produced reasonable efficiencies, but those that did were 1.46% and 0.70%.

nanoparticles that the titanium metal substrate hydrothermal growth processes were researched. Before testing hydrothermal growth coatings on titanium metal, the effect of changing the substrate from FTO/sol-gel to titanium was characterized. To do this, cells were made with the common P25 dispersion deposited by doctor blading on titanium metal. The titanium metal complicates the cell build design because it is an opaque, thin sheet of metal as compared to a thicker sheet of insulating glass with only a thin conductive layer on one side. Using the catalytic platinum electrode combats the opacity, but the thinness of the metal allows the liquid electrolyte to reach the backside of the titanium and causes a short circuit. It was difficult to find sealing methods that allowed for efficient cells. A layer of Scotch tape worked as an insulator, but did not have surface tension values that kept the electrolyte confined to the area between electrodes. On the contrary, a thin coating of clear nail polish kept the metal insulated and the electrolyte in the cell. This method was used with the hot melt sealing method in the cells shown in figure 6.1.28. The electrolyte tested was the volatile $\text{CH}_3\text{CN}/\text{MPN}$. In figure 6.1.29, titanium metal cells were hot melt sealed with no backside insulator coating, but an ionic liquid electrolyte was used (Electrolyte 2). The increased viscosity of the electrolyte kept the cell from short circuiting.

6.2: Discussion of Hydrothermal Growth Method

6.2.1: Morphology

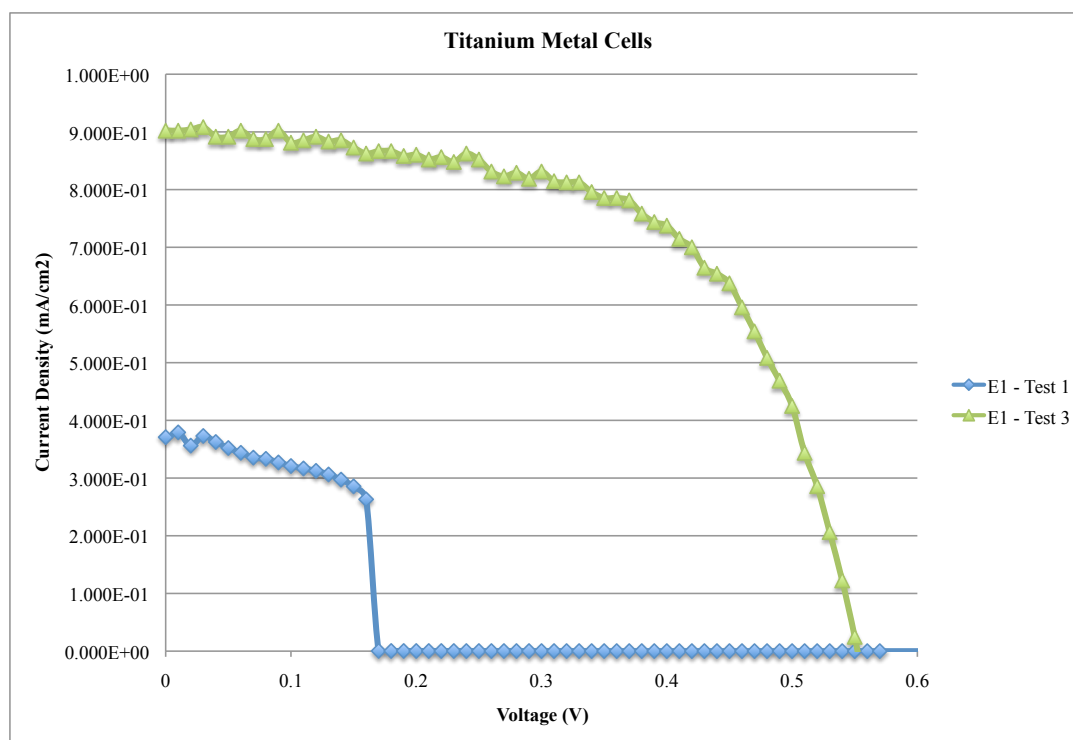
The objective of this portion of the research was to produce high aspect ratio nanostructures that could be used to form films with high surface area. Two ways of doing this were researched, the first, a solution method of hydrothermally reacted titania



	Area (cm ²)	Isc (mA/cm ²)	Voc (V)	PP (mW/cm ²)	Vpp (V)	Ipp (mA/cm ²)	FF	Efficiency
A1	1.4	4.80	0.74	2.09	0.51	4.11	58.97%	2.33%
A2	1.35	4.43	0.75	2.03	0.52	3.91	61.22%	2.26%
AT1 - SC	unk	0.00	#N/A	0.01	1	0.01	#N/A	0.01%
AT2	1.2	1.48	0.74	0.56	0.53	1.06	51.47%	0.63%
AT2 - 2	1.2	1.48	0.74	0.58	0.52	1.12	53.28%	0.65%

(cell comparison 110508.xls)

Figure 6.1.28. IV curves and characteristics comparing cells made with dip coated P25 on FTO/sol-gel with those made on titanium metal. These cells were tested with a volatile electrolyte.



	Area (cm ²)	Isc (mA/cm ²)	Voc (V)	PP (mW/cm ²)	Vpp (V)	Ipp (mA/cm ²)	FF	Efficiency
D2	0.56	0.00	✓ 0.70	0.00	✓ 0.28	✓ 0.00	16.35%	0.00%
E1	0.48	0.90	✓ 0.55	0.30	✓ 0.40	✓ 0.74	59.46%	0.33%

Figure 6.1.29. Titanium metal cells sealed with hot melt and tested with an ionic liquid electrolyte. An interesting point to note is the short circuit that occurred during test 1, demonstrating the difficulty of building titanium metal cells.

nanoparticles in sodium hydroxide with powder products, and the second, a similar hydrothermal reaction on a titanium metal substrate with and without titania as a reactant. Although these reactions appear similar, it was found that very different morphological products could be formed. In the case of the solution reactions, the products ranged from spherical nanoparticles to long nanofibers, whereas in the substrate growth, the structures formed can be large micron-sized platelets or different width nanofibers.

The specific dimensions of the nanostructures produced in the solution process are dependent on the temperature and the concentration of sodium hydroxide, but general high aspect ratio nanostructures can be made at a variety of reaction conditions. Reactions that occur at 90-100°C produce spherical nanoparticles that are very similar in size and shape to the P25 nanoparticles used as a starting material. At higher temperatures, in the 150°C to 200°C range, high aspect ratio nanostructures were formed; however, nanotubes were only seen at 150°C. As the temperature was increased, the width of the nanostructures decreased and the structure became needle-like. The effect of the NaOH concentration was shown in figure 6.1.9. The spherical particles form at 1M NaOH while higher concentrations, in the 5-10M NaOH range, produce high aspect ratio structures. The addition of P25 nanoparticles varied from 0.5g to 5.0g and nanotubes were consistently formed throughout this range as long as the temperature remained at 150°C. The larger reactant concentration did lead to a higher volume of unreacted particles in the final solution, which are visible in the TEM images found in section 6.1.2. The morphology of the end products also was found to be independent of reaction time in the range of 6-24 hours. This demonstrates that the solubility limit was most likely realized at 6 hours, so further increases in reaction time did not affect the reaction.

In the substrate growth process, there were three types of structures that formed: preliminary ruffles, large platelets and thin nanofibers and examples of these are shown in figure 6.1.17. The images in the left column demonstrate the ruffles and in the rest of the images, the platelets are clearly seen on a background of nanofibers. As the concentration of sodium hydroxide increases in the range of 5-10M, the size and number of platelets increases. When titanium dioxide nanoparticles are added to the hydrothermal solution, platelet growth is hindered and only the wide ribbons and nanofibers form. The wide ribbons are produced when low concentrations of sodium hydroxide react with titanium or titania, independent of whether titanium dioxide is added to the solution. The nanofibers appear to be the product of the reaction between titanium dioxide and concentrated (5-10M) sodium hydroxide, similar to that which occurs in the solution based growth reactions. A background layer forms on the titanium when no additional TiO_2 is present because there is a thin passivation layer on the titanium metal due to oxidation in air. Once the passivation layer is removed by reaction with NaOH and formation of nanofibers, either the reaction with titania continues with the particles in solution or the NaOH reacts with the minimal titanium metal available, forming platelets instead of nanofibers. As the reaction between NaOH and TiO_2 could either precipitate the nanofibers from a solution reaction or continue growth of the nanofibers from the titanium passivation layer, it was important to determine which occurred. This was done by imaging both sides of a reacted titanium metal substrate. Figure 6.2.1 portrays sample H031308A and B which are the top and bottom sides of the titanium metal, respectively, after reaction at an angle shown in figure 4.2.1. The hypothesis of these growth patterns are reinforced by reacting sol-gel coated titanium

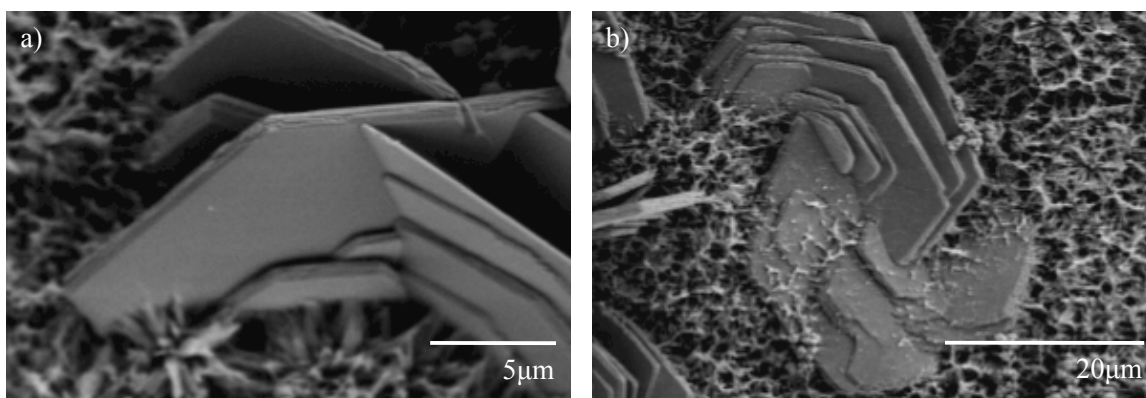


Figure 6.2.1. FESEM images of the a) top and b) bottom sides of the titanium metal substrate after hydrothermal reaction in 5M NaOH at 150°C for 18 hours.

metal with no additional TiO_2 . In this case, nanofibers are still the main growth product, since the NaOH reacts with the thicker layer of sol-gel titania. As this layer is still on the order of only 30-50nm, a few platelets are still formed in some areas, and their number reduces as the thickness of the sol-gel layer increases.

It was important to characterize the effect of the acid wash and annealing on the morphology of the products in order to ensure that the structures were not damaged by the post treatment process. In the solution growth system, figure 6.1.3 is evidence that the nanotube structure is maintained even after three acid washes. In this case it can be seen that the nanotubes are actually enhanced by the acid wash. It is believed that the structure is not affected directly by the acid wash, but that the disordered, partially reacted intermediates are rinsed out in the post treatment process. This leads to a greater yield and a clearer image of the nanotubes in the final product images. When the substrate products are treated with even one acid wash, the surface area of the films is greatly diminished, as shown in figure 6.1.23. In these images, while the high aspect ratio nanostructures remain, the openness of the films is greatly damaged by the post treatment process. For this reason, a second treatment technique was tested that could be used for proton exchange, but that maintained the porous nature of the films. The warm water wash simply involved placing the hydrothermally grown titanium metal in 80°C water for 3 days. As this was simply a trial, the time and temperature were not optimized for sodium removal, but this method does remove a large amount of sodium, as the EDS in figure 6.1.24 demonstrates. It is also shown in figure 6.1.22 that this process maintains the high surface area of the coating. Annealing the products up to 500°C for 0.5-1 hours does not damage the nanostructures in either the solution or substrate growth.

6.2.2: Phase and Composition of Hydrothermal Growth Products

The composition sequence of the products of the solution growth process is shown through XRD patterns in figure 6.1.1. In the initial phase, there are numerous peaks that need to be matched. The first peak sits at 15.9° and to illustrate the difficulty in matching this peak, table 6.2.1 compares similar peaks in numerous titanate products. While this peak could be easily ascribed to $\text{Na}_2\text{Ti}_3\text{O}_7$, as is often the case in the literature, it is important to look at the other peaks in both the sample being analyzed and the chosen phase. In this case, $\text{Na}_2\text{Ti}_3\text{O}_7$ has a peak with 100% intensity at 10.5° that simply does not exist in the H090606 XRD pattern. Figure 6.2.2 includes charts for the same sodium titanate compounds found in table 6.2.1 with their entire XRD pattern. Matching the three biggest peaks in the initial product of H090606 leads to the conclusion that the product could be $\text{Na}_2\text{Ti}_8\text{O}_{13}$, NaTiO_2 or Na_4TiO_4 . It appears that since the peaks cannot all be matched to any one phase of sodium titanate, that the product may be an agglomeration of numerous phases. In this case, it is reasonable that the 15.9° peak matches NaTiO_2 , the 44.5° peak equates to $\text{Na}_2\text{Ti}_8\text{O}_{13}$ and the 37.3° to Na_4TiO_4 . The peak at 24.6° is from the unreacted titania that still remains in the initial product. As the sequence continues and the products are acid washed, the composition changes due to proton exchange. This is evidenced by the salt product that is found in the supernatant after acid washing is complete due to the reaction of the chlorine anions with the removed sodium cations. Finally, with water rinsing, the proton exchanged titanate converts to a combination of anatase and rutile titania. The XRD patterns of these materials are found in figure 6.2.3 and can be compared to the final product results shown in section 6.1.

Table 6.2.1. Intensity and Position of Closest Peak to 15.9° in Various Sodium Titanate Compounds

Composition	Peak Nearest 15.9°	Intensity (/100)
NaTiO ₂	16.5	75
NaTi ₈ O ₁₃	14.5	59
Na ₄ TiO ₄	16.5	10
Na ₄ Ti ₅ O ₁₂	16.17	10
Na ₂ TiO ₃	16.88	87
Na ₂ Ti ₃ O ₇	15.8	30
Na _{1.7} Ti ₆ O ₁₁	16.8	39

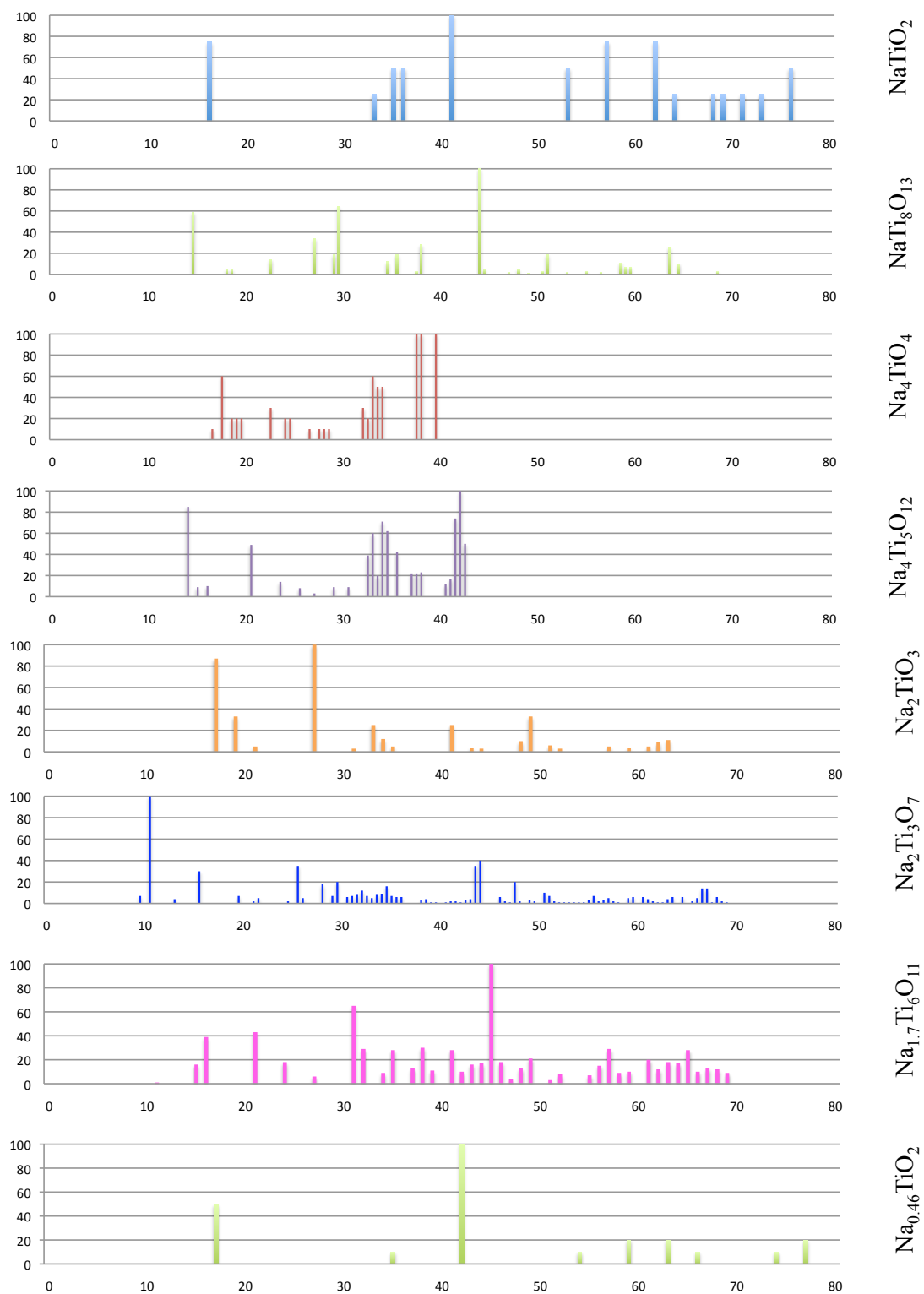


Figure 6.2.2. Charts of the pdf cards for a variety of sodium titanate phases.

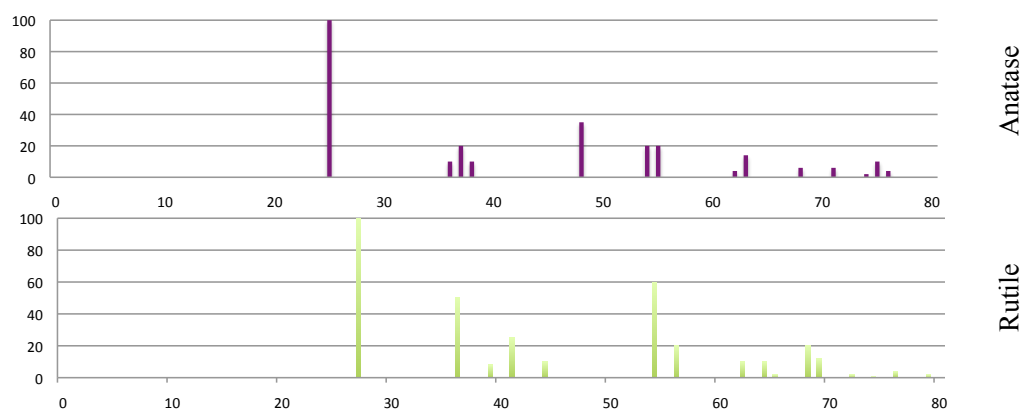


Figure 6.2.3. Graphs of the pdf cards for anatase and rutile TiO_2 .

The composition of the substrate materials is separated into three phases because the preliminary ruffle-like structures, the platelets and the nanofibers each have a distinct composition, although there is some overlap as they grow in combination with one another. Their distinct XRD patterns are shown in figures 6.1.19, 6.1.20 and 6.1.21. When these are compared to the control sample of untreated titanium metal on a glass substrate, whose XRD pattern is illustrated in figure 6.2.4, it is evident that the preliminary ruffle structure is most likely disordered as their XRD patterns have no diffraction signal beyond what is seen with untreated titanium. It is unlikely that the sample is simply too thin to produce a pattern because the peaks at approximately 24.6° and 27° in the pattern from the hydrothermal reaction with additional TiO_2 , provide evidence that the unreacted titania in the coating can be seen. The XRD patterns from the reactions that produce platelets have high intensity peaks that differ from the control pattern at approximately 19.5° , 27.4° , 34° , and 48.4° . In this structure, the 27.4° matches the pattern to rutile, while the other three peaks match reasonably well to a combination of Na_4TiO_4 and $\text{Na}_{0.46}\text{TiO}_2$. Further characterization was attempted with electron backscatter diffraction; however, it was apparent from these tests that the platelets have a disordered coating and so could not be characterized with this method either. Using image maps, shown in figure 6.2.5, of the different elements in EDS it appears that there is very little titanium in the platelets as compared to the nanofibrous background. Although this is not quantitative data, it lends evidence to the suggested reaction in which the platelets form when there is a limited supply of titanium ions available. The composition of the nanofibers is either disordered or a combination of anatase and rutile titania. It is unlikely that the products shown in figure 6.1.21 are disordered as they have

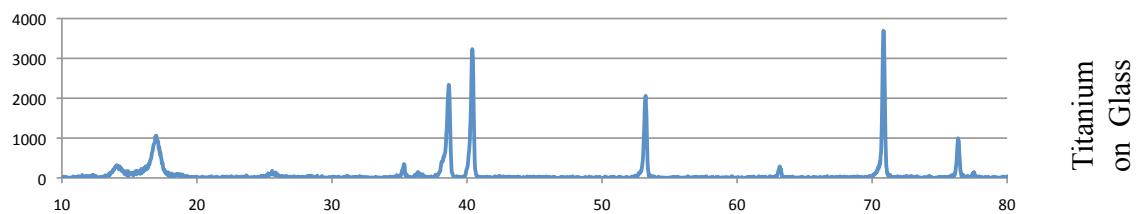


Figure 6.2.4. XRD pattern taken from untreated Ti metal sheet used in the hydrothermal substrate reactions.

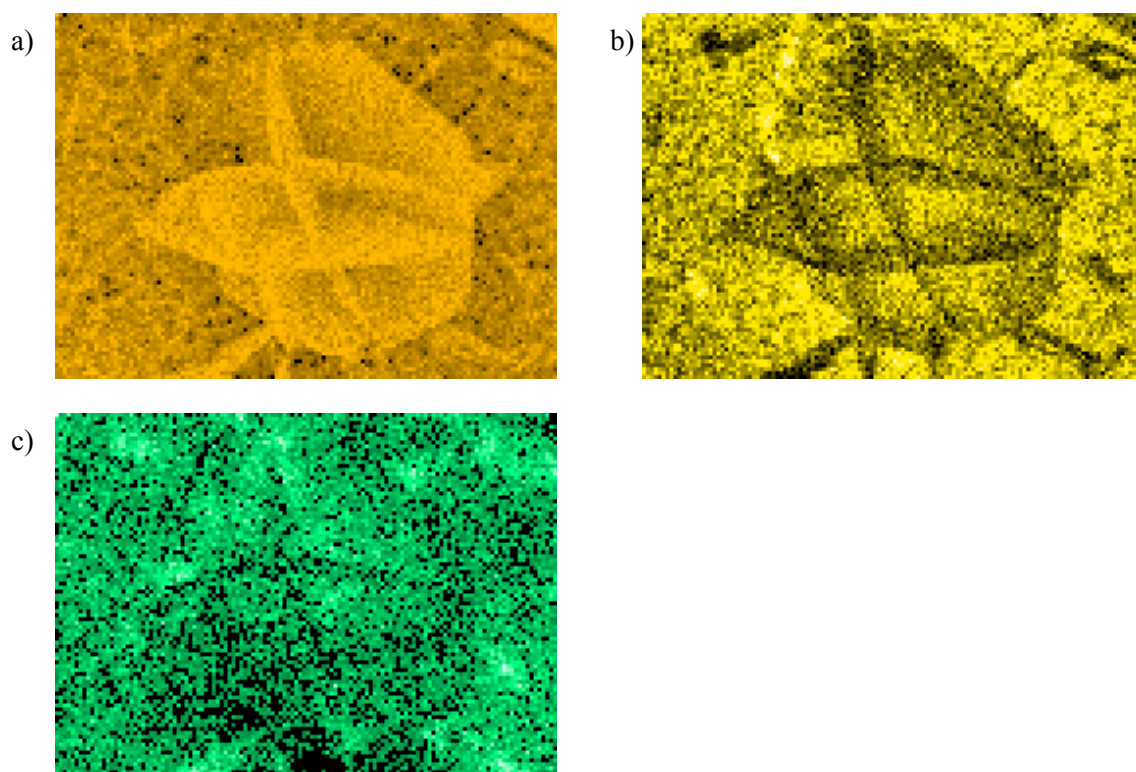


Figure 6.2.5. Image mapping of the sodium and titanium content of platelet structures.
a) Map of the gold coating, b) titanium map and c) sodium map.

been heat treated to 500°C for 30 minutes. If the heat treatment had not been done, the titania phase could be ascribed to unreacted particles embedded in the coating. However, it is apparent that the nanofibers grown on titanium metal in the presence of sodium hydroxide and excess titania are titanium dioxide after post treatment processing.

6.2.3: High Aspect Ratio and Titanium Substrate Solar Cells

Two types of cells were tested in this stage of the research, those with deposited hydrothermal products on FTO/sol-gel substrates and those with the P25 dispersion on titanium metal substrates. In the first set, the high aspect ratio nanostructures grown in the hydrothermal solution reaction process were dispersed with a surfactant in ethanol and spray coated onto the FTO/sol-gel substrates. The second set of cells consisted of a thin titanium metal sheet acting as the substrate for the P25 dispersion. This research illustrates a proof of concept that the high aspect ratio nanostructures can be used in a dye sensitized solar cell, and that if thick coatings are hydrothermally grown on titanium metal, the cells can be built and tested. In comparison with the spray coated cells made with spherical P25 nanoparticles, the high aspect ratio nanostructures did have lower efficiencies. The efficiency of this type of cell was shown to be approximately 0.85% when acid washed nanotubes were utilized. Higher efficiencies, up to 1.46%, were seen with structures from hydrothermal reactions at 90-100°C; however, as shown in figure 6.1, the morphology of these products is spherical nanoparticles. It became apparent that the nanotubes were more difficult to deposit than the spherical nanoparticles, as there was a lot of variation in the coatings.

For this reason, the tests on titanium metal were conducted in order to remove the difficult deposition step from the process. The cells made with titanium metal required a slightly different build design since the platinum electrode now needed to have transparency since the titanium metal substrate is opaque. The increased conductivity of the titanium metal in comparison to the FTO lowered the series resistance in the cell. However, a greater number of short circuits were seen since the volatile electrolyte easily reached the backside of the titanium metal. Once the optimization of the build design included an insulating coating on the backside of the titanium metal, and the use of ionic liquid electrolytes with increased viscosity, the cells made on titanium metal were made with good reproducibility. Cells tested with the volatile electrolyte still produced higher efficiencies in this design as was similarly noticed with the P25/FTO cells. The hydrothermally grown titania nanofibrous coatings on titanium metal were tested in preliminary solar cells, but the coatings were too thin to produce a measurable current output.

CHAPTER 7: CONCLUSIONS

7.1: Dye Sensitized Solar Cells

This portion of the research focused on producing and characterizing dye sensitized solar cells with a variety of materials to better understand this photovoltaic system. Initial experiments tested solar cells with spherical titania nanoparticle films as the semiconducting layer, a catalytic platinum back electrode, and a commercially available volatile liquid electrolyte. Based on research into the effect of different materials on the efficiency, changes were made to the construction process of the cells. Sputtered platinum replaced the catalytic platinum due to its higher conductivity and reflective coating. A barrier layer of spun-coat sol-gel titania was introduced to reduce interaction between the electrolyte and the FTO electrode. Different sealing methods were utilized based upon the goals of the cell. The binder clip method, with very limited electrolyte space, produced the highest efficiency cells, but the efficiency decreased to zero rapidly as the electrolyte volatilized in air, whereas the hot melt sealing method allowed for testing of the cells over a number of days, though at a slightly lower efficiency. The effect of the titania film itself was analyzed to determine the optimal deposition method. Spray coating was found to produce higher efficiency cells due to increased surface area; however, doctor blading was chosen as the deposition method for most cells as more uniform films could be produced. Overall, cells with an efficiency of 2-3% could be made reproducibly with the chosen cell design.

The design of the pore structure of the titania coating and its interaction with the electrolyte were studied by producing films templated with PS spheres and characterizing

them with both volatile and ionic liquid electrolytes. Ionic liquid electrolytes improve the lifetime of the cell as they have a higher viscosity and are confined to the titania film more easily; however, most still use a volatile solvent so sealing is still necessary.

Depending on the size of the templated PS spheres, organized or disordered macropores are formed in the pore structure of the titania film. PS spheres with sizes from 160nm to 1 μ m were tested with the hypothesis that the thicker ionic liquid electrolytes would have better penetration in these films than in coatings with only mesoporosity. The results of this study demonstrated that there is a period of time needed for the ionic liquid electrolyte to permeate all the pores of the titania coating. These cells were not optimized for thickness and it is believed that with increased thickness, their efficiency could be better than that of the baseline mesoporous films. With their similar surface area, but increased pore size, the electrolyte has a simpler pathway to traverse. Especially with the more viscous ionic liquid electrolytes, these larger pathways allow for better penetration, which would increase the speed of reduction of the dye molecules.

The most important parameter for the titania films in DSSC's is to have maximum dye adsorption. For this to occur, the coating must have high surface area, good light harvesting efficiency, and strong bonding between the dye molecule and the titania film. The thickness of the film must be optimized for the highest current output. The current initially increases with film thickness, but tends to plateau as recombination of the electrons occurs before they can be transported all the way to the back electrode. The pore volume and pore structure of the film need to be designed based on the electrolyte being tested as larger pore volumes need thicker coatings for the same dye adsorption,

which is a negative for volatile electrolytes with fast ionic conduction, but may be necessary for increased efficiency with ionic liquid electrolytes.

7.2: Hydrothermal Growth of High Aspect Ratio Nanostructures

The objective of this portion of the research was to form high aspect ratio titanium dioxide particles to test in DSSC's. The first stage of research involved hydrothermal reaction of titania nanoparticles in sodium hydroxide solution where titania nanotubes were produced after post treatment with acid. In the second stage, nanofibers were formed by the hydrothermal growth of titanium metal in a sodium hydroxide solution with titania nanoparticles. Hydrothermal growth is a low temperature process with simple reaction conditions that allow it to be useful for flexible substrates in solar cells. However, understanding the reactions that occur in these processes can be difficult.

In the solution system, reactions run at 150°C for 6-24 hours produce sodium titanate nanotubes. After treatment with either hydrochloric or nitric acid, proton exchange occurs and the sodium titanate is converted to hydrogen titanate. After rinsing with distilled, deionized water, anatase titania nanotubes are produced. Characterization by TEM and XRD illustrated that they have a nanotube morphology, unless treated at higher temperatures where nanofibers were likely to form, and that their final composition was anatase titania. Research in the literature reports that the nanotubes are formed by a scrolling mechanism where sheets of sodium titanate that initially form in solution have surface energy asymmetry that drives them to roll into a multiwalled, open ended nanotube. However, in the present research, initial growth structures include disordered "flowers," but no intermediate scrolls were found. The composition of the

sodium titanate is most likely a combination of phases with $\text{Na}_2\text{Ti}_3\text{O}_7$, $\text{Na}_2\text{Ti}_8\text{O}_{13}$ and Na_4TiO_4 as the major constituents.

When titanium metal is added to the hydrothermal reaction as a substrate, an interesting set of morphologies forms. The preliminary thin ruffle structures form at low concentrations of sodium hydroxide or low reaction times. It appears that these are intermediates to the reaction and that in these cases, the reaction has not gone to completion. As the reaction time is increased to 6 hours and the sodium hydroxide concentration to 5M, platelet structures form with a background of nanofibers across the entirety of the titanium metal substrate, including the backside. The platelets are large, several microns in diameter, and increase in size with the sodium hydroxide concentration. It was necessary to encourage the growth of the nanofiber background and hinder platelet formation in order to produce high surface area coatings on the titanium metal that could be used in DSSC's. To form only nanofibers, titanium dioxide nanoparticles were added to the hydrothermal reaction solution. Due to excess Ti^{4+} ions in the reaction from the dissolution of the nanoparticles, the nanofibers grow continuously and create an interconnected mesh-like coating. No platelets are seen when abundant TiO_2 precursor to the charge. The hypothesis for this lack of growth is that they are a reaction between the Ti^0 from the metal and the sodium hydroxide, and that the reaction with Ti^{4+} is favored when its concentration is high enough. The nanofibrous mesh is produced when no additional TiO_2 is added to the solution because titanium metal has a passivation layer of titania due to rapid oxidation in air. Evidence of this reaction process was supported by our experiments where sol-gel coated titanium metal was reacted without additional TiO_2 nanoparticles. The products of this hydrothermal

reaction included mainly nanofibers with only a small number of platelets throughout the coating. The sol-gel layer acts like a source of Ti^{4+} and so produces nanofibers, but with some platelets as the concentration is lower than when nanoparticles are used. Also, as the thickness of the sol-gel layer increased, the number of platelets diminished. It was found that the products from the sol-gel coating reactions had better uniformity and a more open pore structure than those with the added titania in solution. It is likely that when the TiO_2 is in solution, some sedimentation occurs on top of the growth, although the nanofibrous coverage of both sides of the titanium substrate does illustrate a growth mechanism. The composition of the different structures was characterized with XRD. The preliminary thin ruffles are disordered and the platelets are a sodium titanate composition. The nanofibers, however, after an acid wash treatment are anatase titania. The hypothesis is that these react similarly to the nanotubes grown in solution and that after proton exchange, the titania is produced.

7.3: The Use of High Aspect Ratio Nanostructures in DSSC's

The parameters for the titania coating in DSSC's are high surface area, strong dye adhesion, and fast electron conduction to the back electrode. The use of high aspect ratio titania nanostructures is believed to increase the electron conduction and lower recombination because there are fewer defects and grain boundaries that lead to trapping of the electrons. High surface area can be maintained either with very thin, on the order of 10-20nm, nanorods or by using a composite of nanorods and nanoparticles. As the composition of the titania is the same in both the nanoparticle and the nanorod structures,

the dye adhesion is unlikely to change, although the light harvesting efficiency could be increased with greater light scattering from the larger particles.

DSSC's were tested with deposited titania nanotubes from the solution hydrothermal reactions and these showed proof of concept although the efficiencies were low since they had not been optimized for thickness or packing. The packing of the nanotubes is quite important to maintaining high surface area. Cells with a titanium metal substrate were tested with the P25 spherical nanoparticle solution as the cell design is quite different due to the opacity of this electrode. There are increased losses in these cells, including those due to transmission through the catalytic platinum electrode and electrolyte solution and increased interaction between the electrolyte and the titanium metal. This research demonstrated that a nanotube titania film can be utilized in a DSSC and that titanium metal can be used as the back electrode.

CHAPTER 8: FUTURE WORK

It is apparent that DSSC's must become more efficient in order to compete with more readily available silicon cells while maintaining their price advantage. Nanorods and/or nanotubes are improving the efficiencies of DSSC's by reducing recombination rates and speeding electron transfer; however, current methods of either depositing powder products from solution growth or anodizing titanium for aligned nanotubes still require either a number of steps or a difficult commercialization process. Combining these two and using hydrothermal growth methods to produce high aspect ratio nanostructures grown on thin, flexible titanium metal offers ease of production and low cost. While this research made much progress in this direction, further optimization of the DSSC's and growth of thicker titania films are necessary. Transferring the light input from the titania/FTO substrate to the Pt/FTO electrode decreases light transmission and needs further experimentation to produce cells of comparable efficiency. The thickness of the titania films is necessary to increase the dye content and therefore, the current in the cells. It is believed that the nanofibers reduce recombination, which allows the cells to be even thicker than the 10-12 μm normally used with spherical nanoparticles. However, testing of the electrical characteristics of the hydrothermal growth products is necessary to better understand how they effect charge transport in the solar cells. Longer reaction time or producing a second hydrothermal layer by coating the fibrous film with a sol-gel layer should be tested. As these films are directly placed into solar cells, composites with nanoparticles are a good option for higher efficiency due to the large open pore structure. The nanoparticles would be able to increase the surface area of the

coatings while the nanofibers increase the speed of electron transfer and reduce recombination. For future solar cell production, the platinum electrode should also be studied to determine if a flexible substrate could replace the FTO/glass substrate. With the titanium metal, a completely flexible DSSC could be produced and the hydrothermal coating appears to have enough pore structure and mechanical stability that it will be appropriate for this use.

In terms of better understanding of the hydrothermal growth methods, further characterization work should be done so that the aggregate of compositions are known for both the solution and substrate growth products. Currently, the substrate growth products are inherently more interesting and understanding the mechanism behind the formation of nanofibers and platelets is important to being able to design thicker coatings and optimize the process as a whole. To do this, the intermediates of the process would need to be characterized more stringently. At short time intervals, the reaction would be stopped and TEM characterization of the coating products would be able to determine small changes in the product over time.

REFERENCES

- (1) Matson, R.; Energy, U. S. D. o., Ed.; NREL: 2007.
- (2) Kazmerski *NREL* **2007**.
- (3) Gratzel, M. "Solar Energy Conversion by Dye-Sensitized Photovoltaic Cells." *Inorganic Chemistry* **2005**, *44*, 6841-6851.
- (4) Nazeeruddin, M. K.; De Angelis, F.; Fantacci, S.; Selloni, A.; Viscardi, G.; Liska, P.; Ito, S.; Takeru, B.; Gratzel, M. "Combined Experimental and DFT-TDDFT Computational Study of Photoelectrochemical Cell Ruthenium Sensitizers." *Journal Of The American Chemical Society* **2005**, *127*, 16835-16847.
- (5) O'Regan, B.; Gratzel, M. "A low-cost, high-efficiency solar cell based on dye-sensitized colloidal TiO₂ films." *Nature* **1991**, *353*, 737-740.
- (6) Fungo, F.; Otero, L.; Durantini, E. N.; Silber, J. J.; Sereno, L. E. "Photosensitization of Thin SnO₂ Nanocrystalline Semiconductor Film Electrodes with Metallodiporphyrin." *Journal of Physical Chemistry B* **2000**, *104*, 7644-7651.
- (7) Kay, A.; Gratzel, M. "Artificial Photosynthesis. 1. Photosensitization of TiO₂ Solar Cells with Chlorophyll Derivatives and Related Natural Porphyrins." *Journal of Physical Chemistry* **1993**, *97*, 6272 - 6277.
- (8) Kay, A.; Humphry-Baker, R.; Gratzel, M. "Artificial Photosynthesis. 2. Investigations on the Mechanism of Photosensitization of Nanocrystalline TiO₂ Solar Cells by Chlorophyll Derivatives." *Journal of Physical Chemistry* **1994**, *98*, 952-959.
- (9) Papageorgiou, N. "Counter-electrode function in nanocrystalline photoelectrochemical cell configurations." *Coordination Chemistry Reviews* **2004**, *248*, 1421-1446.
- (10) Hagfeldt, A.; Bjorksten, U.; Lindquist, S. E. "Photoelectrochemical studies of colloidal TiO₂ films: the charge separation process studied by means of action spectra in the UV region." *Solar Energy Materials And Solar Cells* **1992**, *27*, 293-304.
- (11) Eastman, D. E. "PHOTOELECTRIC WORK FUNCTIONS OF TRANSITION, RARE-EARTH, AND NOBLE METALS." *Phys. Rev., B ;2: 1-2(1 Jul 1970)*. **1970**.
- (12) Vogel, R.; Hoyer, P.; Weller, H. "Quantum-Sized PbS, CdS, Ag₂S, Sb₂S₃, and Bi₂S₃ Particles as Sensitizers for Various Nanoporous Wide-Bandgap Semiconductors." *Journal of Physical Chemistry* **1994**, *98*, 3183-3188.
- (13) Sakohara, S.; Tickanan, L. D.; Anderson, M. A. *Journal of Physical Chemistry* **1992**, *96*, 11086.
- (14) Redmond, G.; O'Keefe, A.; Burgess, C.; MacHale, C.; Fitzmaurice, D. *Journal of Physical Chemistry* **1993**, *97*, 11081.
- (15) Rensmo, H.; Keis, K.; Lindstrom, H.; Sodergren, S.; Solbrand, A.; Hagfeldt, A.; Lindquist, S. E. "High Light-to-Energy Conversion Efficiencies for Solar Cells Based on Nanstructured ZnO Electrodes." *Journal of physical Chemistry B* **1997**, *101*, 2598-2601.
- (16) Bedja, I.; Hotchandani, S.; Kamat, P. V. *Journal of Physical Chemistry* **1994**, *98*.
- (17) Bjorksten, U.; Moser, J. E.; Gratzel, M. *Chemistry Of Materials* **1994**, *6*, 858-863.

- (18) Sayama, K.; Sugihara, H.; Arakawa, H. "Photoelectrochemical Properties of a Porous Nb₂O₅ Electrode Sensitized by a Ruthenium Dye." *Chemistry Of Materials* **1998**, *10*, 3825-3832.
- (19) Hodes, G.; Howell, I. D. J.; Peter, L. M. "Nanocrystalline Photoelectrochemical Cells: A New Concept in Photovoltaic Cells." *Journal of the Electrochemical Society* **1992**, *139*, 3136-3140.
- (20) Tsubomura, H.; Matsumura, M.; Nomura, Y.; Amamiya, T. "Dye sensitised zinc oxide: aqueous electrolyte: platinum photocell." *Nature* **1976**, *261*, 402-403.
- (21) Gratzel, M. "Conversion of sunlight to electric power by nanocrystalline dye-sensitized solar cells." *Journal Of Photochemistry And Photobiology A-Chemistry* **2004**, *164*, 3.
- (22) Bach, U.; Tachibana, Y.; Moser, J. E.; Haque, S. A.; Durrant, J. R.; Gratzel, M.; Klug, D. R. "Charge Separation in Solid-State Dye-Sensitized Heterjunction Solar Cells." *Journal Of The American Chemical Society* **1999**, *121*, 7445-7446.
- (23) Pelet, S.; Moser, J. E.; Gratzel, M. "Cooperative effect of adsorbed cations and iodide on the interception of back electron transfer in the dye sensitization of nanocrystalline TiO₂." *Journal Of Physical Chemistry B* **2000**, *104*, 1791-1795.
- (24) Hagfeldt, A.; Gratzel, M. "Light-Induced Redox Reactions in Nanocrystalline Systems." *Chemical Reviews* **1995**, *95*, 49-68.
- (25) Diebold, U. "The surface science of titanium dioxide." *Surface Science Reports* **2003**, *48*, 53-229.
- (26) Li, Y. X.; Hagen, J.; Schaffrath, W.; Otschik, P.; Haarer, D. "Titanium dioxide films for photovoltaic cells derived from a sol-gel process." *Solar Energy Materials And Solar Cells* **1999**, *56*, 167-174.
- (27) Fan, Q.; McQuillin, B.; Bradley, D. D. C.; Whitelegg, S.; Seddon, A. B. "A solid state solar cell using sol-gel processed material and a polymer." *Chemical Physics Letters* **2001**, *347*, 325-330.
- (28) Nazeeruddin, M. K.; Kay, A.; Rodicio, I.; Humphry-Baker, R.; Muller, E.; Liska, P.; Vlachopoulos, N.; Gratzel, M. "Conversion of Light to Electricity by cis-X₂Bis(2,2'-bipyridyl-4,4'-dicarboxylate)ruthenium(II) Charge-Transfer Sensitizers on Nanocrystalline TiO₂ Electrodes." *Journal of the American Chemical Society* **1993**, *115*, 6382-6390.
- (29) Burnside, S. D.; Shklover, V.; Barbe, C.; Comte, P.; Arendse, F.; Brooks, K.; Gratzel, M. "Self-Organization of TiO₂ Nanoparticles in Thin Films." *Chemistry Of Materials* **1998**, *10*, 2419-2425.
- (30) Kavan, L.; O'Regan, B.; Kay, A.; Gratzel, M. *Journal of Electroanalytical Chemistry* **1993**, *346*, 291.
- (31) Vlachopoulos, N.; Liska, P.; Augustynski, J.; Gratzel, M. "Very efficient visible light energy harvesting and conversion by spectral sensitization of high surface area polycrystalline titanium dioxide films." *Journal Of The American Chemical Society* **1988**, *110*, 1216-1220.
- (32) Nazeeruddin, M. K.; Kay, A.; Rodicio, I.; Humphry-Baker, R.; Mueller, E.; Liska, P.; Vlachopoulos, N.; Gratzel, M. "Conversion of light to electricity by cis-X₂bis(2,2'-bipyridyl-4,4'-dicarboxylate)ruthenium(II) charge-transfer sensitizers (X = Cl-, Br-, I-, CN-, and SCN-) on nanocrystalline titanium dioxide electrodes." *Journal Of The American Chemical Society* **1993**, *115*, 6382-6390.

- (33) Nazeeruddin, M. K.; Pechy, P.; Renouard, T.; Zakeeruddin, S. M.; Humphry-Baker, R.; Comte, P.; Liska, P.; Cevey, L.; Costa, E.; Shklover, V.; Spiccia, L.; Deacon, G. B.; Bignozzi, C. A.; Gratzel, M. "Engineering of Efficient Panchromatic Sensitizers for Nanocrystalline TiO₂-Based Solar Cells." *Journal of the American Chemical Society* **2001**, *123*, 1613-1624.
- (34) Gratzel, M. "Mesoporous oxide junctions and nanostructured solar cells." *Current Opinion In Colloid & Interface Science* **1999**, *4*, 314-321.
- (35) Desilvestro, J.; Gratzel, M.; Kavan, L.; Moser, J. E.; Augustynski, J. "Highly Efficient Sensitization of Titanium Dioxide." *Journal of the American Chemical Society* **1985**, *107*, 2988-2990.
- (36) Renouard, T.; Fallahpour, R. A.; Nazeeruddin, M. K.; Humphry-Baker, R.; Gorelsky, S. I.; Lever, A. B. P.; Gratzel, M. "Novel Ruthenium Sensitizers Containing Functionalized Hybrid Tetradentate Ligands: Synthesis, Characterization and INDO/S Analysis." *Inorganic Chemistry* **2002**, *41*, 367-278.
- (37) Zakeeruddin, S. M.; Liska, P.; Gratzel, M. "A Quasi-Solid-State Dye-Sensitized Solar Cell Based on a Sol-Gel Nanocomposite Electrolyte Containing Ionic Liquid." *Chemistry Of Materials* **2003**, *15*, 1825-1829.
- (38) Asbury, J. B.; Ellingson, R. J.; Ghosh, H. N.; Ferrere, S.; Nozik, A. J.; Lian, T. "Femtosecond IR Study of Excited-State Relaxation and Electron-Injection Dynamics of Ru(dcbpy)₂(NCS)₂ in Solution and on Nanocrystalline TiO₂ and Al₂O₃ Thin Films." *Journal of Physical Chemistry* **1999**, *103*, 3110-3119.
- (39) Nusbaumer, H.; Moser, J. E.; Zakeeruddin, S. M.; Nazeeruddin, M. K.; Gratzel, M. "Co(II)(dbbip)₂(2+) Complex Rivals Tri-iodide/Iodide Redox Mediator in Dye-Sensitized Photovoltaic Cells." *Journal Of Physical Chemistry B* **2001**, *105*, 10461-10464.
- (40) Oskam, G.; Bergeron, B. V.; Meyer, G.; Searson, P. C. "Pseudohalogens for Dye-Sensitized TiO₂ Photoelectrochemical Cells." *Journal Of Physical Chemistry B* **2001**, *105*, 6867-6873.
- (41) Matsumoto, M.; Miyazaki, H.; Matsuihiro, K.; Kumashiro, Y.; Takaoka, Y. "A dye sensitized TiO₂ photoelectrochemical cell constructed with polymer solid electrolyte." *Solid State Ionics* **1996**, *89*, 263-267.
- (42) Nogueira, A. F.; De Paoli, M. A.; Montanari, I.; Monkhouse, R.; Nelson, J.; Durrant, J. R. "Electron Transfer Dynamics in Dye Sensitized Nanocrystalline Solar Cells Using a Polymer Electrolyte." *Journal Of Physical Chemistry B* **2001**, *105*, 7517-7524.
- (43) Cao, F.; Oskam, G.; Searson, P. C. "A Solid State, Dye Sensitized Photoelectrochemical Cell." *Journal of Physical Chemistry* **1995**, *99*, 17071-17073.
- (44) Cao, F.; Oskam, G.; Meyer, G.; Searson, P. C. "Electron Transport in Porous Nanocrystalline TiO₂ Photoelectrochemical Cells." *Journal of Physical Chemistry* **1996**, *100*, 17021.
- (45) Hao, Y.; Yang, M.; Li, W.; Qiao, X.; Zhang, L.; Cai, S. "A photoelectrochemical solar cell based on ZnO/dye/polypyrrole film electrode as photoanode." *Solar Energy Materials And Solar Cells* **2000**, *60*, 349-359.

- (46) Shklover, V.; Ovchinnikov, Y. E.; Braginsky, L. S.; Zakeeruddin, S. M.; Gratzel, M. "Structure of Organic/Inorganic Interface in Assembled Materials Comprising Molecular Components. Crystal Structure of the Sensitizer Bis[(4,4'-carboxy-2,2'-bipyridine)(thiocyanato)]ruthenium(II)." *Chemistry Of Materials* **1998**, *10*, 2533-2541.
- (47) Chopra, N. G.; Luyken, R. J.; Cherrey, K.; Crespi, V. H.; Cohen, M. L.; Louie, S. G.; Zettl, A. "Boron Nitride Nanotubes." *Science* **1995**, *269*, 966-967.
- (48) Gong, D.; Grimes, C. A.; Varghese, O. K.; Hu, W. C.; Singh, R. S.; Chen, Z.; Dickey, E. C. "Titanium oxide nanotube arrays prepared by anodic oxidation." *Journal Of Materials Research* **2001**, *16*, 3331-3334.
- (49) Mor, G. K.; Varghese, O. K.; Paulose, M.; Grimes, C. A. "Transparent highly ordered TiO₂ nanotube arrays via anodization of titanium thin films." *Advanced Functional Materials* **2005**, *15*, 1291-1296.
- (50) Mor, G. K.; Varghese, O. K.; Paulose, M.; Mukherjee, N.; Grimes, C. A. "Fabrication of tapered, conical-shaped titania nanotubes." *Journal Of Materials Research* **2003**, *18*, 2588-2593.
- (51) Sugimura, H.; Uchida, T.; Kitamura, N.; Masuhara, H. "SCANNING TUNNELING MICROSCOPE TIP-INDUCED ANODIZATION OF TITANIUM - CHARACTERIZATION OF THE MODIFIED SURFACE AND APPLICATION TO THE METAL RESIST PROCESS FOR NANOLITHOGRAPHY." *Journal of Vacuum Science & Technology B* **1994**, *12*, 2884-2888.
- (52) Zhang, Z. H.; Yuan, Y.; Fang, Y. J.; Liang, L. H.; Ding, H. C.; Shi, G. Y.; Jin, L. T. "Photoelectrochemical oxidation behavior of methanol on highly ordered TiO₂ nanotube array electrodes." *Journal of Electroanalytical Chemistry* **2007**, *610*, 179-185.
- (53) Hoyer, P. "Formation of a Titanium Dioxide Nanotube Array." *Langmuir* **1996**, *12*, 1411-1413.
- (54) Miao, L.; Tanemura, S.; Toh, S.; Kaneko, K.; Tanemura, M. "Fabrication, characterization and Raman study of anatase TiO₂ nanorods by a heating-sol-gel template process." *Journal Of Crystal Growth* **2004**, *264*, 246-252.
- (55) Sander, M. S.; Cote, M. J.; Gu, W.; Kile, B. M.; Tripp, C. P. "Template-assisted fabrication of dense, aligned arrays of titania nanotubes with well-controlled dimensions on substrates." *Advanced Materials* **2004**, *16*, 2052-2057.
- (56) Zhang, M.; Bando, Y.; Wada, K. "Sol-gel template preparation of TiO₂ nanotubes and nanorods." *Journal Of Materials Science Letters* **2001**, *20*, 167-170.
- (57) Zhao, Y. N.; Lee, U. H.; Suh, M.; Kwon, Y. U. "Synthesis and characterization of highly crystalline anatase nanowire arrays." *Bulletin of the Korean Chemical Society* **2004**, *25*, 1341-1345.
- (58) Yang, X.; Konishi, H.; Xu, H.; Wu, M. "Comparative Sol-Hydro(Solvo)thermal Synthesis of TiO₂ Nanocrystals." *European Journal of Inorganic Chemistry* **2006**, 2229-2235.
- (59) Zhang, Z.; Zhong, X.; Liu, S.; Li, D.; Han, M. "Aminolysis Route to Monodisperse Titania Nanorods with Tunable Aspect Ratio." *Angewandte Chemie* **2005**, *117*, 3532-3536.

- (60) Bavykin, D.; Parmon, V.; Lapkin, A.; Walsh, F. "The effect of hydrothermal conditions on the mesoporous structure of TiO₂ nanotubes." *Journal of Materials Chemistry* **2004**, *14*, 3370-3377.
- (61) Kasuga, T.; Hiramatsu, M.; Hoson, A.; Sekino, T.; Niihara, K. "Formation of Titanium Oxide Nanotube." *Langmuir* **1998**, *14*, 3160-3163.
- (62) Nian, J.-N.; Teng, H. "Hydrothermal Synthesis of Single-Crystalline Anatase TiO₂ Nanorods with Nanotubes as the Precursor." *Journal Of Physical Chemistry B* **2006**, *110*, 4193-4198.
- (63) Tian, Z. "Large Oriented Arrays and Continuous Films of TiO₂-based nanotubes." *Journal of the American Chemical Society* **2003**, *125*, 12384-12385.
- (64) Zhang, S.; Peng, L. M.; Chen, Q.; Dawson, G.; Du, G. H.; Zhou, W. Z. "Formation Mechanism of H₂Ti₃O₇ Nanotubes." *Physical Review Letters* **2003**, *91*, 256103.
- (65) Andersson, S.; Wadsley, A. D. "The Crystal Structure of Na₂Ti₃O₇." *Acta Crystallographica* **1961**, *14*, 1245-1249.
- (66) Kasuga, T.; Hiramatsu, M.; Hoson, A.; Sekino, T.; Niihara, K. "Titania Nanotubes Prepared by Chemical Processing." *Advanced Materials* **1999**, *11*, 1307-1311.
- (67) Kasuga, T.; Hiramatsu, M.; Hirano, M.; Hoson, A.; Oyamada, K. "Preparation of TiO₂-based powders with high photocatalytic activities." *Journal Of Materials Research* **1997**, *12*, 607-609.
- (68) Tsai, C. C.; Teng, H. "Structural Features of Nanotubes Synthesized from NaOH Treatment on TiO₂ with Different Post-Treatments." *Chem. Mater.* **2006**, *18*, 367-373.
- (69) Chen, Q.; Du, G. H.; Zhang, S.; Peng, L. M. "The structure of trititanate nanotubes." *Acta Crystallography: Section B* **2002**, *58*, 587-593.
- (70) Chen, Q.; Zhou, W. Z.; Du, G. H.; Peng, L. M. "Trititanate Nanotubes made via a Single Alkali Treatment." *Advanced Materials* **2002**, *14*, 1208-1211.
- (71) Du, G. H.; Chen, G.; Peng, L. M. "Preparation and structural analysis of titanium oxide nanotubes." *Applied Physics Letters* **2001**, *79*, 3702-3704.
- (72) Ferreira, O. P.; Souza Filho, A. G.; Filho, J. M.; Alves, O. L. "Unveiling the Structure and Composition of Titanium Oxide Nanotubes through Ion Exchange Chemical Reactions and Thermal Decomposition Processes." *Journal of the Brazilian Chemical Society* **2006**, *17*, 393-402.
- (73) Poudel, B.; Wang, W. Z.; Dames, C.; Huang, J. Y.; Kunwar, S.; Wang, D. Z.; Banerjee, D.; Chen, G.; Ren, Z. F. "Formation of crystallized titania nanotubes and their transformation. into nanowires." *Nanotechnology* **2005**, *16*, 1935-1940.
- (74) Suzuki, Y.; Yoshikawa, S. "Synthesis and thermal analyses of TiO₂-derived nanotubes prepared by the hydrothermal method." *Journal Of Materials Research* **2004**, *19*, 982-985.
- (75) Thorne, A.; Kruth, A.; Tunstall, D.; Irvine, J. T. S.; Zhou, W. "Formation, Structure, and Stability of Titanate Nanotubes and Their Proton Conductivity." *Journal Of Physical Chemistry B* **2005**, *109*, 5439-5444.
- (76) Sun, X. M.; Li, Y. D. "Synthesis and characterization of ion-exchangeable titanate nanotubes." *Chemistry-A European Journal* **2003**, *9*, 2229-2238.

- (77) Zhang, Q.; Gao, L.; Sun, J.; Zheng, S. "Preparation of Long TiO₂ Nanotubes from Ultrafine Rutile Nanocrystals." *Chemistry Letters* **2002**, 31, 226.
- (78) Seo, D.-S.; Lee, J.-K.; Kim, H. "Preparation of nanotube-shaped TiO₂ powder." *Journal Of Crystal Growth* **2001**, 229, 428-432.
- (79) Yuan, Z.-Y.; Su, B.-L. "Titanium oxide nanotubes, nanofibers and nanowires." *Colloids and Surfaces A: Physicochemical Engineering Aspects* **2004**, 241, 173-183.
- (80) Yuan, Z.-Y.; Zhou, W.; Su, B.-L. "Hierarchical interlinked structure of titanium oxide nanofibers." *Chemical Communications* **2002**, 1202-1203.
- (81) Ma, R.; Fukuda, K.; Sasaki, T.; Osada, M.; Bando, Y. "Structural Features of Titanate Nanotubes/Nanobelts Revealed by Raman, X-ray Absorption Fine Structure and Electron Diffraction Characterizations." *Journal Of Physical Chemistry B* **2005**, 109, 6210-6214.
- (82) Nakahira, A.; Kato, W.; Tamai, M.; Isshiki, T.; Nishio, K.; Aritani, H. "Synthesis of nanotube from a layered H₂Ti₄O₉ center dot H₂O in a hydrothermal treatment using various titania sources." *Journal Of Materials Science* **2004**, 39, 4239-4245.
- (83) Yao, B. D.; Chan, Y. F.; Zhang, X. Y.; Zhang, W. F.; Yang, Z. Y.; Wang, N. "Formation mechanism of TiO₂ nanotubes." *Applied Physics Letters* **2003**, 82, 281-283.
- (84) Tsai, C. C.; Teng, H. S. "Regulation of the physical characteristics of Titania nanotube aggregates synthesized from hydrothermal treatment." *Chemistry Of Materials* **2004**, 16, 4352-4358.
- (85) Sun, X.; Chen, X.; Li, Y. "Large-Scale Synthesis of Sodium and Potassium Titanate Nanobelts." *Inorganic Chemistry* **2002**, 41, 4996-4998.
- (86) Weng, L. Q.; Song, S. H.; Hodgson, S.; Baker, A.; Yu, J. "Synthesis and characterisation of nanotubular titanates and titania." *Journal of the European Ceramic Society* **2006**, 26, 1405.
- (87) Ma, R.; Bando, Y.; Sasaki, T. "Nanotubes of lepidocrocite titanates." *Chemical Physics Letters* **2003**, 380, 577-582.
- (88) Wang, Y. Q.; Hu, G. Q.; Duan, X. F.; Sun, H. L.; Xue, Q. K. "Microstructure and formation mechanism of titanium dioxide nanotubes." *Chemical Physics Letters* **2002**, 365, 427.
- (89) Thorne, A.; Kruth, A.; Tunstall, D.; Irvine, J. T. S.; Zhou, W. *Journal Of Physical Chemistry B* **2005**, 109, 5439-5444.
- (90) Yang, J. J.; Jin, Z. S.; Wang, X. D.; Li, W.; Zhang, J. W.; Zhang, S. L.; Guo, X. Y.; Zhang, Z. J. "Study on composition, structure and formation process of nanotube Na₂Ti₂O₄(OH)(2)." *Dalton Transactions* **2003**, 3898-3901.
- (91) Chi, B.; Victorio, E. S.; Jin, T. "Synthesis of TiO₂-Based Nanotube on Ti Substrate by Hydrothermal Treatment." *Journal of Nanoscience and Nanotechnology* **2007**, 7, 668-672.
- (92) Lee, S.-S.; Byeon, S.-H. "Structural and Morphological Behavior of TiO₂ Rutile Obtained by Hydrolysis Reaction of Na₂Ti₃O₇." *Bulletin of the Korean Chemical Society* **2004**, 25, 1051.

- (93) Knauss, K. G.; Dibley, M. J.; Bourcier, W. L.; Shaw, H. F. "Ti(IV) hydrolysis constants derived from rutile solubility measurements made from 100 to 300°C." *Applied Geochemistry* **2001**, *16*, 1115-1128.
- (94) Lencka, M. M.; Riman, R. E. "Thermodynamic modeling of hydrothermal synthesis of ceramic powders." *Chemistry Of Materials* **1993**, *5*, 61-70.
- (95) Ziemniak, S. E.; Jones, M. E.; Combs, K. E. S. "SOLUBILITY BEHAVIOR OF TITANIUM(IV) OXIDE IN ALKALINE MEDIA AT ELEVATED-TEMPERATURES." *Journal of Solution Chemistry* **1993**, *22*, 601-623.
- (96) Sugimoto, T.; Zhou, X.; Muramatsu, A. "Synthesis of Uniform Anatase TiO₂ Nanoparticles by Gel-Sol Method: 1. Solution Chemistry of Ti(OH)_n(4-n)⁺ Complexes." *Journal of Colloid and Interface Science* **2002**, *252*, 339-346.
- (97) Zhu, Y.; Li, H.; Koltypin, Y.; Hacohen, Y. R.; Gedanken, A. "Sonochemical synthesis of titania whiskers and nanotubes." *Chemical Communications* **2001**, 2616-2617.
- (98) Sasaki, T.; Kooli, F.; Iida, M.; Michiue, Y.; Takenouchi, S.; Yajima, Y.; Izumi, F.; Chakoumakos, B. C.; Watanabe, M. "A Mixed Alkali Metal Titanate with the Lepridrocrocite-like Layered Structure. Preparation, Crystal Structure, Protonic Form, and Acid-Base Intercalation Properties." *Chemistry Of Materials* **1998**, *10*, 4123-4128.
- (99) Ma, R.; Bando, Y.; Sasaki, T. "Directly Rolling Nanosheets into Nanotubes." *Journal Of Physical Chemistry B* **2004**, *108*, 2115-2119.
- (100) Penn, R. L.; Banfield, J. F. "Morphology development and crystal growth in nanocrystalline aggregates under hydrothermal conditions: Insights from titania." *Geochimica et Cosmochimica Acta* **1999**, *63*, 1549-1557.
- (101) Lim, Y. J.; Oshida, Y.; Andres, C. J.; Barco, M. T. "Surface characterizations of variously treated titanium materials." *International Journal of Oral & Maxillofacial Implants* **2001**, *16*, 333-342.
- (102) Chu, C. L.; Chung, C. Y.; Zhou, J.; Pu, Y. P.; Lin, P. H. "Fabrication and characteristics of bioactive sodium titanate/titania graded film on NiTi shape memory alloy." *Journal of Biomedical Materials Research Part A* **2005**, *75A*, 595-602.
- (103) Wang, X.-X.; Hayakawa, S.; Tsuru, K.; Osaka, A. "Improvement of bioactivity of H₂O₂/TaCl₅-treated titanium after subsequent heat treatments." *Journal of Biomedical Materials Research* **2000**, *52*, 171-176.
- (104) Takemoto, S.; Yamamoto, T.; Tsuru, K.; Hayakawa, S.; Osaka, A.; Takashima, S. "Platelet adhesion on titanium oxide gels: effect of surface oxidation." *Biomaterials* **2004**, *25*, 3485-3492.
- (105) Becker, I.; Hofmann, I.; Muller, F. A. "Preparation of bioactive sodium titanate ceramics." *Journal of the European Ceramic Society* **2007**, *27*, 4547-4553.
- (106) Kubota, S.; Johkura, K.; Asanuma, K.; Okouchi, Y.; Ogiwara, N.; Sasaki, K.; Kasuga, T. "Titanium oxide nanotubes for bone regeneration." *Journal of Materials Science: Materials in Medicine* **2004**, *15*, 1031-1035.
- (107) Kim, H. M.; Miyaji, F.; Kokubo, T.; Nakamura, T. "Preparation of bioactive Ti and its alloys via simple chemical surface treatment." *Journal of Biomedical Materials Research* **1996**, *32*, 409-417.

- (108) Yada, M.; Inoue, Y.; Uota, M.; Torikai, T.; Watari, T.; Noda, I.; Hotokebuchi, T. "Plate, Wire, Mesh, Microsphere and Microtube Composed of Sodium Titanate Nanotubes on a Titanium Metal Template." *Langmuir* **2007**, *23*, 2815-2823.
- (109) Yun, H.; Lin, C.; Li, J.; Wang, J.; Chen, H. "Low-temperature hydrothermal formation of a net-like structured TiO₂ film and its performance of photogenerated cathode protection." *Applied Surface Science* **2008**, *255*, 2113-2117.
- (110) Wang, W. L.; Lin, H.; Li, J. B.; Wang, N. "Formation of titania nanoarrays by hydrothermal reaction and their application in photovoltaic cells." *Journal Of The American Ceramic Society* **2008**, *91*, 628-631.
- (111) Ohba, Y.; Baba, Y.; Sakai, E.; Hirata, H.; Sugino, M.; Daimon, M. "Porous anatase layer formed on titanium substrate through hydrothermal processes." *Journal Of Materials Science* **2008**, *43*, 2163-2170.
- (112) Zhang, Q.; Chakraborty, A. K.; Lee, W. I. "Preparation of titania nanotape array and its photocatalytic property." *Journal of Physics and Chemistry of Solids* **2008**, *69*, 1450-1453.
- (113) Adachi, M.; Murata, Y.; Takao, J.; Jiu, J.; Sakamoto, M.; Wang, F. "Highly Efficient Dye-Sensitized Solar Cells with a Titania Thin-Film Electrode Composed of a Network Structure of Single-Crystal-like TiO₂ Nanowires Made by the "Oriented Attachment" Mechanism." *Journal Of The American Chemical Society* **2004**, *126*, 14943-14949.
- (114) Jiu, J.; Isoda, S.; Wang, F.; Adachi, M. "Dye-Sensitized Solar Cells Based on a Single-Crystalline TiO₂ Nanorod Films " *Journal Of Physical Chemistry B* **2006**, *110*, 2087-2092.
- (115) Tan, B.; Wu, Y. "Dye-Sensitized Solar Cells Based on Anatase TiO₂ Nanoparticle/Nanowire Composites." *The Journal of Physical Chemistry B* **2006**, *110*, 15932-15938.
- (116) Zhu, K.; Neale, N. R.; Miedaner, A.; Frank, A. J. "Enhanced Charge-Collection Efficiencies and Light Scattering in Dye-Sensitized Solar Cells Using Oriented TiO₂ Nanotubes Arrays." *Nano Letters* **2007**, *7*, 69-74.
- (117) Ohsaki, Y.; Masaki, N.; Kitamura, T.; Wada, Y.; Okamoto, T.; Sekino, T.; Niihara, K.; Yanagida, S. "Dye-Sensitized TiO₂ Nanotube solar cells: fabrication and electronic characterization." *Physical Chemistry Chemical Physics* **2005**, *7*, 4157-4163.
- (118) Uchida, S.; Chiba, R.; Tomiha, M.; Masaki, N.; Shirai, M. "Application of titania nanotubes to a dye-sensitized solar cell." *Electrochemistry* **2002**, *70*, 418-420.
- (119) Wei, M.; Konishi, Y.; Zhou, H.; Sugihara, H.; Arakawa, H. "Utilization of Titanate Nanotubes as an Electrode Material in Dye-Sensitized Solar Cells." *Journal Of The Electrochemical Society* **2006**, *153*, A1232-A1236.
- (120) Yoon, J.-H.; Jang, S.-R.; Vittal, R.; Lee, J.; Kim, K.-J. "TiO₂ nanorods as additive to TiO₂ film for improvement in the performance of dye-sensitized solar cells." *Journal of Photochemistry and Photobiology A: Chemistry* **2006**, *180*, 184-188.

- (121) Mor, G. K.; Shankar, K.; Paulose, M.; Varghese, O. K.; Grimes, C. A. "Use of Highly-Ordered TiO₂ Nanotube Arrays in Dye-Sensitized Solar Cells." *Nano Letters* **2006**, 6, 215-218.
- (122) Pavasupree, S.; Ngamsinlapasathian, S.; Nakajima, M.; Suzuki, Y.; Yoshikawa, S. "Synthesis, characterization, photocatalytic activity and dye-sensitized solar cell performance of nanorods/nanoparticles TiO₂ with mesoporous structure." *Journal of Photochemistry and Photobiology A: Chemistry* **2006**, 184, 163-169.
- (123) Wang, P.; Zakeeruddin, S. M.; Moser, J. E.; Gratzel, M. "A new ionic liquid electrolyte enhances the conversion efficiency of dye-sensitized solar cells." *Journal Of Physical Chemistry B* **2003**, 107, 13280-13285.
- (124) Luo, H.; Wang, C.; Yan, Y. "Synthesis of Mesoporous Titania with Controlled Crystalline Framework." *Chemistry Of Materials* **2003**, 15, 3841-3846.
- (125) Stergiopoulos, T.; Arabatzis, I. M.; Katsaros, G.; Falaras, P. "Binary polyethylene oxide/titania solid-state redox electrolyte for highly efficient nanocrystalline TiO₂ photoelectrochemical cells." *Nano Letters* **2002**, 2, 1259-1261.
- (126) Ma, T.; Akiyama, M.; Abe, E.; Imai, I. "High-Efficiency Dye-Sensitized Solar Cell Based on a Nitrogen Doped Nanostructured Titania Electrode." *Nano Letters* **2005**, 5, 2543-2547.
- (127) Qi, L.; Sorge, J. D.; Birnie III, D. P. "Dye Sensitized Solar Cells Based on TiO₂ Coatings with Dual Size-Scale Porosity." *Journal Of The American Ceramic Society* **2007**, *Accepted*.
- (128) Many thanks to Steve Dawes.

JUDITH D. SORGE
jdsorge@eden.rutgers.edu

Education

Rutgers University, Piscataway, New Jersey;

Ph.D. candidate, Materials Science and Engineering, 2008; GPA: 3.9

M.S. Materials Science and Engineering, 2006

University of Chicago, Chicago, Illinois; B.S. Chemistry, June 2003; GPA: 3.3

Experience

Rutgers University, Piscataway, New Jersey

Graduate Research Assistant, July 2004 – Current

- ◆ Research topic: “The Effect of Titania Particle Morphology and Crystallographic Orientation on Dye Adsorption for Photovoltaic Applications”
- ◆ Developed method to construct reproducible dye sensitized solar cells in the laboratory
- ◆ Explored hydrothermal reactions of titania in solution and on titanium metal with sodium hydroxide to understand the mechanism of this growth at low temperatures
- ◆ Skilled in using scanning and transmission electron microscopy, as well as X-ray diffraction and atomic force microscopy (AFM) to determine crystal structure, orientation and morphology of titania particles.
- ◆ Oversee and mentor several undergraduates researching a variety of coating and solar cell projects.
- ◆ Group safety coordinator: Develop safety protocols and train new group members
- ◆ Principal Investigator: Dunbar P. Birnie, III

US – India Nanoscale Science and Engineering Institute, Chennai, India

Nanotechnology Tutorial, January 2008

- ◆ Chosen to attend and present on nanoscale titania structures in dye sensitized solar cells; funded by the National Science Foundation
- ◆ Educational experience with invited lecturers on the broad subject of nanotechnology to discuss future directions and to promote collaboration with Indian universities

Corning, Inc., Corning, New York

Research Intern: Display Development and Technology, June 2007 – Aug 2007

- ◆ Mapped residual stress of display substrates after measuring their birefringence and shape in order to understand how forming process affects final stress development
- ◆ Utilized MatLab to create easily manipulated residual stress maps

Pan American Advanced Studies Institute, Santiago, Chile

Transmission Electron Microscopy Workshop, July 2006

- ◆ Selected to be one of 25 TEM focused graduate students to represent the United States; funded by the National Science Foundation
- ◆ Enhanced knowledge of microscopy and microanalysis as well as sample preparation through lectures and hands-on lessons
- ◆ Promoted growth of microscopy in South America through collaborative work

University of Illinois, Champaign, Illinois

Graduate Research Assistant, August 2003 – May 2004

- ◆ Contributed to research in electronic ceramics, especially barium titanate piezoelectric materials

Presentations / Publications

J. D. Sorge and D. P. Birnie, III, Characterization of Structures Grown Hydrothermally on Titanium Metal for Solar Application. Oral presentation and to appear, *Proceedings of the 2008 Materials Science and Technology Conference*, 2008.

S. Phadke, J. D. Sorge, and D. P. Birnie, III, Clustering Effects in Solution-Based Nanoparticle/Template Hybrid Coatings. *Journal of the Society of Information Display*, 2007, 15, 1089-1093.

L. Qi, J. D. Sorge, and D. P. Birnie, III, "Dye Sensitized Solar Cells Based on TiO₂ Coatings with Dual Size-Scale Porosity", submitted to J. Amer. Ceram. Soc., (2008).

S. Phadke, J. D. Sorge, S. Hachtmann, and D. P. Birnie, III, Broad Band Optical Characterization of Sol-Gel TiO₂ Thin Film Microstructure Evolution with Temperature, submitted to Thin Solid Films (2008).

S. Murali, J. D. Sorge, S. Phadke, A. Jackson, J. Stanley, and D. P. Birnie III; Hydrothermal synthesis of titania using different substrates and seed conditions, poster presented at 22nd LSM Annual Meeting, 15 February 2008.

E. Bersch, S. Rangan, J. P. Theisen, R. A. Bartynski, J. D. Sorge, and D. P. Birnie; "Electronic Structure of N3 Dye Molecules on the TiO₂(110) Surface and on Anatase Nanopowder", presented at the Am. Phys. Soc. Annual Meeting, New Orleans, 13 March 2008.

S. Rangan, J. P. Theisen, E. Bersch, R. A. Bartynski, J. D. Sorge, D. P. Birnie III, Z. Duan, and Y. Lu; "Electronic Energy Level Alignment in Dye Sensitized Oxide Surfaces", poster presented Princeton Center for Complex Materials Symposium, June 9-12, 2008.

J. D. Sorge, J. McCarthy, P. Lee, and D. P. Birnie, III, "Investigation of Electrolyte Charge Transfer in a Dye Sensitized Solar Cell", presented, Materials Science and Technology 2007 Conference and Exhibition; September 2007, Detroit, Michigan.

L. Qi, S. Murali, J. D. Sorge, S. Phadke, and D. P. Birnie, III, "Templated TCO/TiO₂ Hierarchical Network Junction for Sensitized Photovoltaics," presented, 31st International Conference & Exposition on Advanced Ceramics & Composites, January 2007, Daytona Beach, FL.

S. Murali, L. Qi, J. D. Sorge, S. Phadke, and D. P. Birnie, III, "Transparent Conducting Oxide Based Templated Structures for Photovoltaic Applications," presented, Materials Science and Technology 2007 Conference and Exhibition; September 2007, Detroit, Michigan.

J. D. Sorge, L. Qi, and D. P. Birnie, III, "TEM Characterization of Nanostructured Titanium Dioxide for Use in Dye Sensitized Solar Cells", poster presentation, Fall 2006 Annual Meeting of MRS, Boston, MA.

S. Phadke, J. D. Sorge and D. P. Birnie, III, "Broad Band Optical Characterization of Sol-Gel TiO₂ Thin Film Microstructure Evolution with Temperature," presented, Materials Science and Technology 2006 Conference and Exhibition; September 2006, Cincinnati, Ohio.

L. Qi, J. D. Sorge, and D. P. Birnie, III, Dye-Sensitized Solar Cells (DSC) with Templated Nanocrystalline TiO₂ Films Having Dual Size-Scale Porosities, presented, Fall 2006 Annual Meeting of MRS, November 30th, 2006, Boston MA.

J. D. Sorge, D. P. Birnie, III, and L. Qi, "Effect of Titania Particle Morphology on Dye Adsorption for Photovoltaic Applications", presented, Fall 2005 Annual Meeting of MRS, Boston MA.

L. Qi, D. P. Birnie, III, and J. D. Sorge, Templated Growth of Highly Porous Titania Films of Closely Packed Pore Network, Poster presentation, Fall 2005 Annual Meeting of MRS, Boston MA.

D. P. Birnie, III, J. D. Sorge, L. Qi, S. Phadke, and S. Hussain, "Nanostructured Solar Oxides", Presented at NJTC/GGSNA Meeting on "Commercializing Nanotechnology in Energy Storage and Conversion", 21 November 2005, Piscataway NJ.

J. D. Sorge and D. P. Birnie, III, "Investigation of TiO₂ Nanoparticle Monolayers by Spin Coating", presented, 107th Annual Meeting of The American Ceramic Society, April 2005, Baltimore MD.

Awards

John Dennis / HED / Malcolm G. McLaren Fellowship,

Rutgers University; September 2004 – June 2006

Hamer Scholarship, University of Illinois; September 2003

Support for Under-Represented Groups in Engineering Fellowship,

University of Illinois; September 2003 – June 2004

Synergistic Activities

Materials Research Society Entrepreneurship Challenge

April 2007

- ◆ International competition pairing materials scientists and business students to develop concepts for materials-based start-up companies
- ◆ Finalist after presentation at the spring Materials Research Society meeting judged by venture capitalists
- ◆ Created business and marketing plan for “cRAM” – a possible start-up company based on a novel memory device

Materials Research Society – Rutgers University Chapter

September 2005 – Current

- ◆ Founding member of the student chapter of the Materials Research Society at Rutgers
- ◆ Organized symposium of graduate students for students and faculty to create open atmosphere for discussion between departments.

Rutgers University

September 2004 – Current

- ◆ Promote Rutgers and its science and research programs by participating in activities such as Engineering Open House, Nano Day and the Society of Women Engineers College Fair.
- ◆ Support Rutgers graduate programs by presenting my fellowship experience at the School of Engineering “Scholarship and Fellowship Reception” in October 2005.

Professional Memberships: American Chemical Society; Sigma Xi; American Ceramics Society; Materials Research Society